Defect Characterization by Acoustic Holography
Volume 1: Imaging in Field Environments

NP-1534, Volume 1
Research Project 605-1

Final Report, September 1980

Prepared by

COE ASSOCIATES
2672 Bayshore/Frontage Road, Suite 1000
Mountain View, California 94043

and

BABCOCK & WILCOX CO.
Research and Development Division
P.O. Box 1260
Lynchburg, Virginia 24505

Principal Investigators
A. Holt
J. Brophy

Prepared for

Electric Power Research Institute
3412 Hillview Avenue
Palo Alto, California 94304

EPRI Project Manager
G. Dau

Reliability, Availability and Economics Program
Nuclear Power Division

ORDERING INFORMATION

Requests for copies of this report should be directed to Research Reports Center (RRC), Box 50490, Palo Alto, CA 94303, (415) 965-4081. There is no charge for reports requested by EPRI member utilities and affiliates, contributing nonmembers, U.S. utility associations, U.S. government agencies (federal, state, and local), media, and foreign organizations with which EPRI has an information exchange agreement. On request, RRC will send a catalog of EPRI reports.

NOTICE

Prepared by
Coe Associates
Mountain View, California
and
Babcock & Wilcox Co.
Lynchburg, Virginia

EPRI PERSPECTIVE

PROJECT DESCRIPTION

Fault detection and characterization are critical aspects of pressure vessel production and in-service inspections. EPRI has initiated a program to improve the reliability and accuracy of nondestructive (NDE) techniques for in-service inspections. While the majority of the NDE research studies are weighted towards improvement of detection reliability, a portion of EPRI's program is devoted to improvement of characterization ability. Acoustic holography laboratory studies indicated that this technique offered a potential for significant improvements in characterization. Two concurrent studies were initiated. One study (RP605), which is the subject of this report, emphasizes expansion of the existing data base pertaining to the application of acoustic holography to heavy section inspections. The second study (RP606) is designed to improve the quality and reliability of acoustic holography systems.

RP605 was designed to provide data that would permit a quantitative definition of the performance expected from the equipment being developed under RP606. Available acoustic holography equipment was used to inspect a variety of components in a field environment. The program included the charge to develop a comparative data base that would allow the results obtained with acoustic holography to be compared to results obtained with destructive tests and by conventional NDE techniques.

PROJECT OBJECTIVES

The objectives of RP605 were to extend the then-existing laboratory data base to a wider range of applications and also explore the implications of operation of acoustic holography equipment in a realistic field environment. A primary goal was to quantify the ability of the existing acoustic holography equipment to characterize defects (i.e., determine the size, shape, orientation, location, and type) in thick-section welds. The test specimens were to include both production components with naturally-occurring and fabrication-induced defects, and nonproduction components with artificially induced defects. Where possible, comparative data were to be obtained with radiographic techniques, conventional ultrasonic techniques, and destructive tests.

PROJECT RESULTS

The RP605 results indicate that acoustic holography can provide accurate dimensional information about defects and their through-wall location. In all cases where comparative results were available, the holographic results were within ± 10 percent of the values determined from destructive inspection. This accuracy is sufficient to meet the measurement requirements for fracture mechanics analysis of flaw significance.

The project also demonstrated that it is possible to obtain useful holographic data in a production environment. This is doubly significant because the equipment used for RP605 represents technology of a decade ago. Thus, improved performance can be expected with more current systems such as the one being developed under RP606.

RP605 included examination of a specially prepared test specimen by teams from different nations using different approaches. This portion of the effort provided comparative information on the different approaches and was an excellent example of international cooperation.

The results of RP605, which are reported in two volumes, are primarily of interest to those engaged in research and development toward improved in-service inspection systems.

Gary J. Dau, Project Manager
Nuclear Power Division

FOREWORD

Research Project 605 (RP-605) is part of an overall program with the goal of making an ultrasonic imaging device available for pre-service and in-service inspections of primary pressure boundary components. The objective of RP-605 is to generate a data base that shows the effects of the field environment on the ease of use and accuracy of an Acoustic Holographic imaging system. In this program Acoustic Holography techniques were applied to the evaluation of flaws in production and non-production vessels, special samples, and clad test blocks.

The results obtained during the RP-605 program are presented in two volumes:

DEFECT CHARACTERIZATION BY ACOUSTIC HOLOGRAPHY
VOLUME I: IMAGING IN FIELD ENVIRONMENTS

DEFECT CHARACTERIZATION BY ACOUSTIC HOLOGRAPHY
VOLUME II: EFFECTS OF CLADDING ON AH IMAGING

Volume I covers the results obtained for production and non-production components and includes American tests of a clad test block supplied by CEN. Volume II covers the results obtained by eleven different groups on a single test specimen.

Prime contractor for the RP-605 effort is Babcock & Wilcox Lynchburg Research Laboratory, (A.E. Holt, Project Manager). The duration of the program was from February 1976 to December 1979.

ABSTRACT

Acoustic Holography (AH) equipment was used in a field environment to characterize defects in thick plate components. The program was successful and a large holographic data base was generated. Both optical and computer reconstruction techniques were used to produce AH images of selected defects. The report covers results on both production and non-production components, and describes the equipment and test configurations used to acquire the data. The portion of the program dealing with the production components includes comparative data for conventional NDE techniques (Radiographic and Ultrasonic), Acoustic Holography and destructive tests. In addition, holographic data developed during the program is on file with the NDE center in Charlotte, North Carolina. Volume I covers AH images obtained with American Equipment using optical reconstruction techniques. Volume II presents results obtained by 11 different Ultrasonic Testing teams that investigated the same test block.

PREFACE

Compliance with the ASME Boiler and Pressure Vessel Code, Section XI, "In-service Inspection of Nuclear Reactor Coolant Systems", is a mandatory requirement for nuclear power station construction and operation licenses in the United States. The code specifies minimum requirements for both pre-service and in-service inspections. Recent editions of the code have required the use of fracture mechanics principles for the evaluation of defect severity. This requires that the inspection method detect the flaw and characterize it in terms of size, orientation, and change with respect to time. The commonly used methods of volumetric inspection, ultrasonics and radiography, are subject to inherent limitations. Only through the acquisition of substantial amounts of data and extensive interpretive effort, can acceptable levels of reliability and precision be obtained. Acoustic Holography inherently generates a large amount of cross-correlated data in a relatively short time. The length of time required to gather the data is governed by the speed of the scanning mechanism and the size of the scan area. The data used in the holographic image formation is a result of signal parameters extracted from a large range of viewing angles. Defect characterization by Acoustic Holography is accomplished through image formation, either optically or computationally. The measured image dimensions then correspond proportionally to the actual defect dimensions. Laboratory tests (and some field tests) have shown that Acoustic Holography, when used for characterization of defects in thick section materials, is capable of better accuracy than conventional ultrasonic or radiographic techniques (Ref. 1).

TABLE OF CONTENTS

ILLUSTRATIONS

Figures

Figures

TABLES

Section 1.0
INTRODUCTION AND SUMMARY

1.1 GENERAL

This report describes the results obtained when Acoustic Holographic (AH) techniques (also known as Ultrasonic Holography) were applied in a field environment to characterization of defects in pressure vessels. The production components contained natural or fabrication induced defects, and the non-production specimens contained artificially induced defects. Seven types of components were evaluated:

a. Production Component-Thick Plate Base Metal (section 3.2)

b. Production Component-Nozzle Weld (section 3.3)

c. Production Component-Circle Seam Weld (section 3.4)

d. Production Component-Long Seam Weld (section 3.5)

e. Non-production Component-Two HSST Thermal Shock Vessels (section 4.2)

f. Non-production Component-Acoustic Emission Pressure Vessel (section 4.3)

g. Non-production Component-Clad Weld Test Block (section 4.4)

The RP-605 program developed a fairly large data base that includes interpreted AH imagery, destructive test photos, and the unprocessed holographic data base.

Illustrative samples of this material were selected for inclusion in this report. The balance of the data is on file at the NDE Center in Charlotte, North Carolina.

1.2 PRODUCTION COMPONENT TESTS

The production component tests were conducted in a field environment with all the schedule constraints associated with a pressure vessel production facility. These field tests involved a variety of geometric arrangements and a wide range of defect sizes and types. Emphasis was on natural and/or fabrication induced defects. The defects that were studied were initially detected with conventional NDE (radiographic or ultrasonic) techniques. When these discontinuities were judged serious enough to warrant removal of a portion of the vessel, AH images of said discontinuities were made. Each of the production AH examinations involved different data acquisition and analysis approaches. The characterization information needed was generally specific to the production components as requested by the fabricator; the production tests were as follows:

a. Base metal studies of thick plate: Thru-wall extent of the discontinuities.

b. Nozzle weld studies: Length, orientation and thru-wall extent of the discontinuities.

c. Circle seam studies: Area of defects.

d. Long seam studies: Defect dimension transverse to the weld seam.

1.3 NON-PRODUCTION COMPONENT TESTS

The non-production component tests were conducted in the field for the Acoustic Emission Pressure Vessel (AEPV) tests; at Oak Ridge National Laboratories for the HSST tests; and in Saclay, France for the Clad Weld Block tests. In these tests, AH images of the defects were obtained in circumstances where conventional NDE and destructive test data on the defects was sparse because the AH project team did not control the NDE or destructive tests. In the non-production tests, AH was used as the primary NDE technique in support of programs with primary objectives other than validation of AH results.

1.4 AH EQUIPMENT AND TEST CONFIGURATIONS

The equipment used for the RP-605 studies represented the state-of-the-art when RP-605 began in 1976. As is true for other fields, improved equipment is now available. In the period 1976-1979, AH was an art rather than a science, and the Babcock and Wilcox team was remarkably successful where other practitioners had been unsuccessful.

1.5 RELATIONSHIP OF VOLUME I AND VOLUME II

The amount of data generated by AH and other advanced testing methods was sufficiently large that a second volume (Volume II) was deemed advisable. Access to all of the RP-605 data would require access to Volume I, Volume II and the data base on file at the NDE Center.

1.6 SUMMARY

Acoustic Holography is a viable technique for expansion of NDE field inspection capability. Acoustic Holography supplements rather than replaces conventional NDE inspection techniques. The results obtained suggest that Acoustic Holography could be the technique of choice for characterization of defects.

The results were obtained with laboratory grade equipment adapted for field use. The operators used to perform the field inspection were highly skilled and the success of the program was in large part attributable to the skill of these operators.

> Image enhancement techniques for AH images derived from optical reconstruction or alternative reconstruction techniques such as those reported in Volume II would materially assist in reducing the dependence of AH on operator skill.

As noted in Section 2.3, field operators will have to be familiar with the physics involved in testing a particular specimen to allow AH usage over the range of specimen configurations that might be encountered in field situations.

The results obtained also suggested avenues of development that could materially improve the effectivity of AH equipment in the field (see Section 5.0).

Section 2.0
BACKGROUND DISCUSSION

2.1 GENERAL

In the period 1972-1976, experiments demonstrated the feasibility of Acoustic Holography techniques. RP-605 was initiated in 1976 to extend AH laboratory results with a more extensive field data base. In part, the program was designed to take advantage of "targets of opportunity" even if the situation was not favorable to rigorous experimental control. The following portions of this section discuss the basic AH technique in the context of conventional NDE techniques. The subsequent discussions present some of the basic considerations that were involved in the production and non-production tests.

2.2 ACOUSTIC HOLOGRAPHY CONCEPT

Conventional ultrasonic (UT) techniques (fixed beam, pulse-echo) are usually based on equipment that propagates a beam of ultrasonic energy in a material, and measures the reflected energy from the beam (Figure 2-1). A physically narrow beam of pulsed energy with a relatively wideband frequency content is used. The search transducer detects any energy of the same frequency band that is reflected from discontinuities in the material back to the transducer (the echo). The technique is known as Backward Wave Propagation. The beam has to be oriented so that it impinges on the discontinuity in the material, and so that the reflected energy will reach the search transducer (see figure 2-2A). The pulse-echo signal is displayed on a cathode ray tube or photographed for later study. While AH also uses a reflected acoustic beam system (see figure 2-2B), there are a number of fundamental differences between the two techniques as follows:

a. A relatively wide cone-shaped beam is used for AH, rather than a narrow beam.

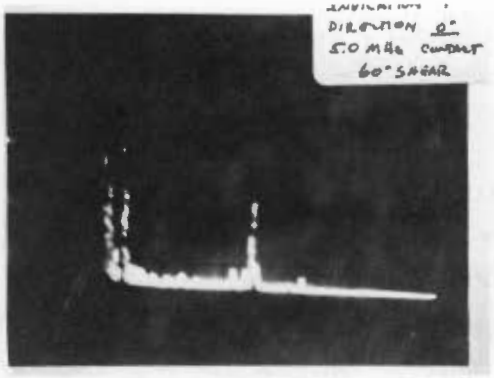

(a)

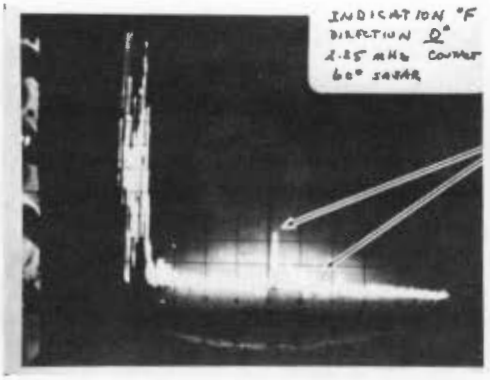

(b)

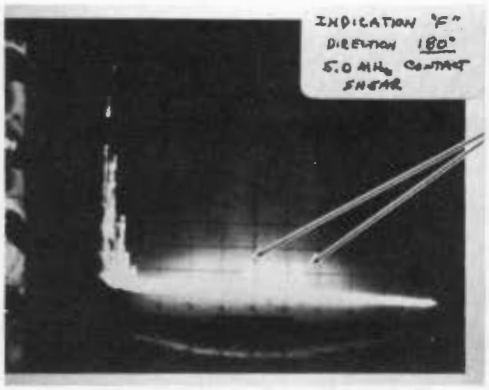

(c)

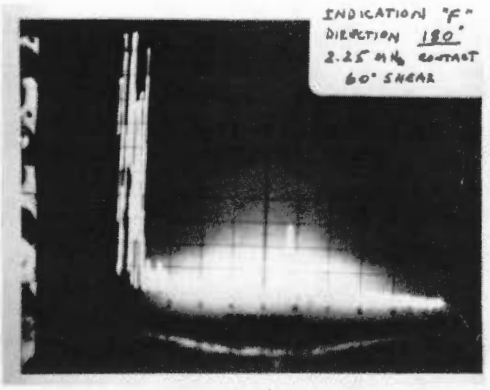

(d)

Figure 2-1 Conventional UT Indications

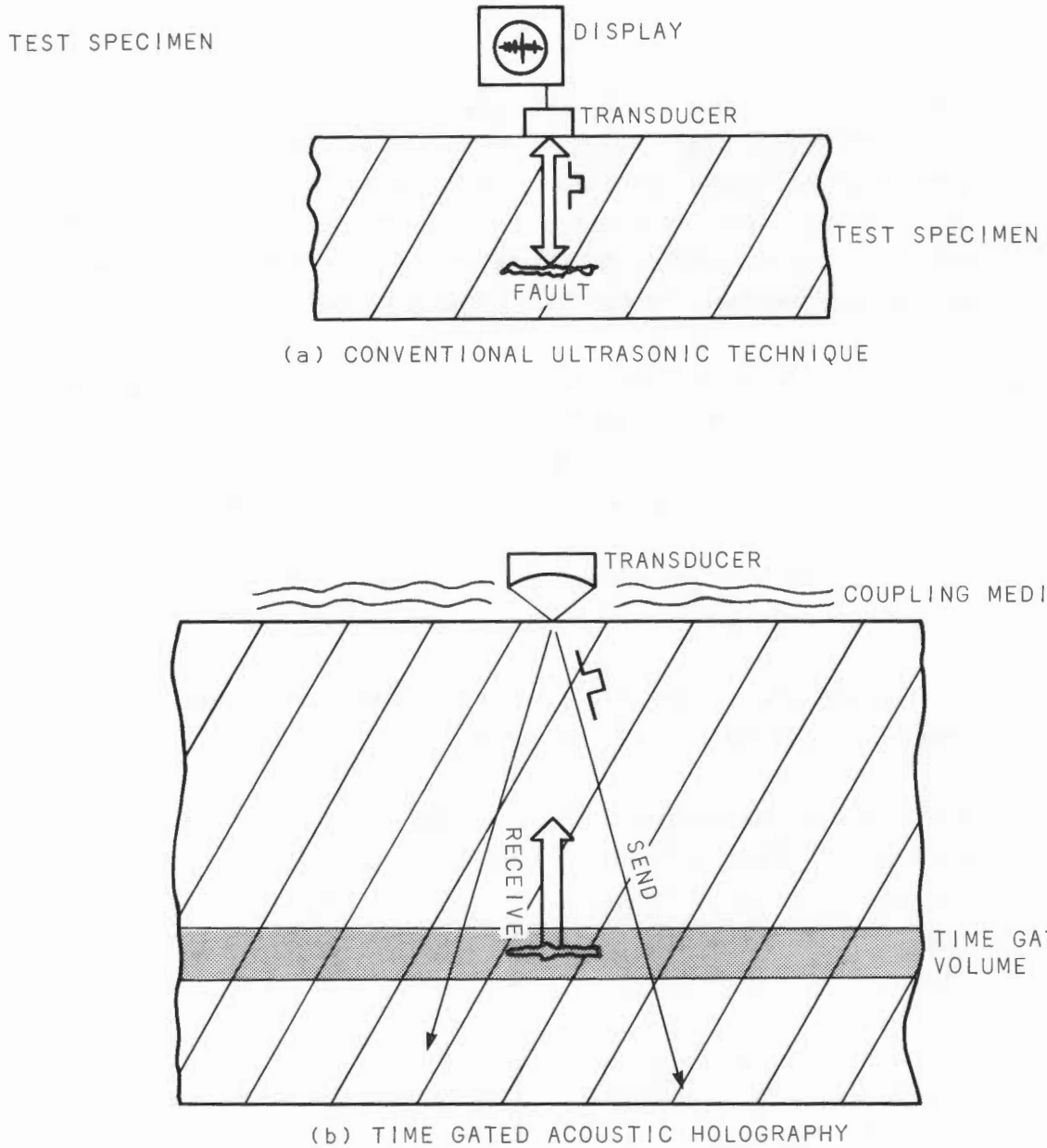

Figure 2-2 AH Concept.

b. A mechanical system is used to continuously translate the AH search transducer (SCANNER), with respect to the test specimen, with a scan pattern analagous to a T.V. screen pattern. Conventional UT scanning is obtained by manual positioning of the search sensor by the operator.

c. Time-gated holography inherently results in a two dimensional image, rather than the single point data of conventional UT (Figure 2-3). Time-gated holography introduces a step that limits the data obtained on a scan to a specific search plane. If the time-gate technique was not used, the holographic data obtained would be for the total volume of the test specimen, rather than a specific plane.

d. The AH transducer is located above the surface of the test specimen and the acoustic energy from this transducer is focused on the surface of the test material, as compared to conventional UT, where the transducer is placed directly on the surface of the test material.

e. AH uses phase coherent signal detection while conventional UT does not.

f. AH images are essentially binary (absent or present), while conventional UT images are analog (amplitude dependent).

g. AH images are interpreted in terms of the location of the points that make up the image, without regard for the intensity of the images or the distribution of intensity within the image. Conventional UT results are interpreted in terms of the intensity of the returned signal.

The use of a cone-shaped beam, as compared to a narrow fixed angle beam, increases the probability of detection of a fault because the cone-shaped beam encompasses a wide range of angles (see Figure 2-4). Since the parameter of interest in AH is the shape of the image, any signal, no matter how weak, that will expose the sensing medium (usually film), is sufficient for a satisfactory result.

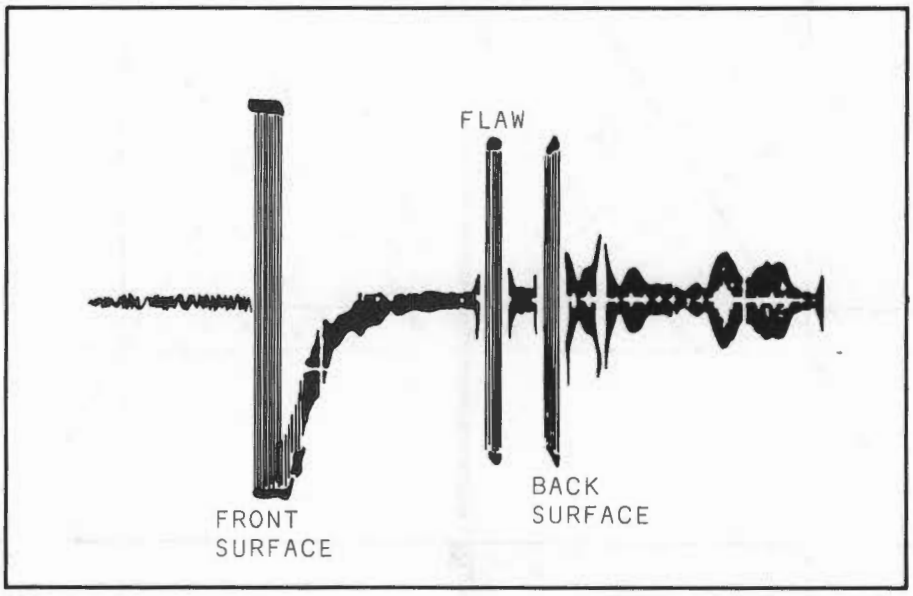

Figure 2-3 AH Signal Return

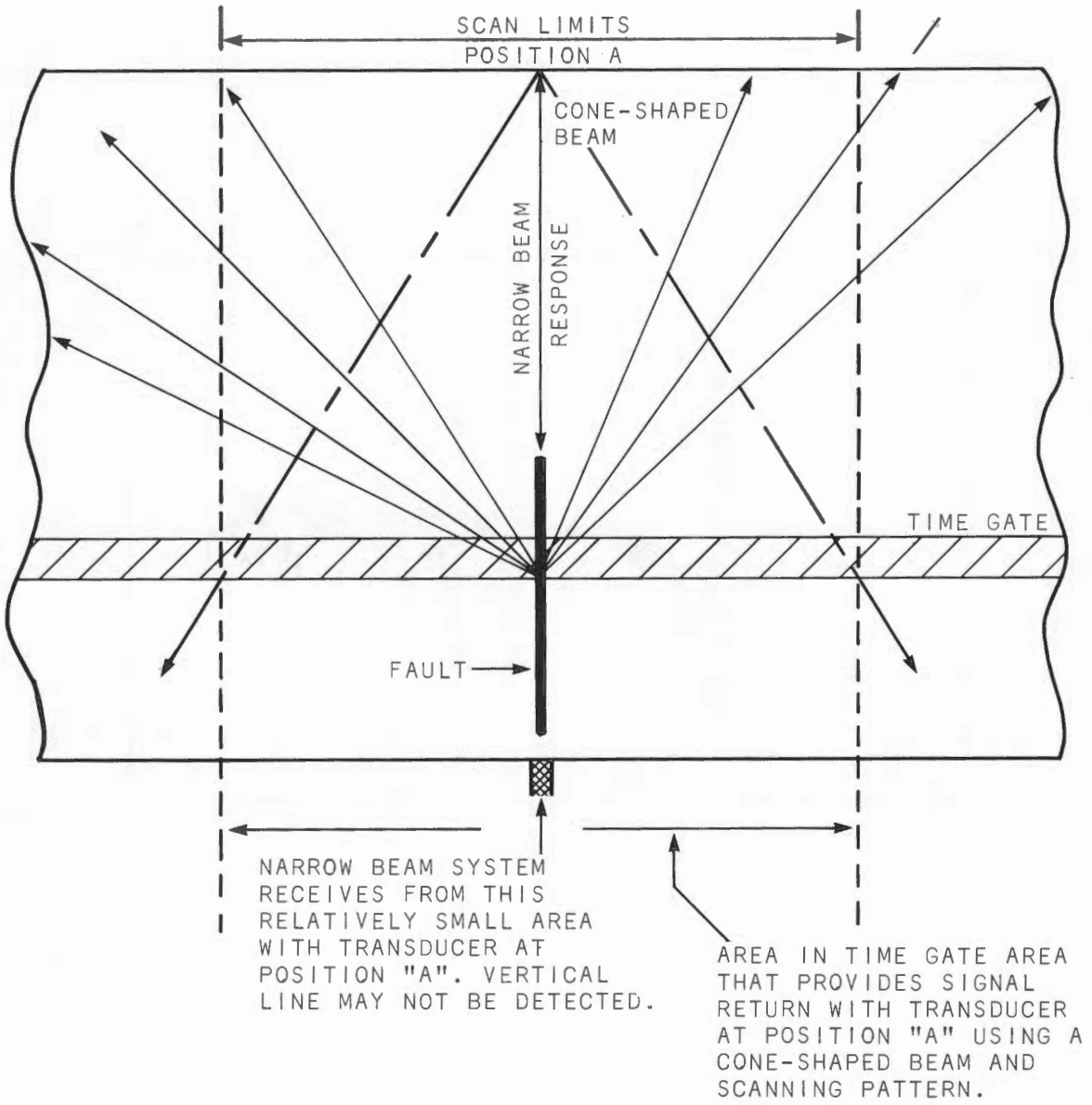

Figure 2-4 Fixed Narrow Beam vs. Cone-shaped Beam

Present day AH systems use a two step approach. In the first step, the holographic data (which looks like a set of rings) is obtained and recorded. The holographic data is then processed to reconstruct the image. At the present time both optical and digital techniques are used for image reconstruction. In the early portion of RP-605, optical reconstruction was used to obtain the AH images (see Figure 2-2).

Figure 2-2 includes a zone that is identified as a Time Gate Zone. The Time Gate Zone allows a particular plane within the material to be selected, and the resultant AH image applies to the specific plane. Moving the Time Gate Zone allows a series of "slices" to be imaged and sized, even when the fault is thin and oriented perpendicular to the surface of the test specimen. In conventional UT, using off-axis techniques, the sizing is based on the amplitude of the return; as a consequence, thin, vertical cracks (which have small net areas) are more difficult to characterize.

2.3 INSPECTION CONSTRAINTS

There are three major constraints affecting the defect characterization process using AH equipment. In the order of priority they are: component geometry and accessibility, physics of the sound beam interaction with the defect, and the optical reconstruction equipment physical limitations. The individual constraints are not independent. Limitations imposed by any one of the three will probably have an impact on the others. Effective defect characterization becomes a process in which the limiting factors are recognized and used to obtain the best compromise in order to characterize a given defect.

Ideally, one would like to optimise the physics of the interaction by imaging from multiple viewing angles and from several surfaces. Also, one would like to scan the defect in a manner so as to decrease the likelihood of unfavorable beam energy scatter. The parameters involved are highly dependent on the geometry of the component being inspected. Very seldom is there opportunity for unlimited access on an inspection surface. The detailed contour of the available surfaces will have an impact on the choice of viewing angles and scanner settings. The direction of scan can also influence the quality of the image. These and other items all play a large role in determining the success of inspection.

Even if the inspection constraints due to the component geometry are negligible, the potential limitations imposed by the defect geometry and type can result in to false or misleading conclusions. In a pulse-echo system, masking of one defect by defects in the immediate vicinity is a real, verified problem. The surface roughness of the defect contour can adversely affect the imaging process if the wavelength of the search beam is improperly chosen. In any specific application there is a long list of possible and probable influencial factors that can complicate defect characterization.

Constraints due to geometry and physics also apply to the optical method of image reconstruction. Initial compromises must be made in the construction of an optical bench. It must be rugged and portable enough for field use, and still have enough versatility to compensate for a fairly wide range of depths, viewing angles and wavelengths. An example is the "Dead Zone" near inspection surfaces that is characteristic of the Optical Bench used for RP605. The "dead zone" was attributable to the fact that the field optical bench was physically limited in size and the viewing monitor lacked the sufficient brightness and resolution to compensate for changes in image size as a function of depth and wavelenth.

The implication that characterization of a naturally occurring defect is difficult is true. However, it does not necessarily follow that it cannot be done. The defect evaluator and data acquisition team must be aware of the potential for misinterpretation and must have a "feel" for the magnitude of the effects on other steps in the complete evaluation process so that appropriate compromises can be made in the data acquisition and image formation process. Fortunately, there usually exists enough data redundancy, even in limited data sets, to adequately characterize most naturally occurring defects.

There has been no attempt made in this discussion to outline all the possible difficulties one might run into during a practical inspection. It suffices to say that at the present time Acoustic Holography is not a straightforward process with a "push-button" solution.

2.4 PRODUCTION INSPECTIONS

2.4.1 Overview

Conventional ultrasonic (UT) inspection techniques are known to have certain limitations with respect to the detection and characterization of defects (flaws, discontinuities) in thick plate made from carbon steel. Standard shop practices are usually based on compliance with applicable codes. Working to code does not assure attainment of the desired result. A major factor that influences the NDE results obtained is the detailed procedure that is used to implement the code. In practice, the code is mute relative to certain physical relationships that pertain to UT techniques, particularly test frequencies or search unit parameters. Previous studies (Ref. 2) have shown that the effectiveness of conventional UT equipment is appreciably affected by the design of the search transducer and the frequency selected for the examination (see Section 3.4 for corroborative test results obtained during RP-605).

Radiographic inspection techniques are inherently limited in that they yield:

a. two dimensional images generated by high energy radiation absorption/attenuation by the material being inspected and

b. exposure of the film on the side opposite the energy source (i.e., the images are profiles perpendicular to the radiation path).

Prior studies (2) have shown that Acoustic Holography can provide certain advantages in the detection and characterization of thick plate defects. RP-605 was established to:

a. build a reportable data base and

b. quantify the degree of degradation (if any) of the AH procedure when used on production vessels in a field environment.

The program was designed to operate on the basis of minimum interference with production operations and with primary reliance on standard ASME Code

procedures for initial detection/characterization of defects. Subsequently AH was used on selected specimens that were flagged by conventional NDE techniques as items of concern.

2.4.2 Technical Considerations

A production environment involves a variety of shapes, surface conditions and surface orientations. AH techniques require effective coupling between the test specimen and the AH transducer. Four field environment problem areas were:

a. the technology involved in coupling the transducers to the test volume;

b. the technology involved in positioning the transducer on the surface of the test vessel;

c. prime power quality and fluctuations and

d. electromagnetic interference.

One characteristic of conventional (straight beam pulse-echo) ultrasonic (UT) examinations is that different frequencies yield different results. Conventional practice assumes that the amplitude of the return signal (pulse-echo) depends only on the area of the defect. This assumption is questionable since different UT transducers yield different results (i.e., the same defect could be judged as acceptable or unacceptable, depending on the transducer used). AH techniques are attractive because they are not dependent upon a reference defect standard for image reconstruction. If all other reconstruction parameters are held constant, it is possible to develop AH scaling factors that are only dependent upon acoustic wavelength and propagation path, rather than transducer characteristics. AH inspections are currently more expensive and difficult to perform than conventional NDE inspections. The existing available commercial equipment (1973) required physical modification before it could be used in the field.

As expected, the field tests showed that some defects were missed with AH techniques due to the physics of the interaction of the acoustic signal and the test specimen. Since no single NDE technique is theoretically infallible, a

combination of NDE techniques is needed in a practical field environment.

Some of the destructive tests were performed with arc-air techniques. While such techniques are well suited to field production uses, they tend to handicap a research program, because arc-air techniques are relatively crude. Where feasible, it would be preferable to use the destructive test techniques that allow more accurate results to be obtained.

A computer program is available to plot the information from the destructive analysis. While this program was only applied to the circle seam tests, it is applicable to any destructive test data set which has a sufficient data base. The computer plots indicate flaw sizes, position, and orientations both in relation to each other and to the material sample as a whole. The program title is FROGS, which is the acronym for Flaw Reconstruction and Orientation Graphics System. Once all necessary data has been supplied, the program can display multiple views of the sample, including angled isometric views. Figures 2-5 through 2-7 are examples of FROGS drawings for the Circle Seam studies, each labeled with the corresponding view. Along with each FROGS plot is the identical view redrawn with the defects labeled. The small scattered dots represent a slight porosity that was evident during the destructive test.

2.5 NON-PRODUCTION INSPECTIONS

2.5.1 Overview

The non-production inspections were part of the overall effort to extend the AH data base. Emphasis was on the AH data per se, rather than comparative data. The field crews did not control the experiments they were supporting and this led to the situation where the comparative data base was minimal or non-existent.

In the non-production inspections AH was used to monitor the position and size of artificially induced faults in the test specimens. The emphasis in these inspections was different for the three different tests as follows:

a. HSST: The experimenters wanted to know if the test procedure used to stress the test specimen resulted in the formation of cracks in the fault zone and what was the extent of any cracks (faults) generated by the stress procedure.

b. AEPV: Defects were intentionally induced in the test specimen by hydrotest prior to stress of the vessel. AH was used to define the characteristics of the faults before and after the hydrotest.

c. Clad weld test block: Primary interest was in the effect of cladding on the quality of AH imagery and the detection capability of the AH equipment (see Volume II of this series for a detailed discussion of cladding effects).

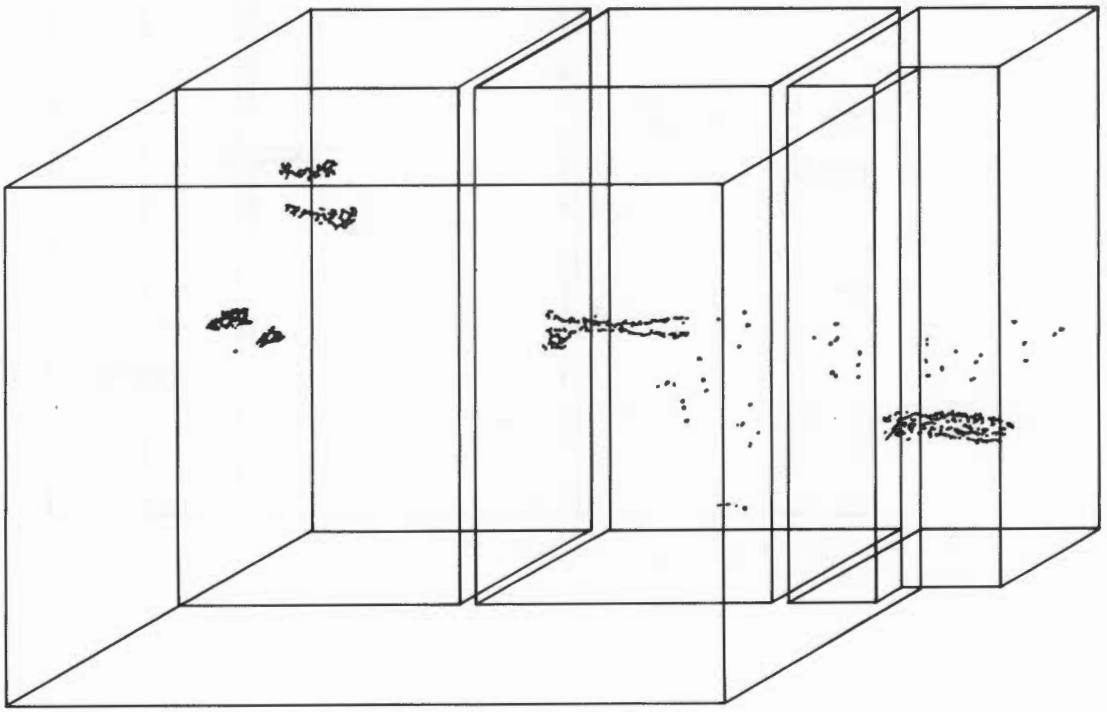

a) COMPUTER DRAWING

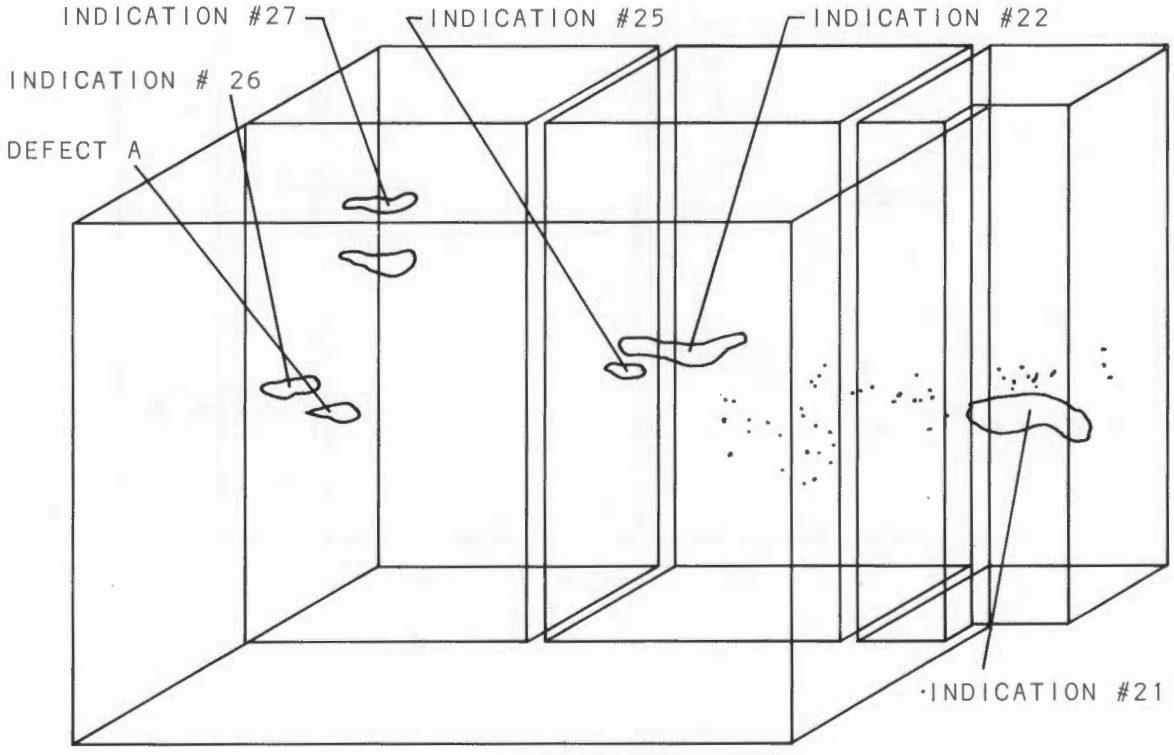

b) REDRAWN AND LABELED

Figure 2-5 FROGS Plot Showing Defect Positions From a 30° Isometric View

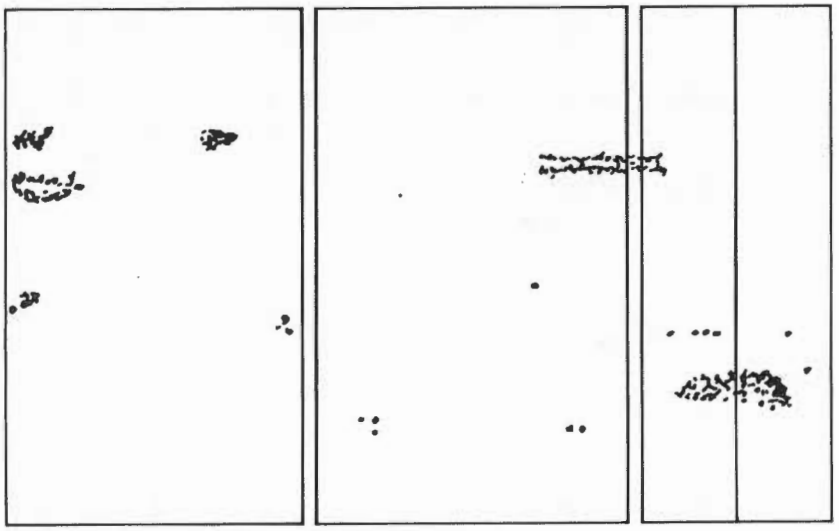

a) COMPUTER DRAWING

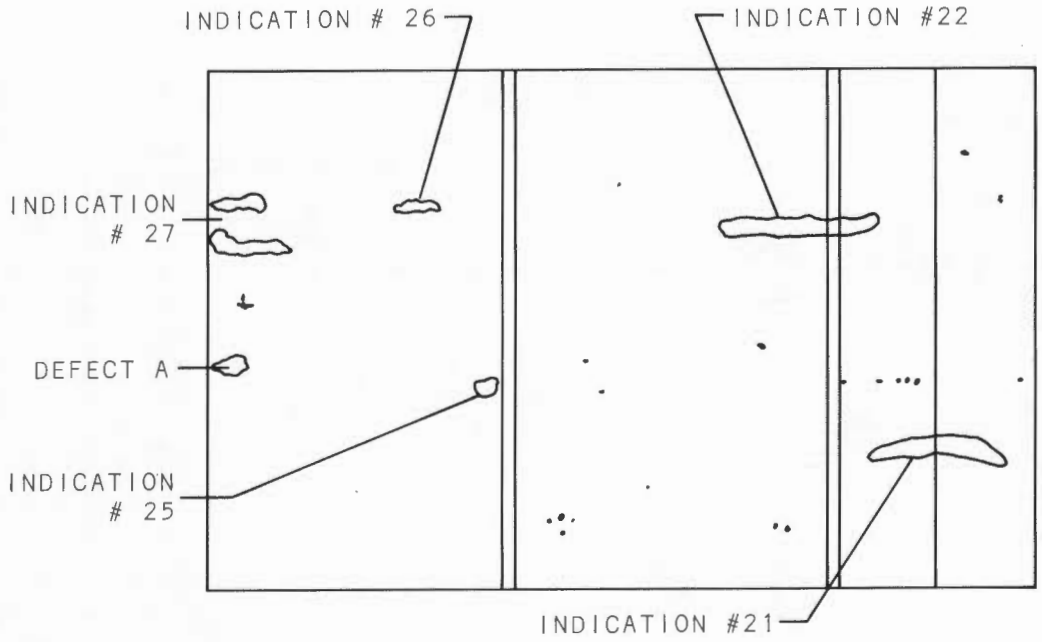

b) REDRAWN AND LABELED

Figure 2-6 FROGS Plot Showing Defect Positions From a Front View

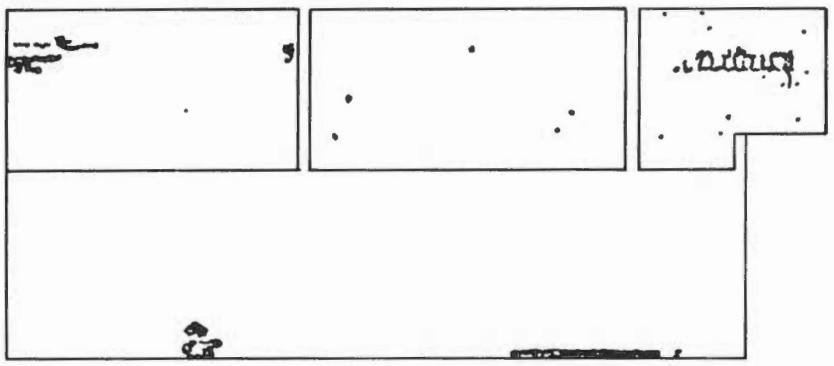

COMPUTER DRAWING

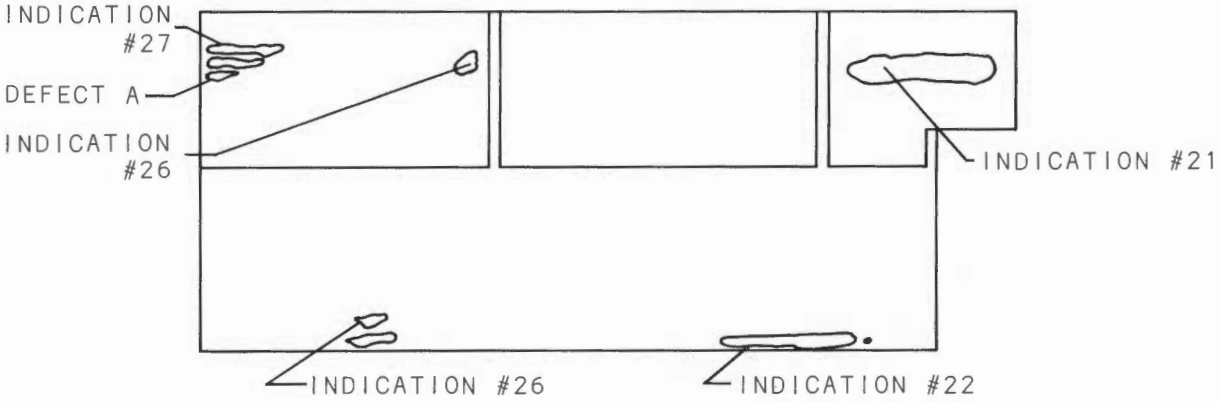

REDRAWN AND LABELED

(a) DEFECT POSITIONS FROM A TOP VIEW

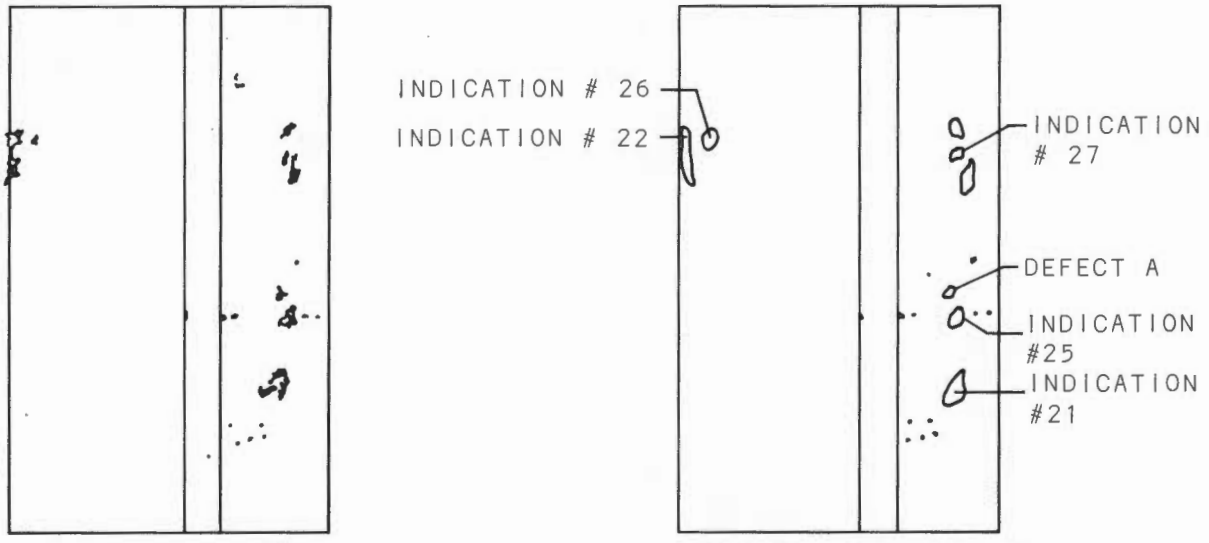

COMPUTER DRAWING

REDRAWN AND LABELED

(b) DEFECT POSITIONS FROM A SIDE VIEW

Figure 2-7 FROGS Plot

Section 3
SPECIFIC FIELD TEST RESULTS
PRODUCTION COMPONENTS

3.1 GENERAL

This section summarizes the field test results. The data includes results obtained with conventional NDE techniques, results obtained with AH techniques, and a comparison of these results with the results of destructive tests of the defects that were studied.

3.2 BASE METAL EXAMINATIONS

3.2.1 General

Radiographic inspection of a large, curved, thick, carbon structural steel plate indicated discontinuities (shrinkage voids) near and possibly in the weld zone of the seam being inspected. The location of these discontinuities is shown in Figure 3-1. Radiographic images indicated that there were a number of stringer -type discontinuities, some of which appeared to extend from the base metal to the weld zone. Five of these defects were selected for AH imaging based on the severity and/or location of the defects. The selected defects were Nos. 1, 2, 4, 5 and 8 (4 and 5 were treated as one area).

The base metal test expanded the data base relative to the size and type of natural flaws that can occur in thick base metal. The results to date indicate that a wide range of sizes and types can occur independently of the welding process.

Both fabrication and in-process detection of naturally occurring shrinkage voids in the base metal are desirable because post-fabrication or post-delivery repair is expensive. Detection and accurate characterization of defects in thick plate, using conventional NDE techniques, are not always successful. There have been cases where the condition was detected after a component was partially completed, rather than prior to fabrication operation. This is the

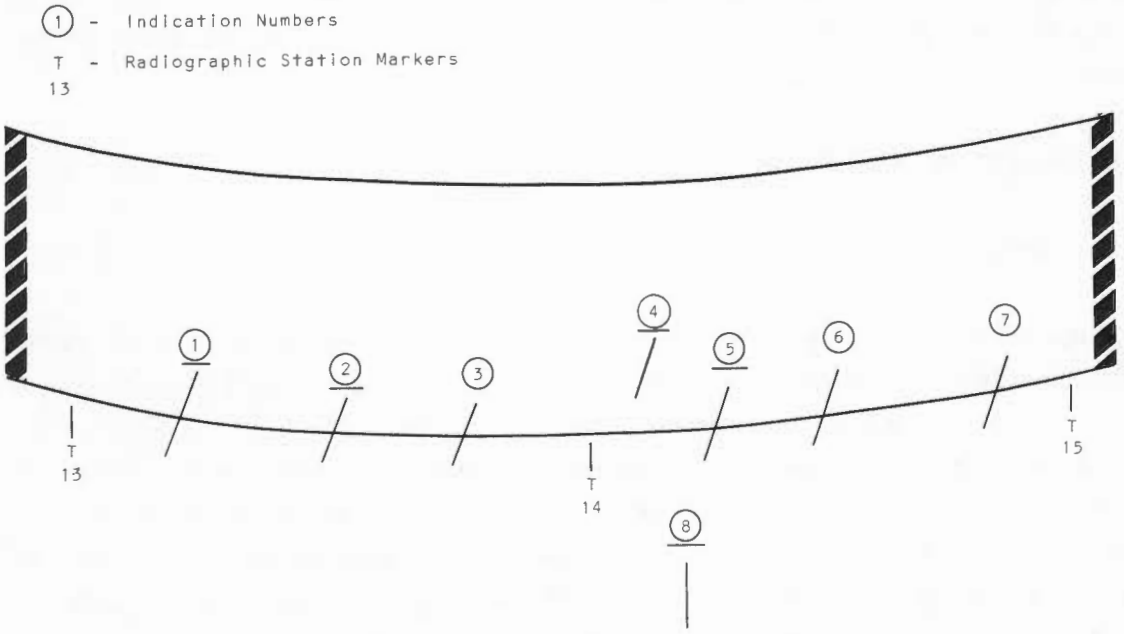

Figure 3-1 Sketch Showing the Location of Indications as Detected by Radiography

case for the studies discussed in this section. AH has been effective in detecting and characterizing discontinuities that were either missed using conventional NDE techniques, or that were difficult to characterize. One of the values of the AH images obtained during the RP 605 studies is the potential for development of improved inspection criteria for conventional inspections.

See Section 5.0 for a discussion of the AH equipment and test configurations.

3.2.2 Test Results

The radiographic results indicated extension of some of the defects into the weld zone. The AH results did not show any extension into the weld zone. Subsequent destructive tests verified the AH results. AH results also differed from radiographic results in that the AH images indicated many discontinuities, whereas the radiographic results showed one defect. Destructive tests showed that there were clusters of defects. The destructive tests also indicated that there was a large intense flaw which was masked by the defect clusters and did not show on the AH images. While such masking can be analytically predicted, the practical consequence is that such large flaws would always be masked in such situations, i.e., an alternative technique would be required to define the large flaw.

An incident beam angle of 45 degrees was used for the AH studies. The beam angle and approximate position of the defects in the AH images are shown in Figure 3-2. Typical results obtained with the AH equipment are presented in Figure 3-3.

Photographs of the results obtained during the destructive tests are presented in Figures 3-4 and 3-5. These photos provide cross sections of the flawed volume, located between 3 inches and 5 inches beneath the vessel surface.

The results obtained with the NDE and destructive tests for indication No. 8 are summarized in Table 3-1. Arc-air destructive tests of No. 8 indicated that there were two individual flaws in clusters of flaws which appeared to be continuous over a thru-wall depth range of 0.75". No discontinuities were detected in the weld zone. All imperfections were detected either in the base material or in the weld to base metal interface. There were clusters of

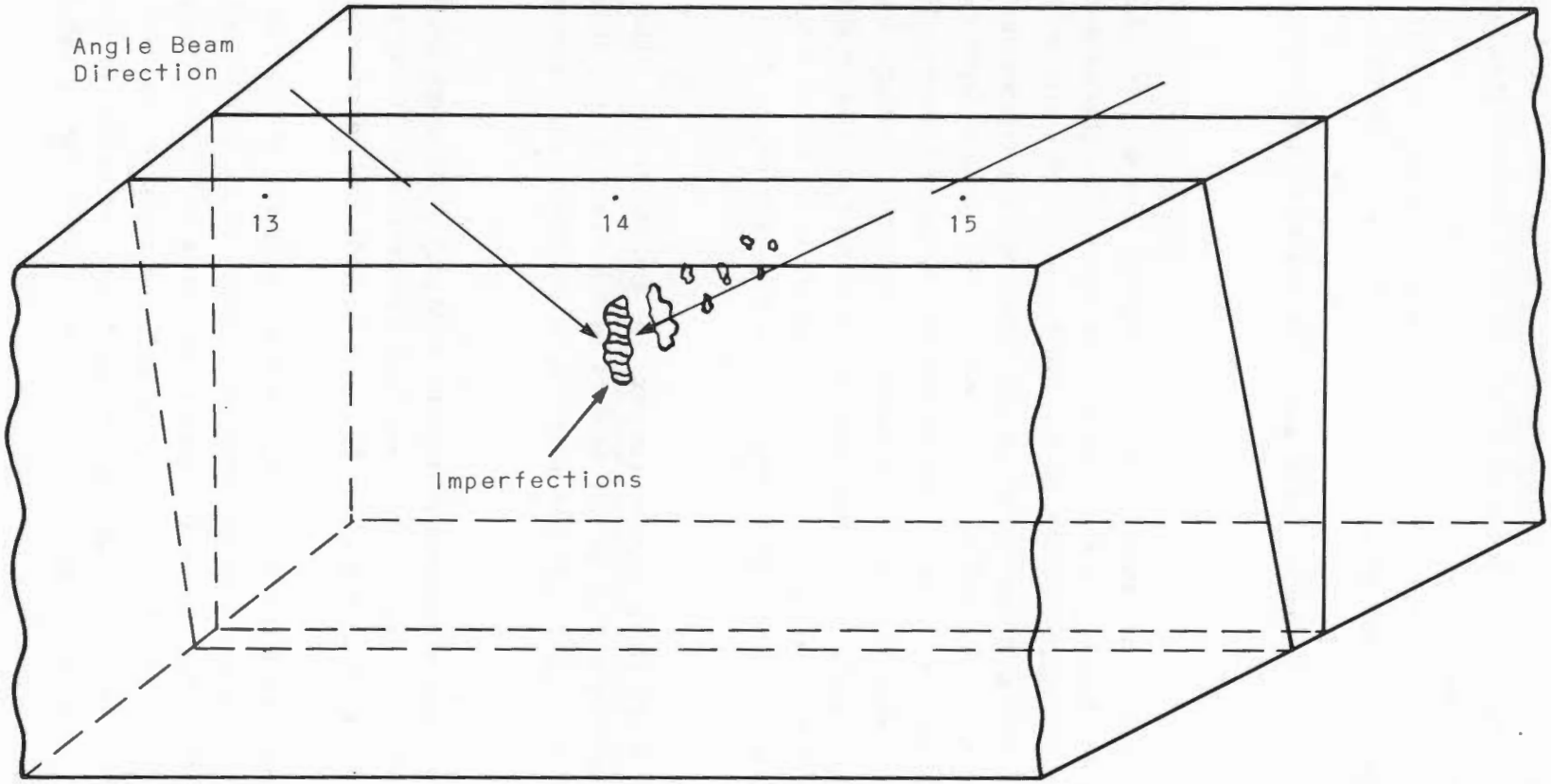

Figure 3-2 Sketch Showing the Angle Beam Directions Used in the Holographic Imaging and Approximate Defect Positions

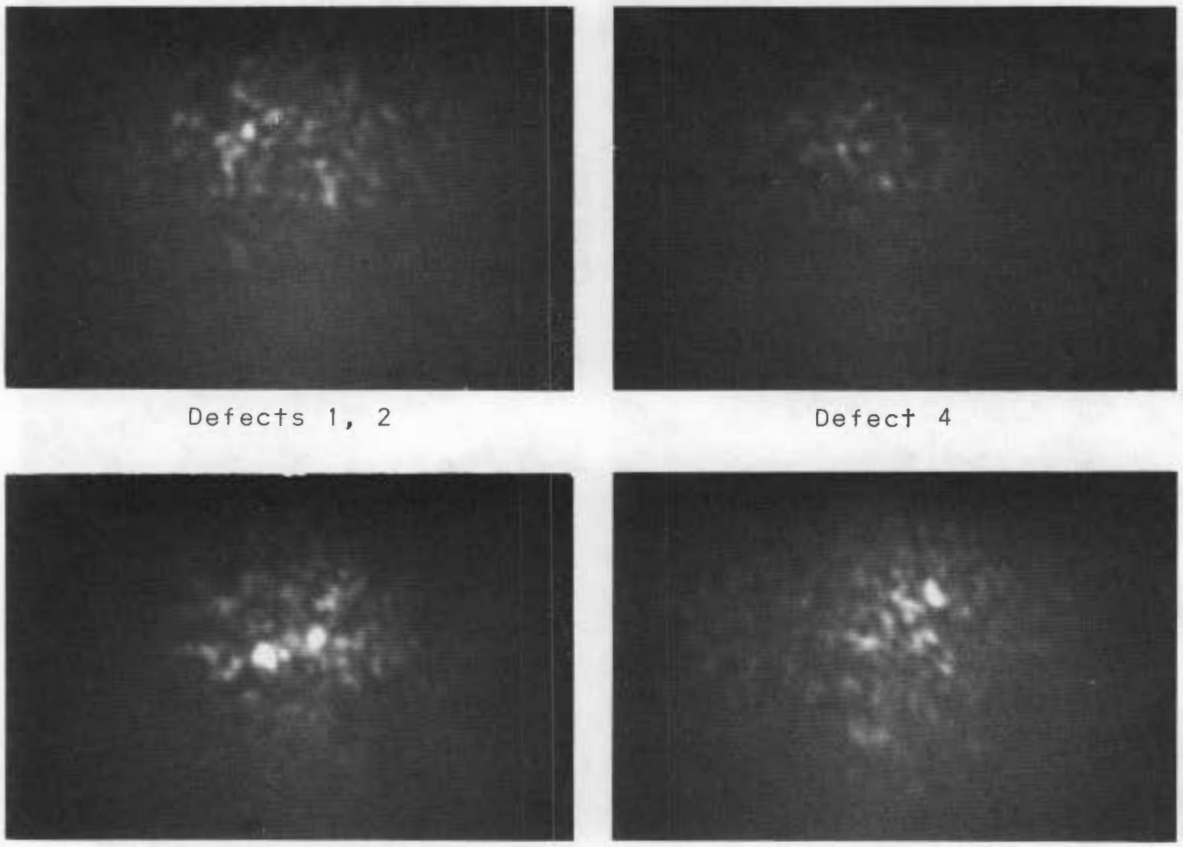

Defects 1, 2

Defect 4

Defect 5

Defect 8

Figure 3-3 Typical AH Images

(a) Cavity Depth 4"
Crack 1/16" x 3/4"

Area Immediately Above Crack
Has Numerous Pinholes

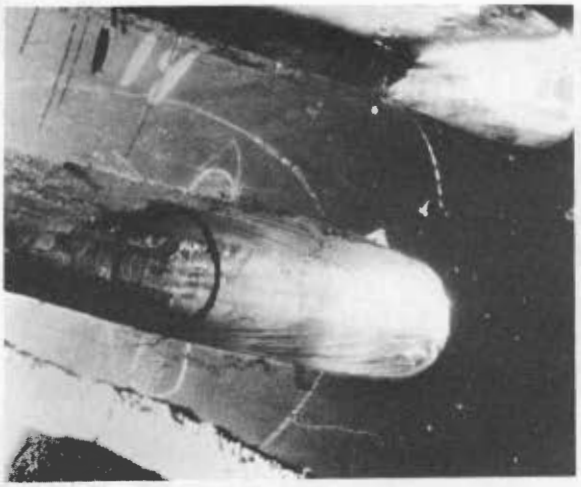

(b) Cavity Depth 4 1/4"
Two Voids
1/2" x 1/2" x 1/4"
1/2" x 3/4" x 1 1/2"

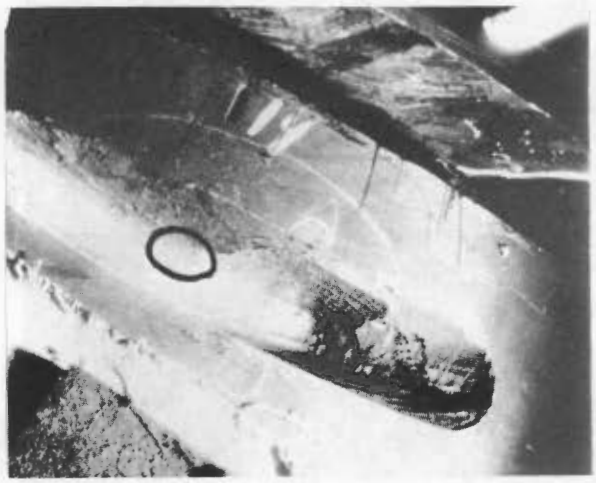

(c) Cavity Depth 4 1/2"
Pinholes and Cracks

(d) Cavity Depth 4 1/2"
New Area Detected

Figure 3-4 Base Metal DT Test Photos - Depth 4 to 4 1/2"

(a) Cavity Depth 5"
New Area Detected

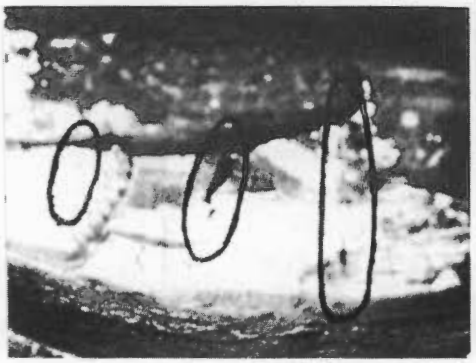

(b)

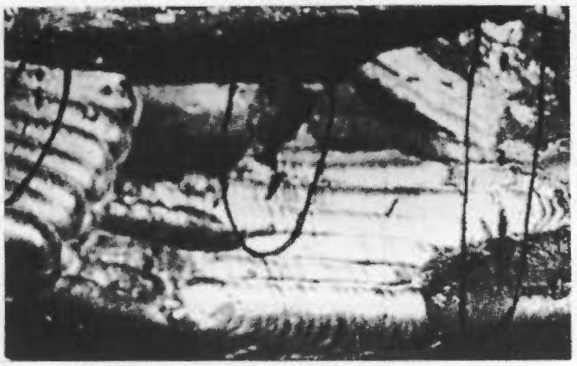

(c)

Cavity in (a) Widened

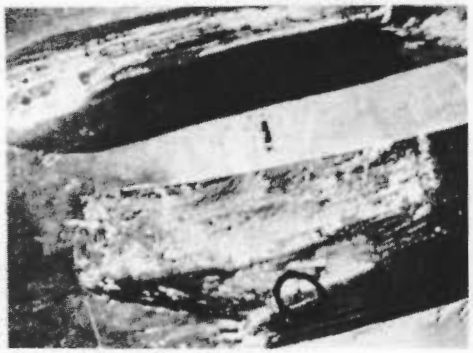

(d)

(e)

Another Void Revealed by Arc-Air

(f)

Appearance of Cavity
After Last Visible
Defect Removed.

Figure 3-5 Base Metal DT Tests Photos - Depth 5" to 5 5/8"

Table 3-1

DT RESULTS FOR INDICATION NO. 8 AND DT VS.
AH SIZE COMPARISON

Depth (inches)	Defect Observed	Defect Size (inches)
3.50	5 Pinholes 1 Crack 2 Pinholes	0.06 diameter 0.06 x 0.50 0.125 diameter
3.75	8 Pinholes	0.06 diameter
4.00	1 Crack 2 Pinholes	0.06 x 0.75 0.125 diameter
4.25	1 Void 1 Void	0.50 x 0.75 x 1.50 0.50 x 0.50 x 0.25
4.50	1 Void 3 Pinholes 1 Crack	0.50 x 0.75 x 1.50 0.125 diameter 0.125 x 3.00
4.75	1 Crack	0.06 x 1.00

COMPARISON OF DT AND AH RESULTS

Parameter	DT Result (inches)	AH Result (inches)
Total Thru Wall Extent	1.5	1.5 (approx)
Length	3.0 (approx)	2.5 (approx)

discontinuities in the areas where radiographic indications were noted. The AH results indicated clusters of discontinuities. There were two large defects oriented perpendicular to the component surface that gave the appearance of stringers standing on end. These large defects were masked in the AH image by the surrounding defect clusters. The clusters were detected and accurately characterized by the AH tests. The proximity and closeness of the individual defects warranted the removal of the discontinuities.

3.3 NOZZLE EXAMINATIONS

3.3.1 General

The AH tests described in this section were conducted over a period of 24 hours. This included the time needed for set-up, test implementation, analysis of the results and removal of the test set-up.

Radiographic inspection of the welds of the nozzles of a pressure vessel indicated defects in two different nozzles. The defects appeared to be transverse to the welds. Pulse-echo ultrasonic examinations were used (2.25 MHz 45^{o} and 60^{o} incident angle) to verify the initial radiographic results. The approximate locations of the defects are shown in Figure 3-6.

The AH tests involved installation of the equipment on vertical surfaces that were prepared for conventional UT inspections. A portion of the clad surface of the nozzle was ground. Refer to Volume II of this series for a discussion of the effects of cladding on the quality of AH imagery (more difficult with cladding). The test equipment and configuration used is discussed in Section 5 of this volume.

The AH tests were successful in accurately detecting and characterizing the defects. The tests were conducted in a field environment with an acceptable time span for implementation of the tests.

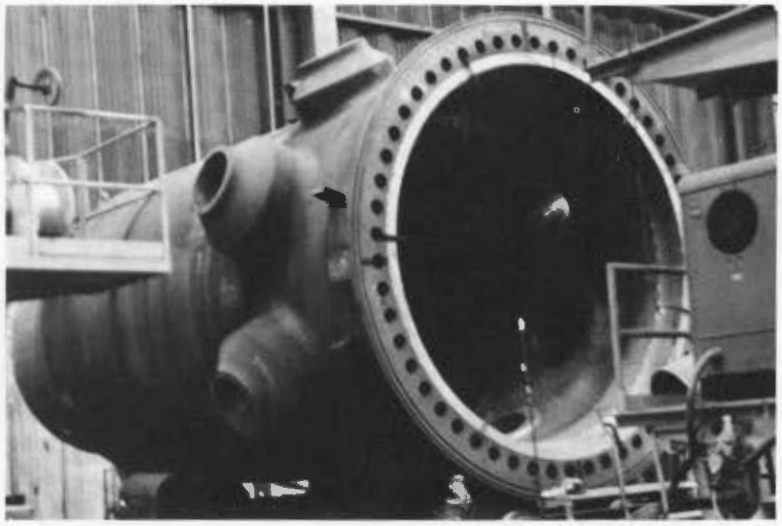

(a) Completed Pressure Vessel, Shown for Reference

(b) Approximate Location and Orientation of Defect in Nozzle

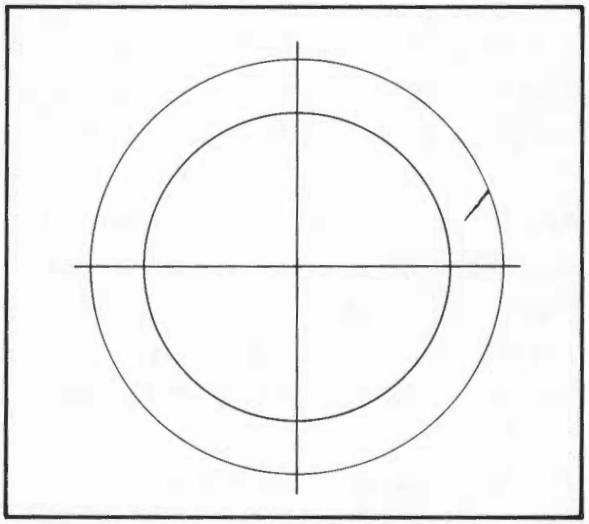

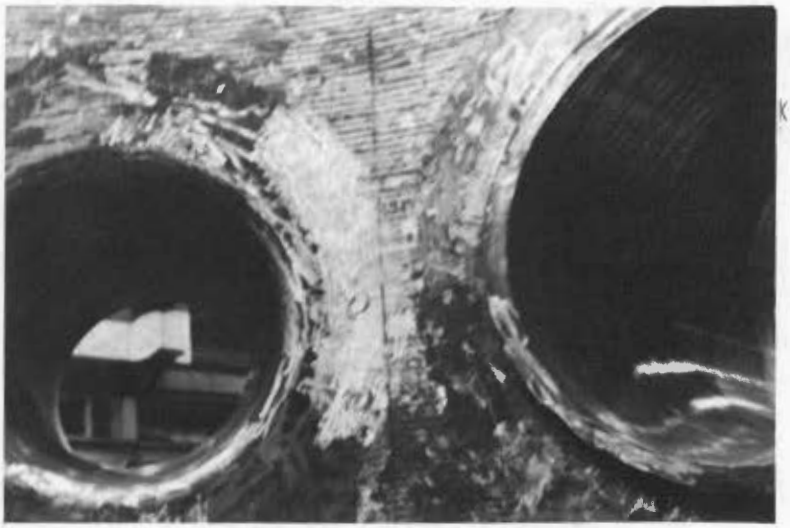

(c) Location of Defects and Area Where Cladding Had Been Ground

Figure 3-6 Approximate Location of Defects

3.3.2 Test Results

The test results are summarized in Table 3-2. The results of the conventional UT tests, which were conducted in accordance with standard ASME code procedures, are not available. Conventional UT tests were conducted from both the inside and outside surface. The inside surface tests produced the maximum signal amplitudes. (200% and 175% of DAC from one view direction for each defect).

Photographs of the AH images are presented in Figure 3-7. The images disclosed by the destructive tests are shown in Figure 3-8. Arc-air techniques were used for the destructive tests. The AH results were verified by the destructive tests.

3.4 CIRCLE SEAM INVESTIGATIONS

3.4.1 General

Ultrasonic examinations of a reactor vessel circle seam indicated the presence of flaws. The results obtained with standard UT shop practices were ambiguous with respect to acceptability of the flaws. Significantly different results were obtained at different ultrasonic frequencies using conventional UT. The location of the defects that were examined is shown in Figure 3-9A.

Acoustic Holography images of the subject defects were obtained on the specimen, prior to removal of the test section in a field environment, using 3 and 5 MHz transducers. The 5 MHz acoustic transducer was damaged during the tests, which limited the data obtained for some of the defects.

The section of the component that was of interest was removed after the initial AH images were obtained (Figure 3-9B). Radiographic images were made of the removed section. Additional tests using conventional UT equipment were made for both contact and immersion type examinations. The additional UT tests were still ambiguous although the immersion procedure did provide higher sensitivity than the contact procedure.

Table 3-2

SUMMARY OF TEST RESULTS
(Dimensions in Inches)

Defect No. 1				Defect No. 2		
Method	Length	Thru-wall Extent	Depth Below Surface	Length	Thru-wall Extent	Depth Below Surface
Radiographic	0.75	----	5.5	1.0	----	5.5
Destructive	2.0	0.56	5.5	2.2	0.8	5.5
AH	1.8	0.6	5.5	2.2	0.8	5.5

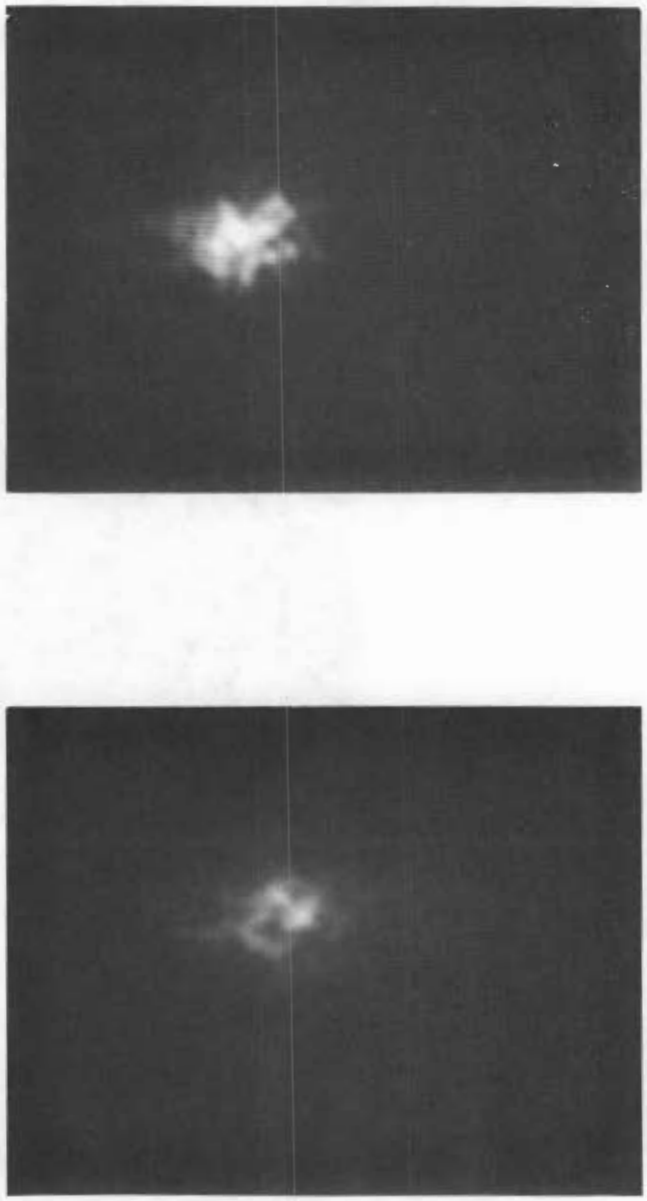

Figure 3-7 AH Images of Nozzle Defects

(a) 5 7/16: Depth

(b) 5 1/2" Depth

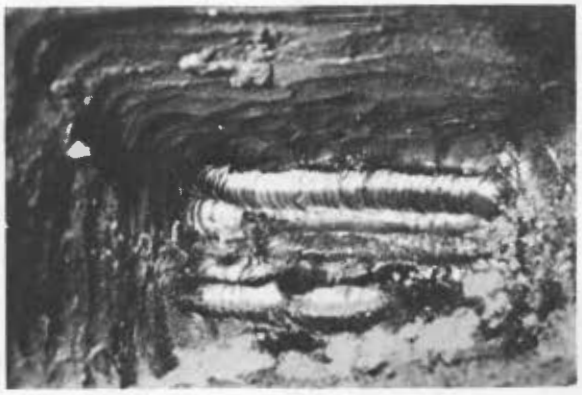

(c) 5 5/8" Depth

(d) 5 3/4" Depth

Figure 3-8 Destructive Test Results

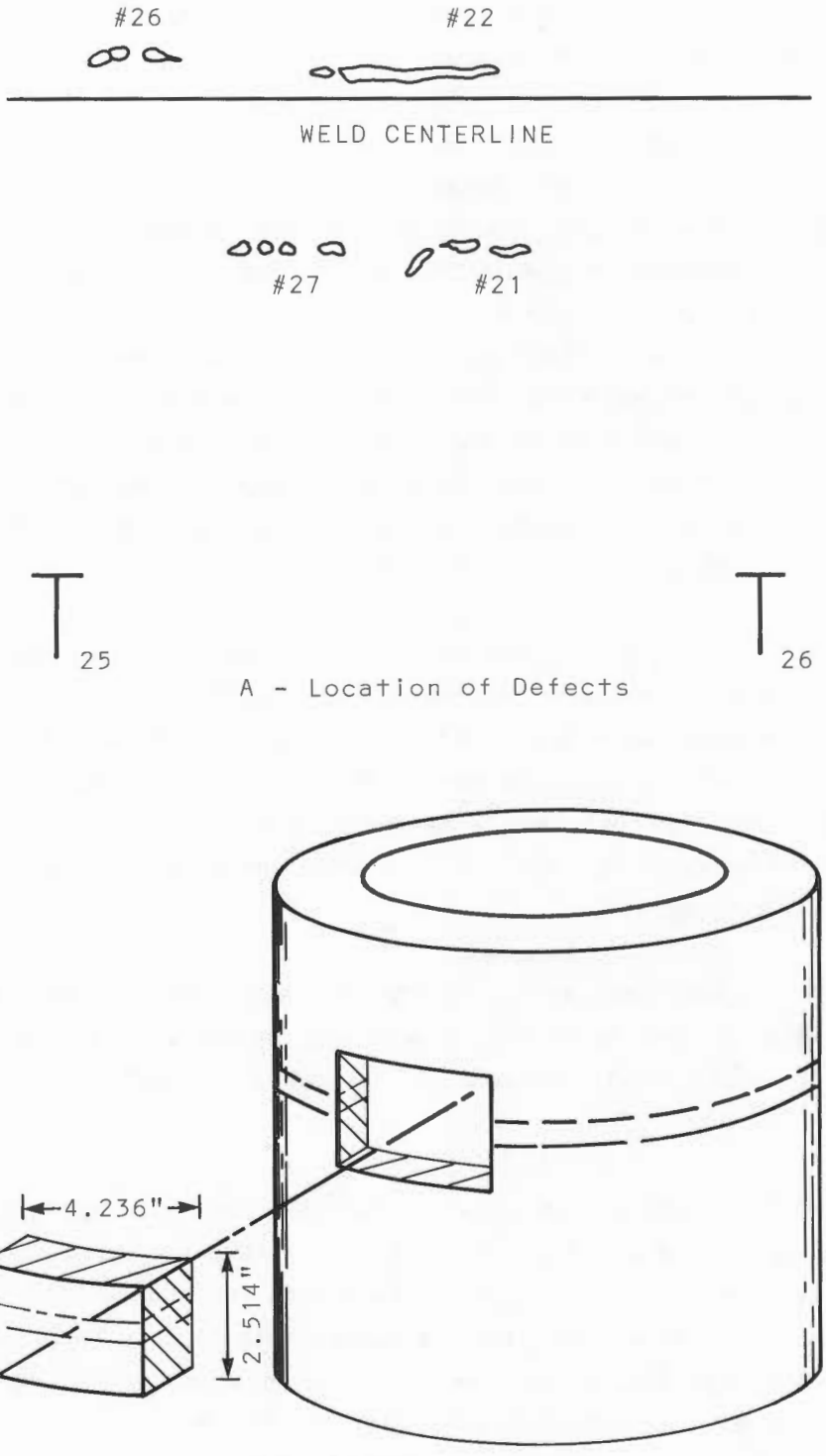

Figure 3-9 Circle Seam Test Sample Location

The results of the circle seam studies challenge the assumption that pulse-echo UT amplitudes depend only on defect area.

Defects Nos. 37 and 46 were imaged in the longitudinal mode at both 3 and 5 MHz. Defects Nos. 22 and 26 were imaged only at 3 MHz. Defect No. 25, which was not imaged at either frequency or by UT pulse-echo procedures, was detected by radiographic techniques. Subsequent to the NDE tests, the removed section was destructively tested to determine the physical location and size of the defects. A combination of cutting and milling techniques were used to locate the defects. Radiographs were made after each major cutting operation to guide the next step. Final exposure of the defects was obtained with a surface grinder set for 0.001" cuts per pass. An optical comparator was set to measure the size of the defects. The destructive tests disclosed a defect (25A) which had not been detected by any of the NDE tests.

The conventional UT and radiographic tests were conducted in accordance with standard shop practices and were calibrated with drilled holes. The UT tests were conducted at both 2.25 MHz and 5MHz. The liquid couplant was Hamikleer and the UT instrument was a Krautkramer USIP-11. Three distinct positions on the weld were found to contain one or more questionable UT indications. Positions were referenced from the initial radiographic weldment markings and given numerical designations.

Table 3-3 lists the UT responses for defects #21, #22, #26, #37, and #46 using particular transducers and inspection frequencies, relative to the established DAC. No data from the in-situ contact UT inspection is available for defects #25 and #27.

A broad range of UT responses was obtained for identical flaws using different search units, and there was a problem in data interpretation. All the UT responses were valid because all were obtained in accordance with standard procedures. It is possible, therefore, to report some flaws detected by UT as acceptable (or rejectable) by simply interchanging transducers. The discrepancies do not indicate problems with the inspection or calibration procedures used. They do indicate the inadequacies of the pulse-echo method as presently used for defect characterization. In particular, the assumption that amplitude depends only upon defect area is not rigorously valid.

Table 3-3

COMPARISON OF IN-SITU CONTACT UT EXAMINATION DATA

Probe Type	Diameter (inches)	Frequency (MHz)		Defect Response (Per Cent DAC)		
		Mfg. Value	Actual	No.21	No.22	No.26
Panametrics	0.75	2.25	1.8	75	70	25
Krautkramer	1.00	2.00	2.0	70	100	--
Krautkramer	1.00	4.00	3.0	26	25	--
Panametrics	0.75	5.00	3.5	15	10	8
Sperry	0.75	5.00	3.5	17	12	--

Table 3-4

COMPARISON OF IMMERSION UT RESPONSES

Probe Number	Diameter (inches)	Frequency (MHz)		Defect Response (Per Cent DAC)			
		Mfg. Value	Actual	No.21	No.22	No.25	No.26
Z-103	0.75	2.25	3.0	40	70	85	None
SIZ-57A3619	0.375	5.00	5.0	50	23	62	None

Additional contact and immersion UT examinations were performed on the section containing the discontinuities. The contact UT tests did not show any significant improvement over the in-situ tests. Immersion UT was accomplished by using two different transducers and the results are shown in Table 3-4. The responses are relative to a 1/8" calibration standard with DAC. No signal could be detected for indication #26. While immersion technique had higher sensitivity than the contact technique, the response variation still led to ambiguous interpretation of the defect sizes.

AH images were obtained at 3 and 5 MHz. The AH images obtained at 3 MHz are shown in Figure 3-10. A comparison of the AH images obtained at 3 and 5 MHz is shown in Figure 3-11. Note that there is essentially no difference in the two images, other than magnification due to frequency.

The test results are summarized in Table 3-5. As shown in Table 3-5, the AH characterization results were validated by the destructive test results. Defect No. 25 was not detected by UT or AH procedures, yet was detected by radiographic techniques. Defect No. 26 was not detected by either pulse-echo UT or radiographic techniques, yet was detected by AH techniques.

Defect No. 25, which did not show the same granular, open structure typical of the other defects, appears to be a solid inclusion of uniform density throughout most of the surface grinding (possibly an electrode tip left in the material). Details on the AH equipment and test configuration are presented in section 5.0.

Destructive test photos of Defects Nos. 21, 22, 25, 27 and "A" are presented in Appendix A.

3.5 LONG SEAM WELD INSPECTION

3.5.1 General

Conventional UT indications of potential defects in a section of a long seam weldment were observed during a routine examination. The ultrasonic inspection data indicated that the discontinuities were oriented in the weld such that the normal to the major reflecting surfaces was parallel to the weld axis. It appeared that the plane containing these cracks was parallel to the longitudinal cross section of the weld (normal to the surface).

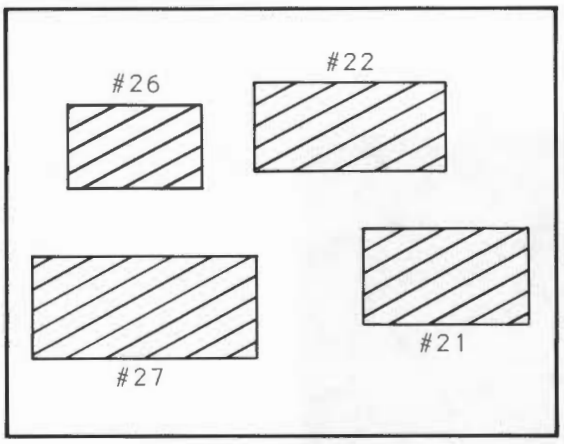

(a)

Sketch of AH Images Obtained with 0° Longitudinal 3MHz Beam.

Photos (b,c,d,e) Obtained at 3MHz

(b) Defect #21

(c) Defect #22

(d) Defect #26

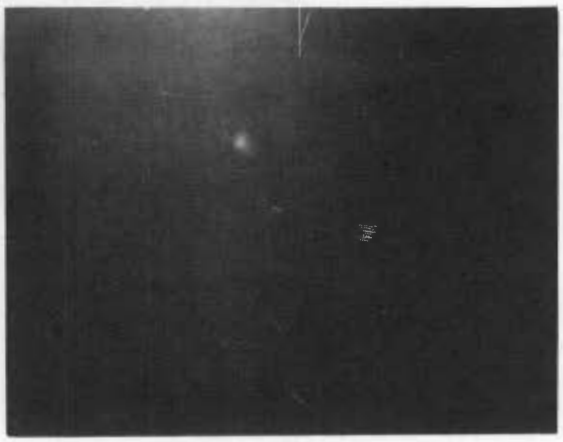

(e) Defect #27

Figure 3-10 AH 3MHz Images - Circle Seam Defects

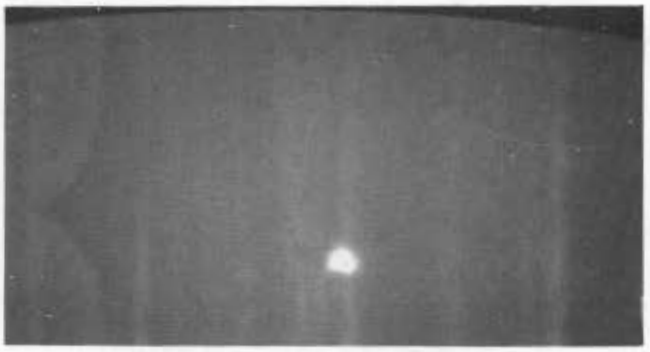

(a) 3MHz AH Image

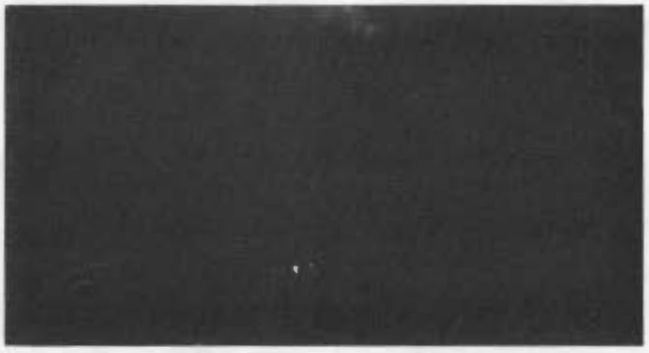

(b) 5MHz AH Image

Figure 3-11 Comparison of 3MHz and 5MHz Images, Defect #37

Table 3-5

DEFECT SIZES AS DETERMINED BY UT, X-RAY, AH, AND DT
(Dimensions in Inches)

Number	UT Length	X-RAY Length	AH (3 MHz)		DT		Depth Below Surface
			Length	Width	Length (Max)	Width (Max)	
21	0.438	0.625	0.45	0.20	0.40*	0.10*	2.875
22	0.188	0.5625	0.80	0.08	0.76	0.088	3.625
25	None	0.156 (Circle)	None	None	0.055	0.03	2.875
26	None	None	Note 1	0.089	Note 2	0.073	3.625
27	0.1875	0.312	0.24	0.144	0.25	0.179	2.875

* Flaw exposed, maximum length exposed and width dimension obtained

Note 1: Two images, 0.14 and 0.19 separated by 0.25 = Total 0.44
Note 2: Two flaws, 0.125 and 0.3 separated by 0.075 = Total 0.50

The ultrasonic tests were conducted using a 60^{o} shear wave, at frequencies of 2.25 MHz and 5 MHz. The locations at which UT were obtained are shown in Figure 3-12, which is a plan view of the weld. The orientation of both the weld and the defects are shown in Figure 3-12A. The scales of Figure 3-12A provide a direct measure of the orientation and position of each defect. The discontinuities designated C, D, E, and F were detected with shear waves directed parallel to the weld centerline plane. Indications AA and BB were thought to be isolated discontinuities of the same type as those indicated by single letters. All of these indications were on one side of the weld. The indications designated XX and YY were on the opposite side of the weld. These discontinuities had different orientations than those listed previously.

Indications C through F, AA and BB were all located between 1.5 and 3 inches from the outer surface of the weld as shown in Figure 3-12B.

Additional conventional UT examinations were performed using 60^{o} and 45^{o} shear wave examinations at 2.25 MHz and 5 MHz. These examinations were conducted using higher sensitivity equipment than was used during the original UT which detected the cracks.

During the conventional UT and AH examinations, ultrasonic energy was directed along the weld axis as shown in Figure 3-13. Note that Figure 3-13 is rotated 90^{o} from the orientation shown in Figure 3-12.

Areas designated C, D, E, and F on Figure 3-12A contained clusters of discontinuities of the type of interest. Indications in areas AA and BB appeared to be isolated discontinuities of the same type as in areas C through F. Conventional UT indicated that the defects in areas XX and YY were of a different type and of different orientation.

Acoustical holograms were obtained for each of these areas with the axis of the diverging conical sound beam oriented toward the weld, using the same designations established for the different directions used with conventional UT (Figure 3-13). Table 3-6 summarizes the AH images that were obtained. The discontinuities in areas C, D, E, F, AA, and BB were oriented so that maximum signal amplitude was obtained from shear waves propagating parallel to the weld. Reconstructed AH images were obtained using scan directions 1, 2, 5, and 6 (Figure 3-14A). The image plane for holograms of areas XX and YY is shown by the dotted line in Figure 3-14B. Holograms of reflectors in areas XX and YY

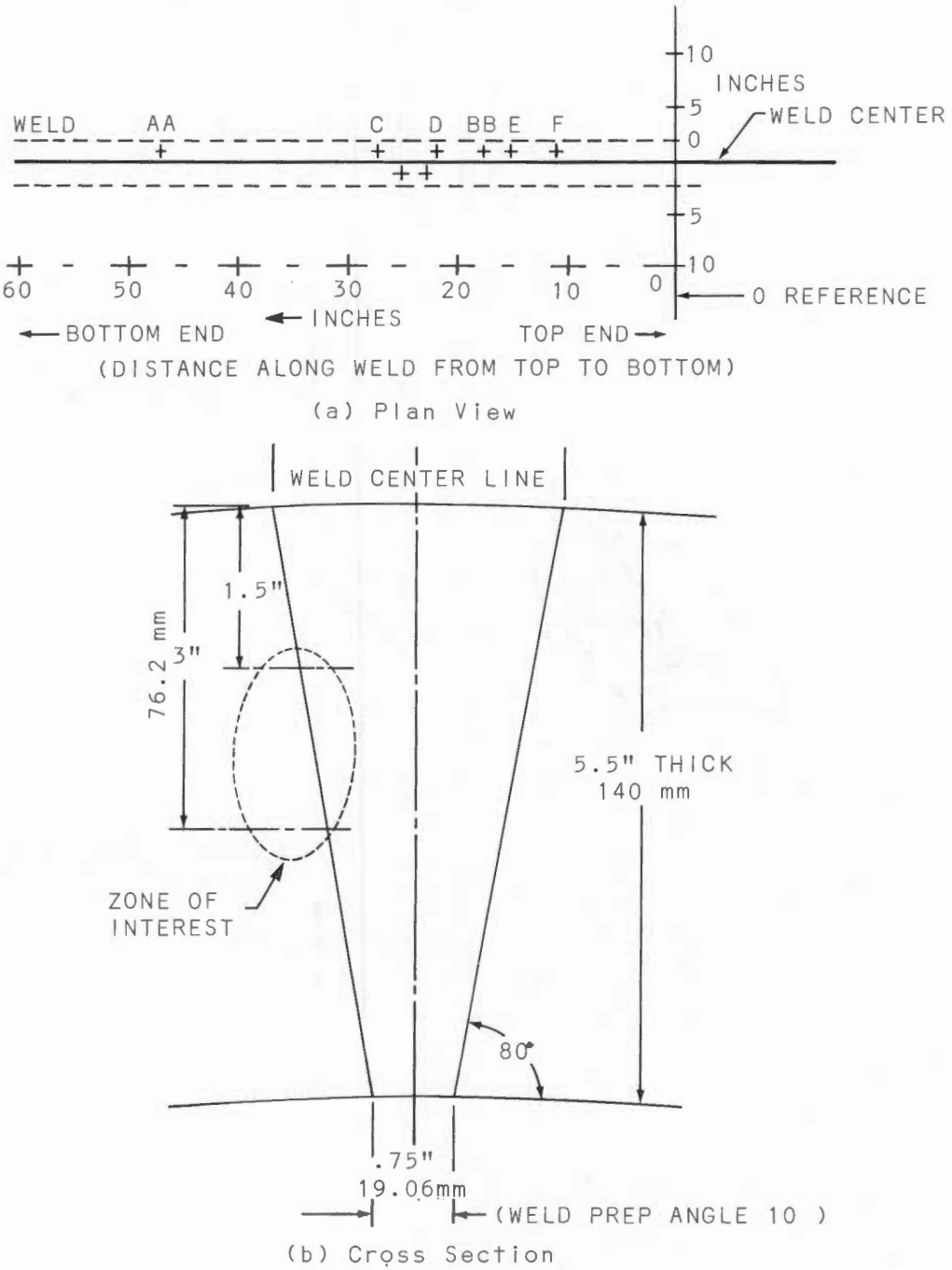

Figure 3-12 Location of Defects

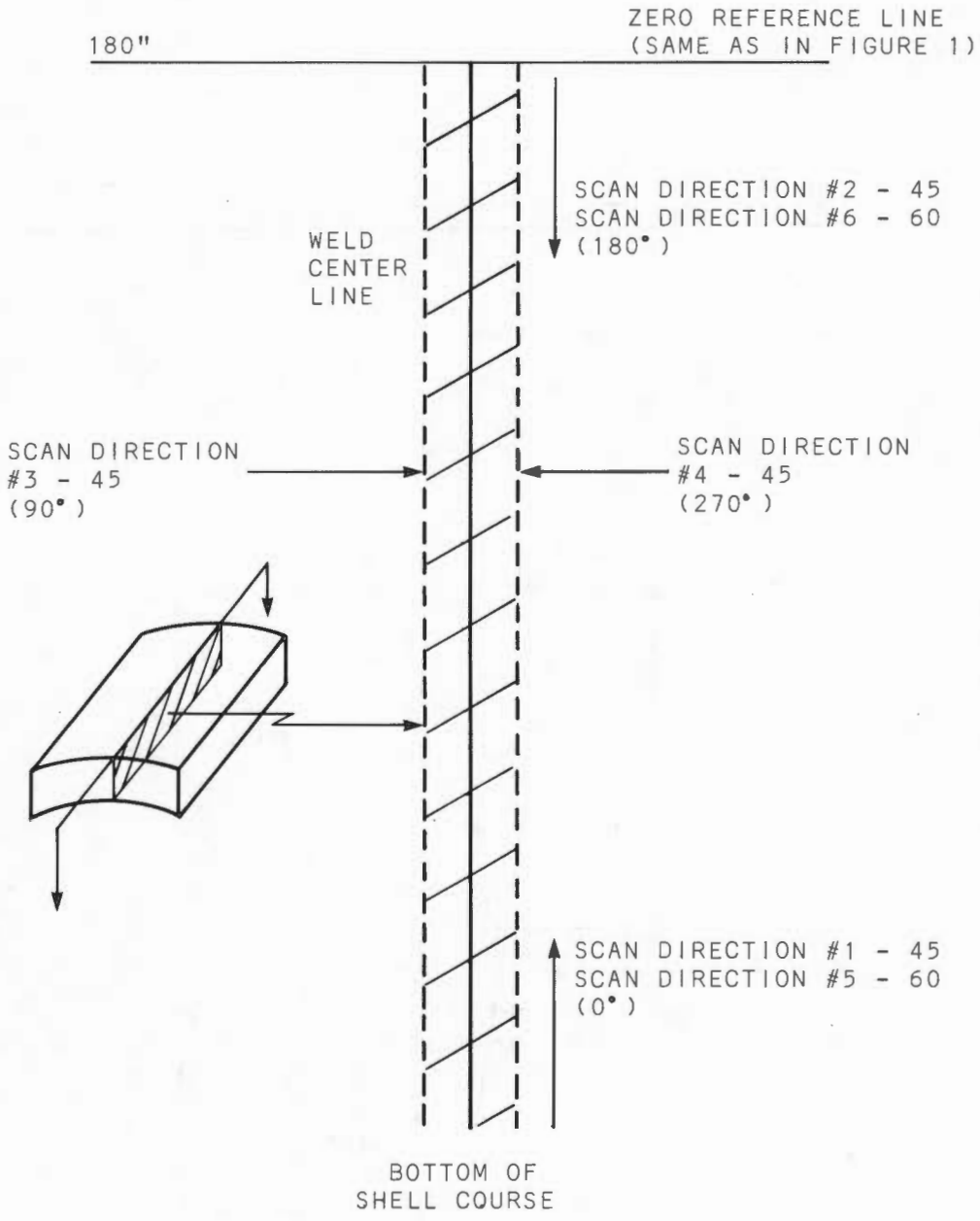

Figure 3-13 Sketch Showing the Four Primary Scan Directions Used for Both Conventional Ultrasonic Tests and for the AH Examination

Table 3-6

LIST OF HOLOGRAPHIC IMAGES
FOR EACH LONG SEAM AREA EXAMINED

Defect	Frequency		Refracted Angle (deg) and Direction						Hologram No.
			(40)	(60)	(45)	(45)	(60)	(45)	
	3MHz	5MHz	1	5	3	2	6	4	
C	X			X					C-5A
		X					X		C-2
	X				X				C-6A
		X	X						C-1A
D		X	X						D-1
	X			X					D-5A
	X						X		D-6A
E		X				X			E-2A
	X		X						E-5A
	X						X		E-6A
	X							X	E-4A
F		X	X						F-1
		X					X		F-2B
	X						X		F-6A
	X					X			F-2H
XX	X							X	XX-4A
	X			X					XX-3A
YY	X							X	YY-4A
	X			X					YY-3A
BB		X				X			BB-2B
AA	This indication determined to be different type (by U. T.) from primary type indication to be imaged. This indication reflected deviation energy from 90^{o} and 27^{o} scan direction as well as for 0^{o} and 180^{o}.								

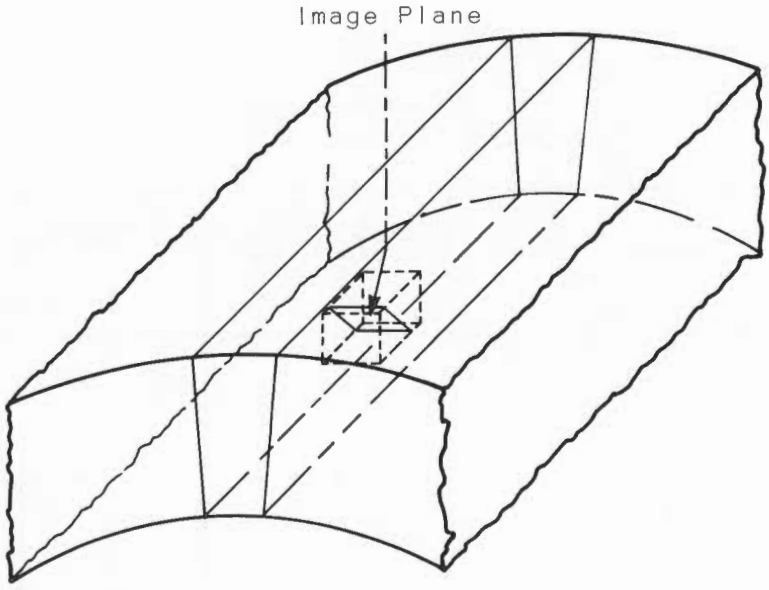

(a)- Scan Directions 1, 2, 5, and 6.

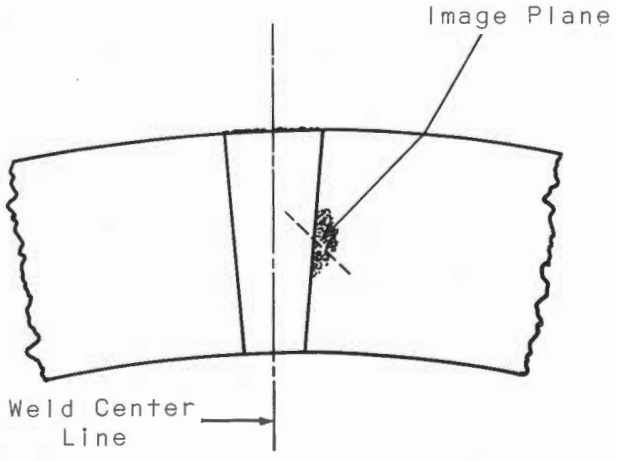

(b)- Scan Directions 3 and 4

Figure 3-14 Orientation of Image Planes

were obtained in directions 3 and 4. Holograms of XX and YY were taken in other directions (the ultrasound propagating along the weld), but the apparent defect orientation was unfavorable for these directions.

Holograms were attempted from all directions at each area indicated in Figure 3-13. With the exception of area AA, which appeared to be an omnidirectional reflector, the discontinuities were oriented such that usable holograms were obtained with the ultrasonic energy directed either along the weld or transverse to the weld, but not in both directions. The discontinuities in areas XX and YY did provide some reflected signals when the ultrasonic energy was directed along the weld. However, much larger signals were obtained with the ultrasonic energy propagating in a transverse direction.

Destructive tests (DT) of core plugs from areas D, E, and F were conducted that did not quantify the transverse dimension of the defect (see Figure 3-15). Additional DT results are incorporated in Appendix B. DT was performed at a site and by personnel that were not under the control of the RP-605 team. The transverse orientation of the defect was verified and the thru-wall extent measured.

The results obtained with AH are summarized in Table 3-7. AH images of some of the defects are shown in Figure 3-16, 3-17 and 3-18. Additional results are incorporated in Appendix B which includes:

Destructive Test Photos in Appendix B

Photo		Magnification
B-1	Crack in D	X10
B-2	Crack in D	X100
B-3	Crack in E	X6
B-4	2nd Crack in E	X25
B-5	Largest Crack in E	X25
B-6	Third Crack in E	X100
B-7	Aluminum in Crack E	X100
B-8	Crack in F	X10
B-9	Crack in F	X1000

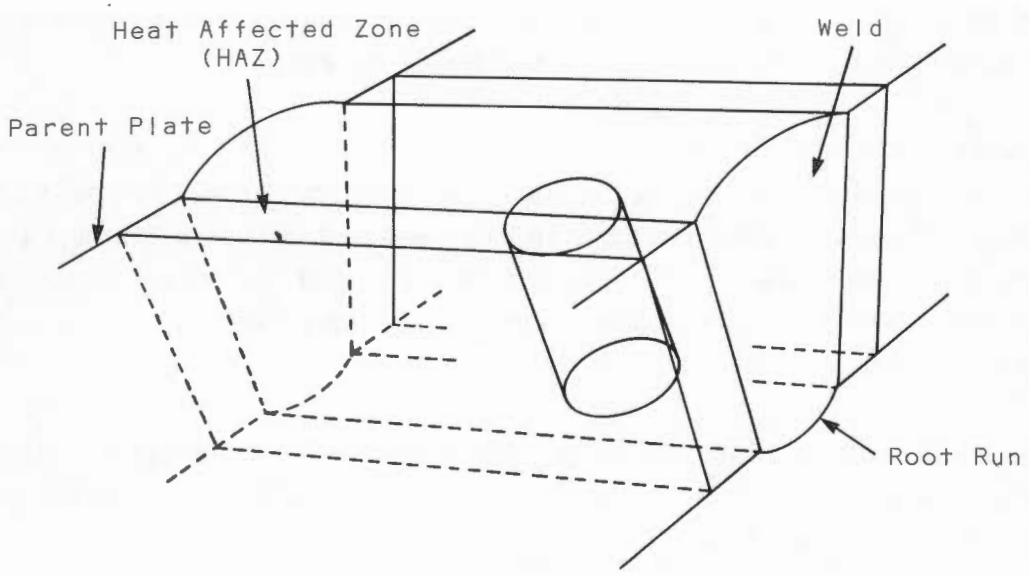

Figure 3-15 Position and Orientation of Core Plug Sample

Table 3-7

SUMMARY OF LONG SEAM AH RESULTS

Defect No.	Direction	Dimension in Inches						
		Depth			Transverse Length			Thru-Wall Extent
		3 MHz		5MHz	3MHz		5MHz	3 MHz
		(A)	(B)	(A)	(A)	(B)	(A)	(B)
BB	2B			1.8			0.12	
C	1A			1.8			0.04	
	6A		1.8			0.04 TO 0.24		
	2						0.10 TO 0.36	
	5A		1.9			0.12 TO 0.32		0.25
D	6A		1.8 TO 2.0			0.20		0.20
	5A		1.8			0.10 TO 0.21		
	1			2.0			0.06 TO 0.20	
E	4A	2.3			0.21*			
	6A		1.8 TO 2.0			0.09 TO 0.18		0.15
	5A		2.0 TO 2.4			0.08 TO 0.24		
	2A			2.2			0.32	
F	1			2.0			0.15	
	2B			1.8			0.15	
	2H	1.9		0.05 TO 0.3				0.15
	6A			1.8 TO 2.4		0.04 TO 0.23		
XX	4A (1.5 EXT.)	3.0			LONG 0.10 TO 0.16			
	3A (0.75 EXT.)	2.7			LONG 0.10 TO 0.25			
YY	3A	2.8			LONG 0.22			
	4A (1.6 EXT.)	2.8			LONG 0.10 0.19			

A - 45 Degrees Shear Angle B - 60 degrees Shear Angle
LONG - Defect Longitudinal to Weld * Longitudinal to Weld
EXT - Distance Between Extremes

Direction 1, 5MHz,
45° Shear Angle

Direction 5, 3MHz,
60° Shear Angle

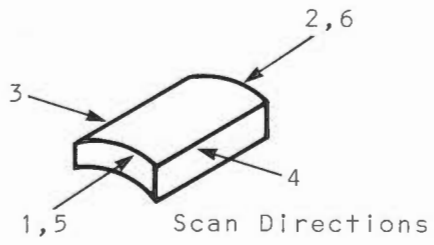

Direction 6, 3MHz,
60° Shear Angle

Figure 3-16 AH Images of Defect "D"

Direction 2, 5MHz, 45°

Direction 5, 3MHz, 60°

Direction 4, 3MHz, 45°

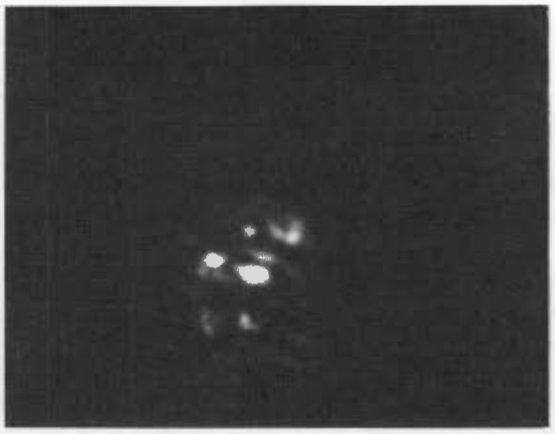

Direction 6, 3MHz, 60°

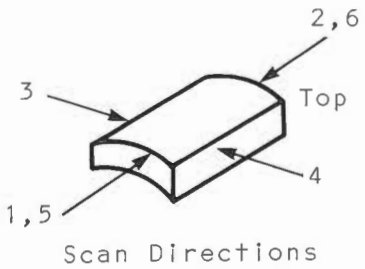

Scan Directions

Figure 3-17 AH Images of Defect E

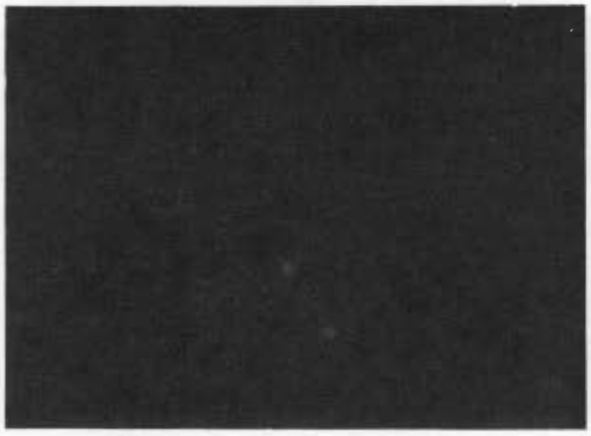

Direction 1, 5MHz, 45°

Direction 2, 5 MHz, 45°

Direction 2, 3MHz, 45°

Direction 6, 13MHz, 60°

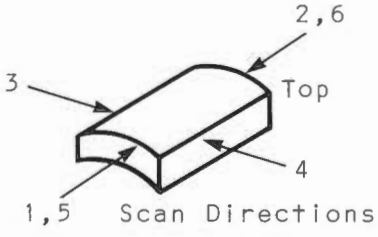

Figure 3-18 AH Images of Defect "F"

The destructive tests indicated:

a. In area D a crack was found to be present in the plate material immediately adjacent to the heat affected zone (HAZ), at a depth of 1.89" (48 mm) below the weld surface (see Appendix B, Figures B-1 and B-2). Closer examination of the crack showed it to be intergranular and further grinding showed the defect to be 0.07" (1.8 mm) in the thru-wall dimension parallel to the weld. The transverse nature of the crack was verified, but the dimension was not recorded.

b. In area E, a macro-section (see Appendix B, Figure B-3) showed two cracks to be present. The larger crack was at a depth of 1.96" (50 mm), with a thru-wall dimension of 0.43" (11 mm). The other crack, which had a thru-wall of 0.08" (2 mm), was near the bottom of the plug at a depth of 2.4" (61 mm). In both of these cases, the cracks were oriented transverse to the weld, similar to the crack in area D. Appendix B, Figures B-4 and B-5, shows that these cracks were also intergranular in nature.

c. An additional crack was found in area E at a depth of 1.77" (45 mm). This crack was oriented in a horizontal plane, i.e., in a plane at right angles to the other cracks in this area. The dimensions of this crack were 0.04" X 0.004" (1 mm X 0.1 mm) (see Appendix B, Figures B-6 and B-7).

d. In area F the crack found was also transversely oriented relative to the weld axis. The defect was at a depth of 1.81" (46 mm) (see Appendix B, Figure B-8). It was not possible to accurately measure the thru-wall extent of this crack since it had been partly removed by machining. Appendix B, Figure B-9 also showed this crack to be intergranular in nature.

The destructive results, while not being comprehensive, did verify that the cracks were in the plate material adjacent to the HAZ, and that they were oriented transverse to the weld axis with a single exception. Also the range of depths and dimensions obtained was comparable to the AH results, so that the AH results were verified relative to the main features of the defects.

Section 4
SPECIFIC TEST RESULTS-NON PRODUCTION COMPONENTS

4.1 GENERAL

This section summarizes the field test results on the non-production components in which the "field" involved different locations in both the United States and France.

4.2 SUPPORT OF HSST THERMAL SHOCK TESTS

4.2.1 General

These tests involved two test vessels of the Heavy Section Steel Technology (HSST) program with induced fault zones (see Figure 4-1). Electron beam welding was used to generate the fault zone on the interior surface of the test specimen. One specimen (HSST 1) was notched prior to welding (see Figure 4-1). The purpose of the HSST tests was to simulate a Loss of Coolant Accident with the attendant emergency core coolant dump following the coolant loss. AH was used to establish the pre-shock baseline and to inspect the specimen after exposure to thermal shock.

A set of overlapping scans was used to inspect the test specimens (see Figure 4-2 for the baseline scan patterns). The pattern for HSST 1 was limited for the baseline scan and then modified for subsequent tests (see Figure 4-3 for the post-test scan patterns). All HSST holographic inspections were obtained using 45 degree shear waves, with the scanner offset to the left or right of the normal to the Electron Beam (EB) weld (see Figure 4-4).

The test specimens were equipped with strain gages. HSST No. 1 was shocked once before the baseline hologram for this specimen was generated. The strain gages did not indicate that any cracks had developed during the first shock test. The baseline AH images for HSST No. 2 were obtained prior to any shock testing of this specimen.

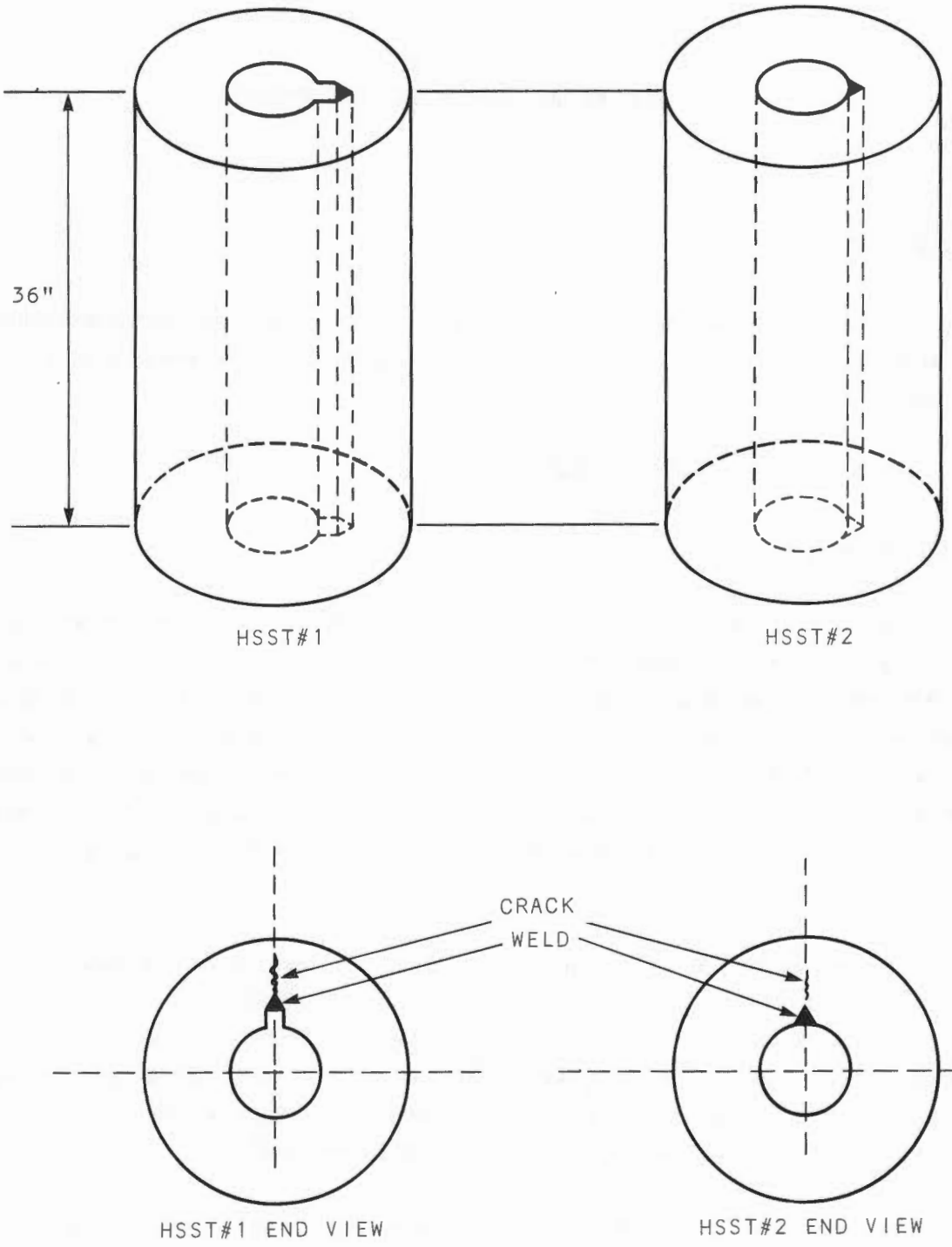

Figure 4-1 HSST Specimens

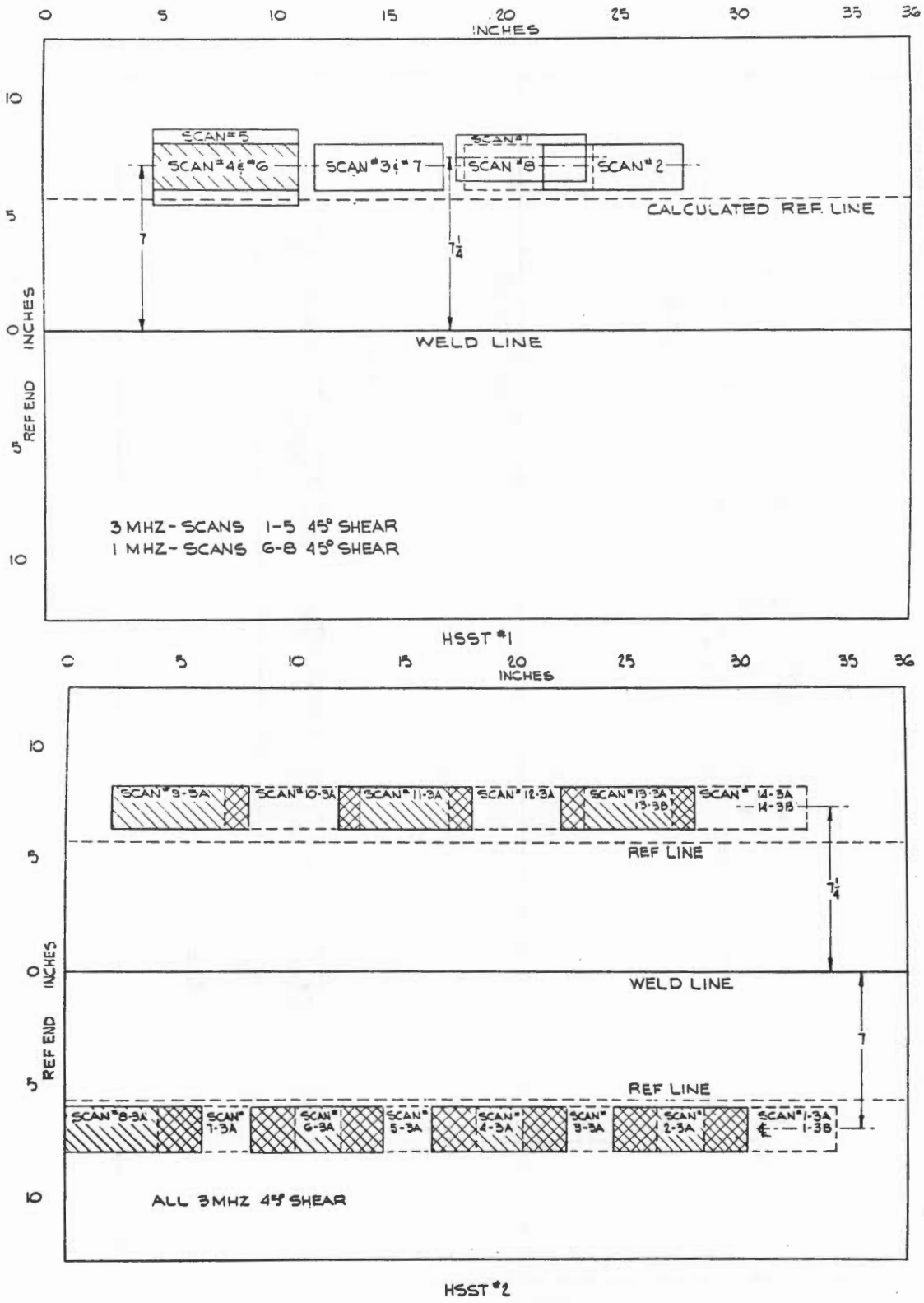

Figure 4-2 Baseline Scan Patterns

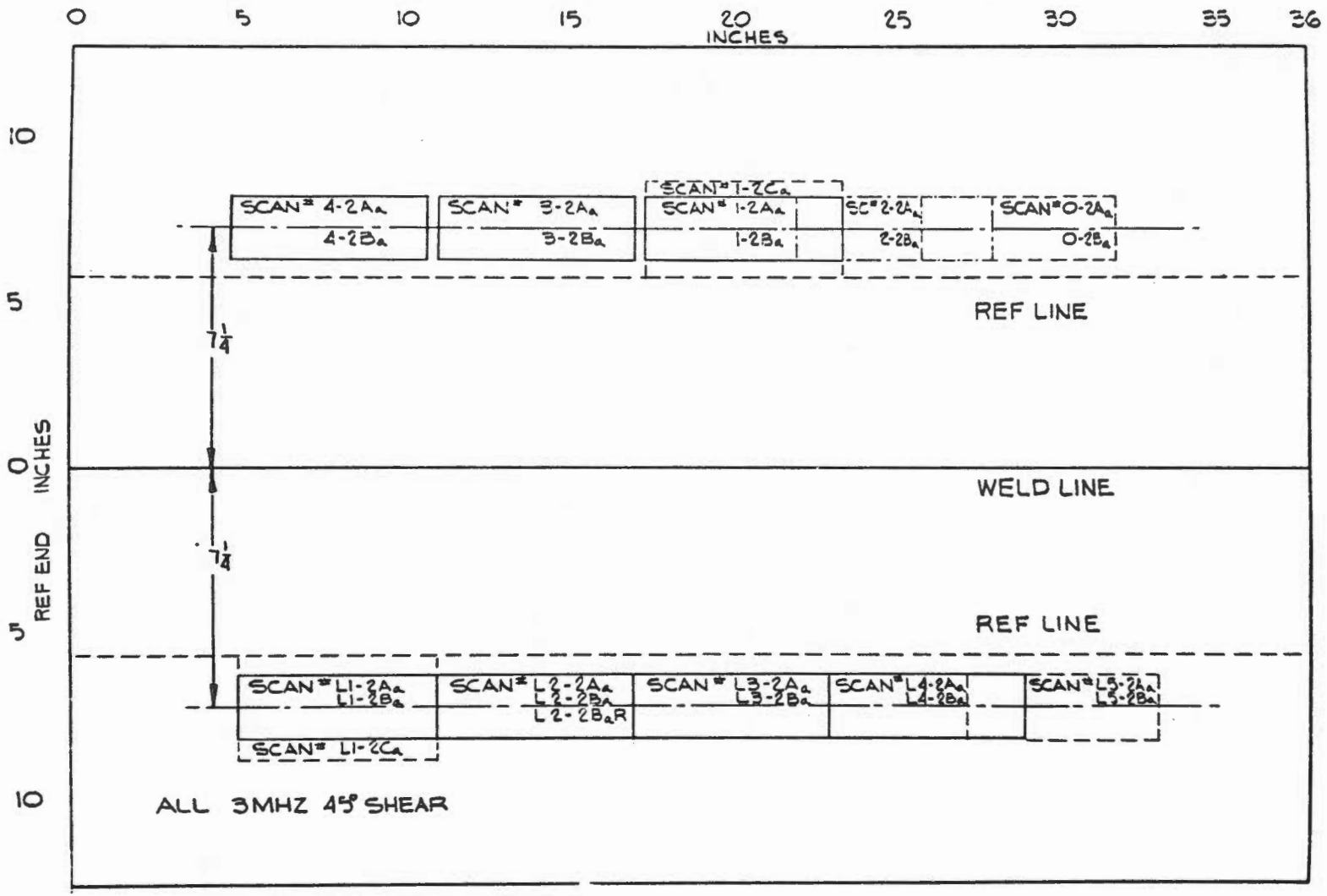

Figure 4-3 Post-test Scan Patterns, HSST#1

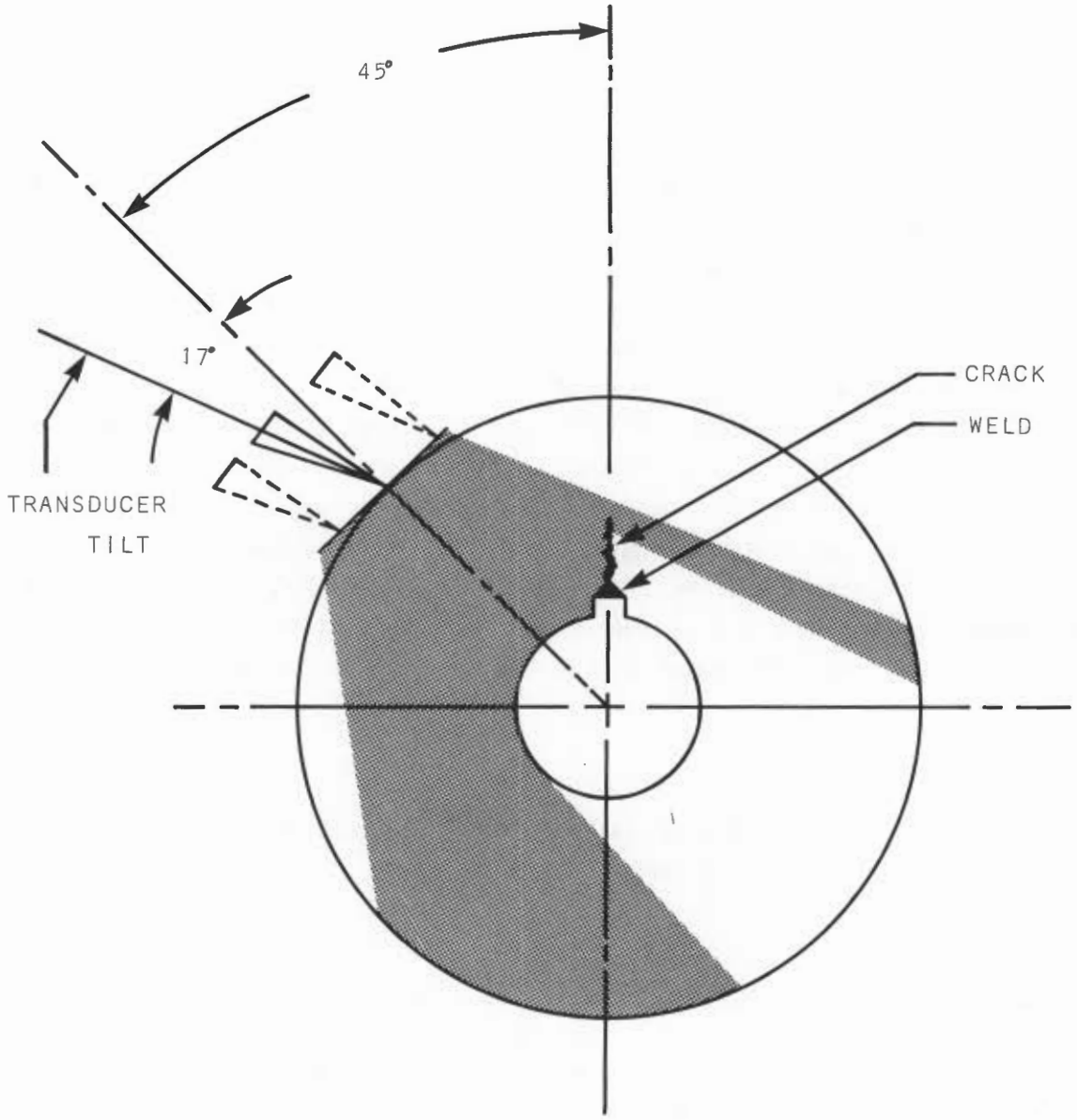

Figure 4-4 HSST#1 End View

The AH inspections were conducted at Oakridge National Laboratory in Oakridge, Tenn.

4.2.2 Test Results

HSST No. 1 had two trepans removed after the first thermal shock. The baseline AH images indicated that the size of the insert that was installed in the holes, created by the trepans, was within 5% of the actual size. The relationship of the trepans to the test specimen is shown in Figure 4-5. The baseline and post test AH images are shown in relationship to the test specimen and the scan segments in Figure 4-6 (HSST No. 1) and Figure 4-7 (HSST No. 2). The HSST No. 1 AH images showed that the thermal shock did create a crack and that the extent of the crack increased in the area of the trepan replacements. The trepan replacements consisted of inserts that were welded in place at the outer surface of the pressure vessel. Post-shock destructive tests indicated that the AH results were accurate and valid (see Table 4-1). The AH derived measurement of the thru-wall extent of the crack was within 10% of the actual value. The HSST No. 2 AH images also agreed with the destructive test results.

Table 4-1
COMPARISON OF HOLOGRAPHIC AND DESTRUCTIVE
ANALYSIS FEATURES

Feature	Analysis Technique	
	Holography	Destructive
HSST #1		
EB Weld Zone	0.5 in (1.25 cm)	0.5 in (1.25 cm)
Trepan Diameter	0.9 in (2.5 cm)	1.0 in (2.54 cm)
Maximum Crack Extent	1.55 in (3.9 cm)	1.7 in (4.3 cm)
HSST #2		
EB Weld Zone	0.5 in (1.25 cm)	0.5 in (1.25 cm)
Average Crack Extent	0.5 in (1.25 cm)	0.5 in (1.25 cm)

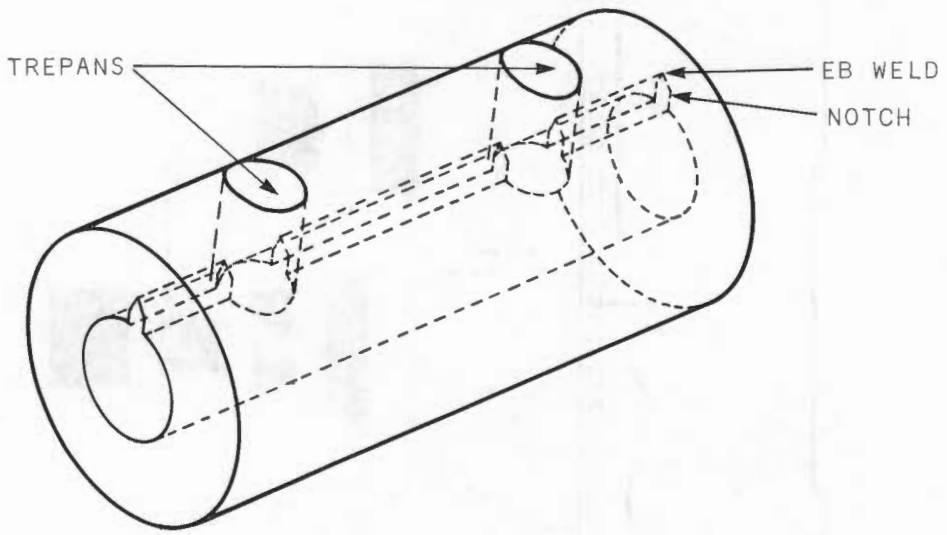

Figure 4-5 Location of HSST#1 Trepans

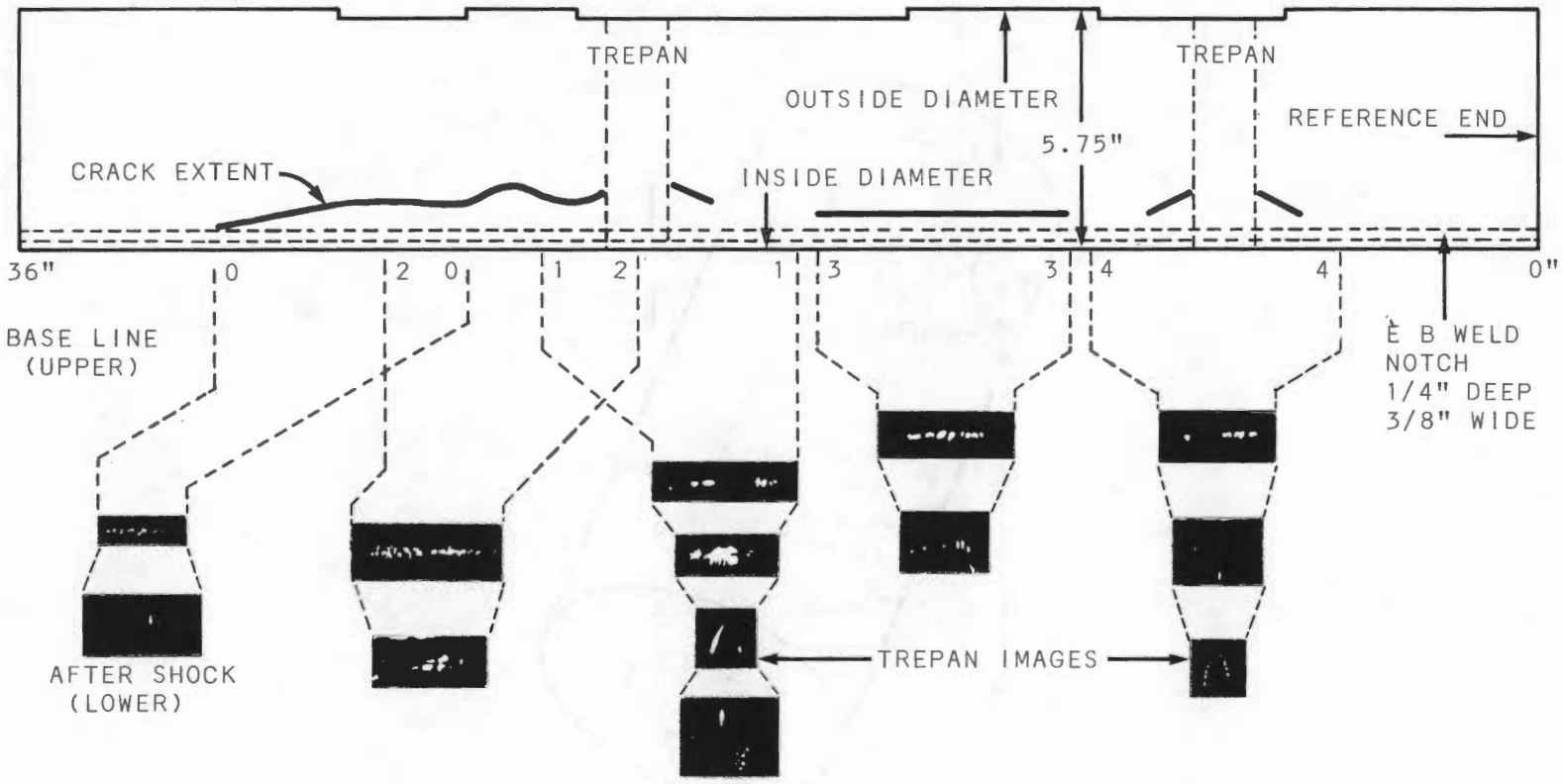

Figure 4-6 Baseline and Post-shock AH Images, HSST#1

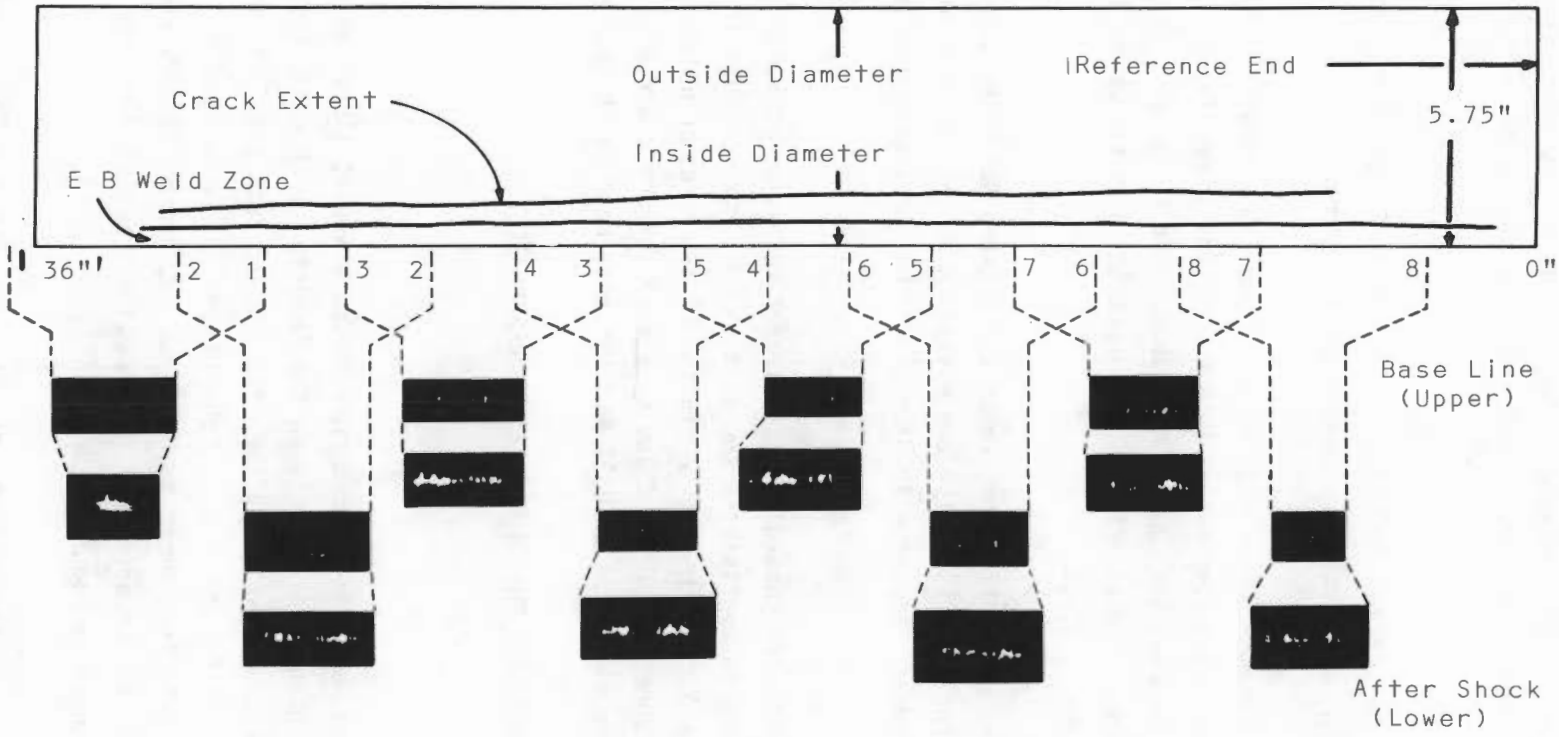

Figure 4-7 Baseline and Post-shock Images, HSST#2

The test sample were curved samples. An analysis of the corrections required to compensate for vessel curvature indicated that little or no correction was required.

A photograph of the crack in HSST No. 1 is shown in Figure 4-8. The notch, EB weld zone and crack can be clearly seen in this picture.

Core samples were removed from HSST No. 2. Figure 4-9 shows the EB weld zone and crack for three core samples of HSST No. 2. The objective of the EB weld was used to induce a 0.5 inch deep fault zone. The AH images indicated that this objective was achieved and the destructive tests of HSST No. 2 corroborated the AH findings.

AH techniques were appropriate for use as the primary NDE technique for support of HSST thermal shock tests. With the exception of predictable areas at the ends of the cylinders, accurate AH images of the shock-generated cracks were obtained.

The HSST experiment also showed that the trepan operation appeared to introduce an additional fault susceptibility the test results showed that the cracks in HSST No. 1 were larger in the vicinity of the trepan holes. While the undisturbed weld zone in HSST No. 2 led to a more uniform crack whose thru-wall extent was smaller than that of HSST No.1 vicinity near the trepan holes.

4.3 SUPPORT OF ACOUSTIC EMISSION PRESSURE VESSEL TESTS

4.3.1 General

The tests involved an Acoustic Emission Pressure Vessel (AEPV) which had been fabricated with intentional defects in the head to shell weld. (see Figure 4-10). The defects in the weld and the radiographic test stations, used for the test, are shown in Figure 4-11. Conventional UT was used to locate and characterize the defects. Shear angles of 0, 45, and 60 degrees were used for the conventional UT inspections. Composite results for the RT and UT inspections are shown in Figure 4-12.

Calibration for the UT inspections was obtained with a 0.125" flat bottom hole for the 0 degree beam, and with 0.188" side drilled holes for the 45 and 60

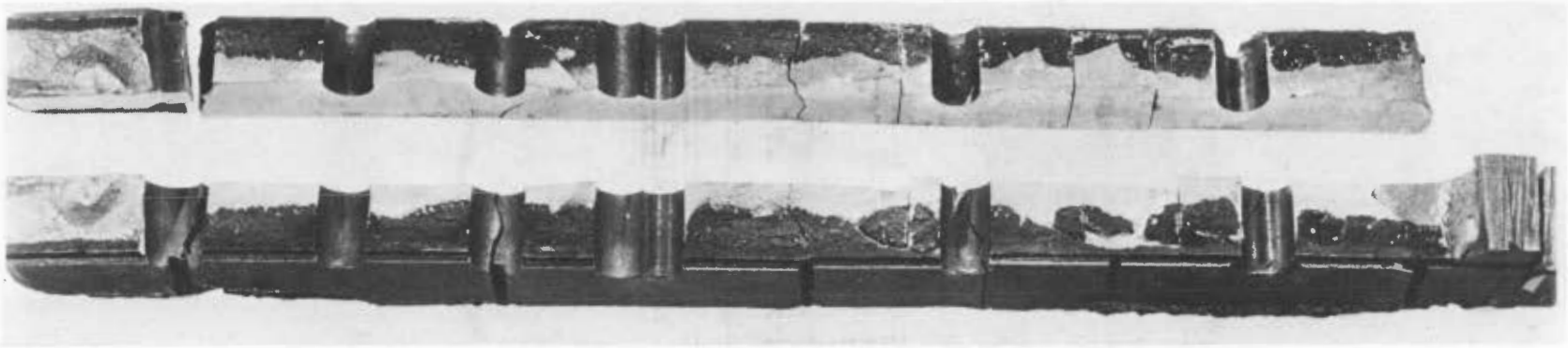

Figure 4-8 Cutaway View of Crack in HSST#1

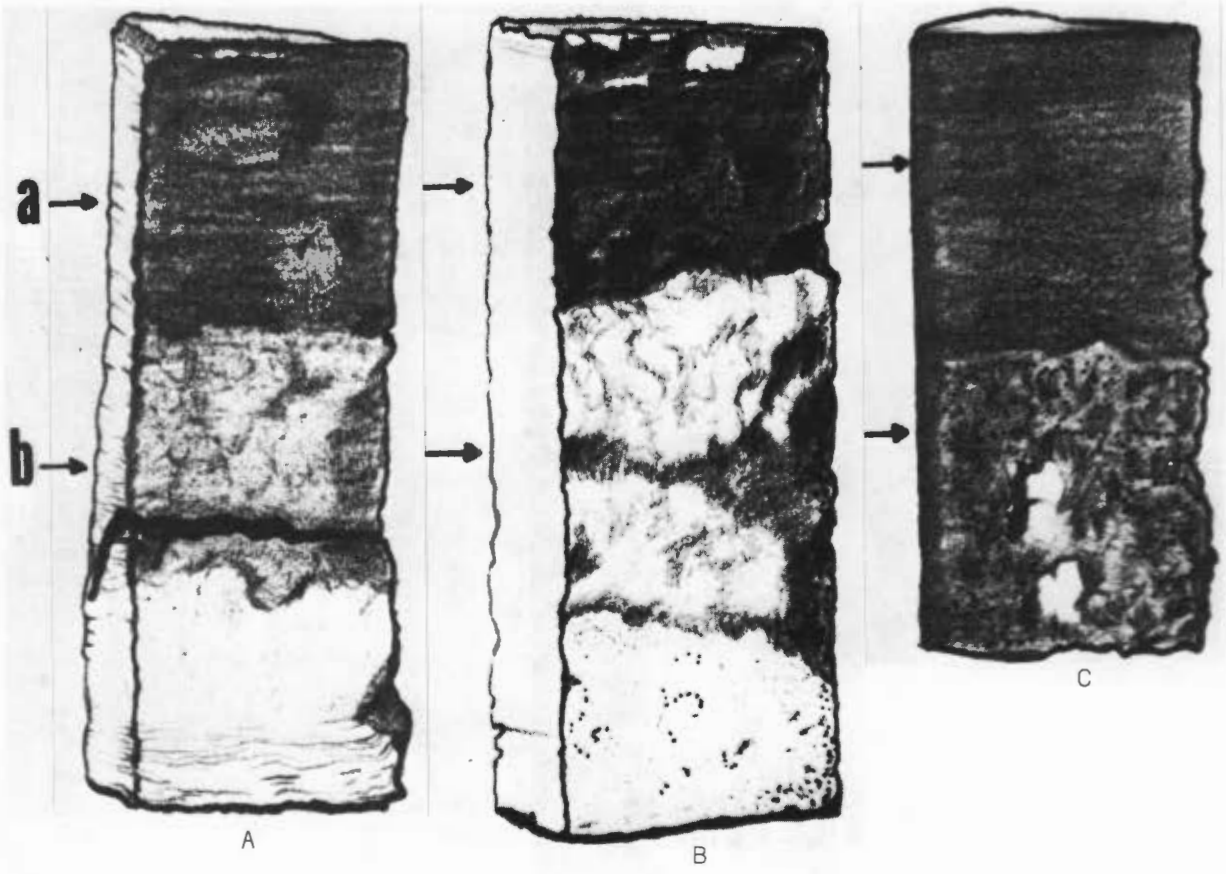

ARROWS POINT TO EXTENT OF EB WELD AREA (a)
AND EXTENT OF CRACK AREA (b)

Figure 4-9 Cross-section of HSST#2 Core Samples

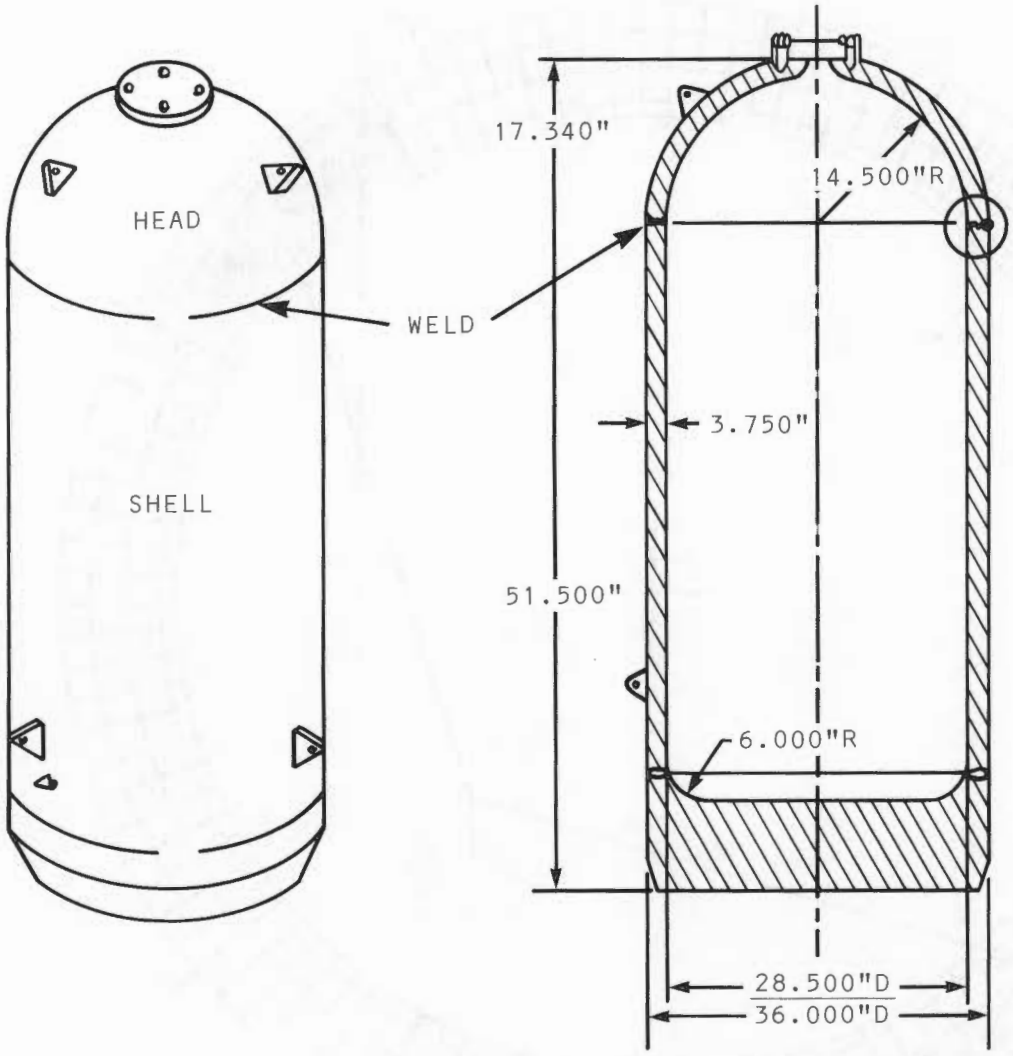

Figure 4-10 Acoustic Emission Pressure Vessel

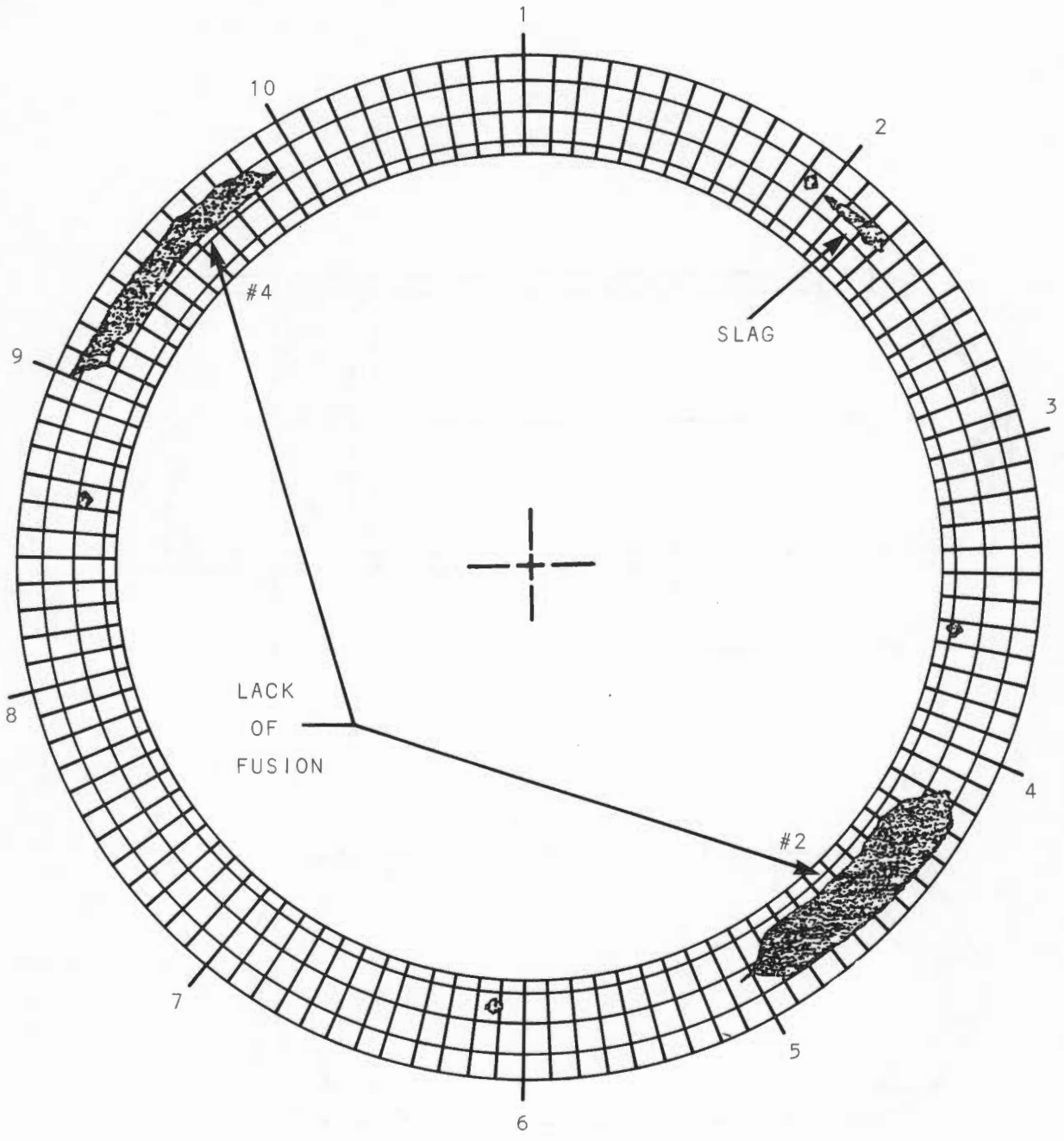

Figure 4-11 Cross-sectional View of Head Weld Defects and Radiographic Test Stations

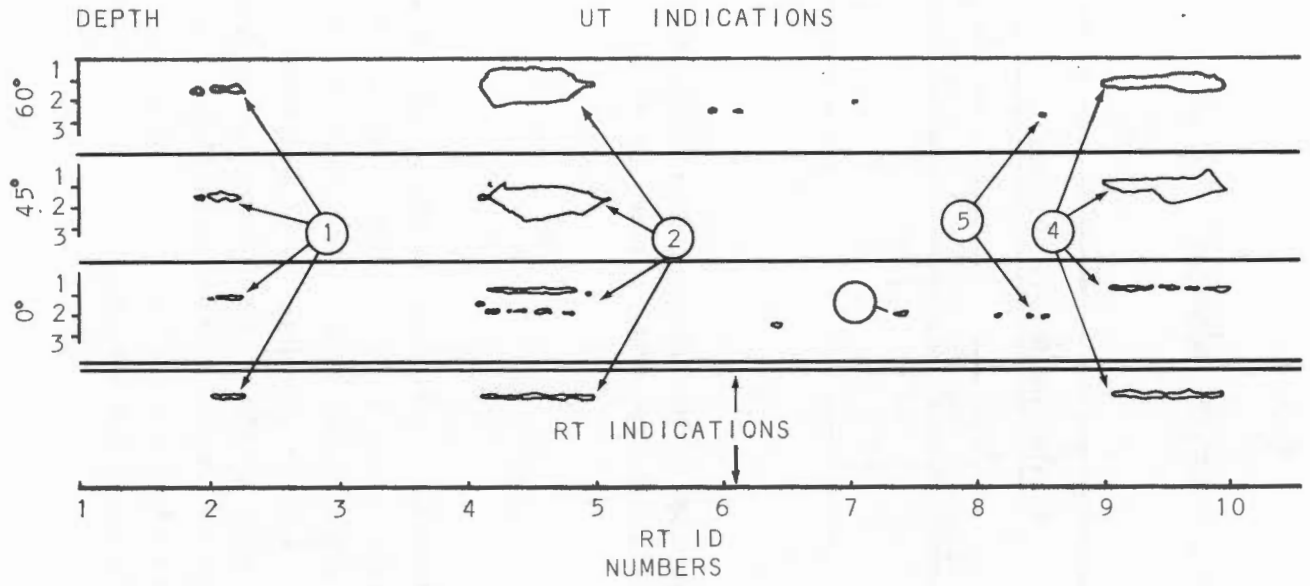

Figure 4-12 Composite UT and RT Results on AEPV

degree beams. RT was performed in accordance with ASME Section III code. Two defects (No. 2 and No. 4) were selected for AH imaging. The characteristics of these two defects are given in Table 4-2 as determined from the UT and RT inspections.

Table 4-2

AEPV DEFECT DIMENSIONS

Defect No.	Examination Results (Inches)					
	UT				RT	
	Length	Width	Thru-wall	Depth	Length	Width
2	11	0.21	1.27	2.2	10.5	0.20
4	11.5	0.17	1.04	0.75	11	0.24

The AH inspections were conducted in the Babcock and Wilcox production facility in Baberton, Ohio. The relationship of the scanner to the flaw is shown in Figure 4-13.

4.3.2 Test Results

AH images of defects No. 2 and No. 4, prior to hydrotest, are shown in Figures 4-14 and 4-15, respectively. These images were obtained at a frequency of 1 MHz. Post hydrotest AH images of defect No. 2 are presented in Figure 4-16, for a 1 MHz beam. Both the acoustic emission and AH procedures indicated that hydrotest did not induce defect growth. This finding was corroborated by the subsequent destructive tests. Detail differences between the initial and finalAH images was attributed to minor changes in scanner orientation with respect to the defects. The overall dimensions for both set of images was in agreement.

The destructive tests were performed by removing 0.5 inch samples from the ends and middle of the defects. Composite photos of the total fracture of defects No. 2 and No. 4 are shown in Figures 4-17 and 4-18, respectively.

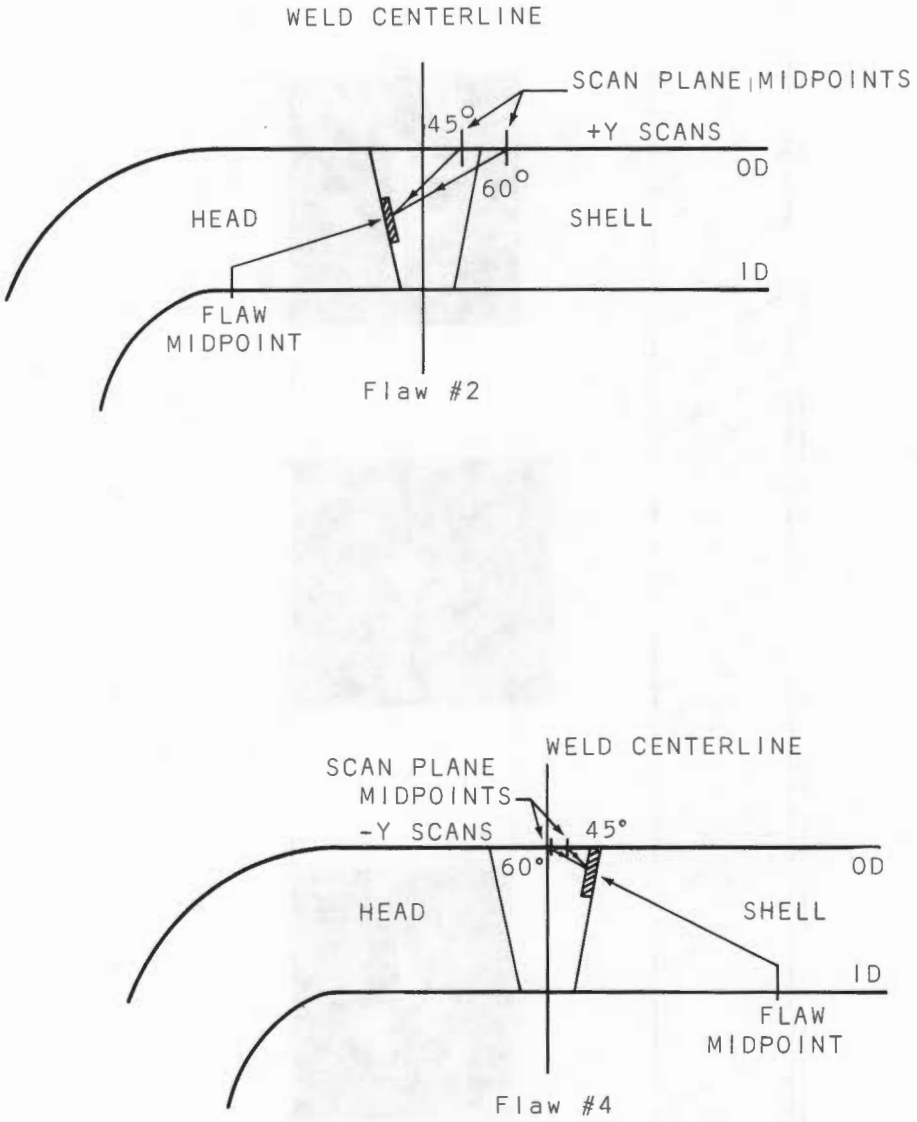

Figure 4-13 Relationship of Scanner to Flaws

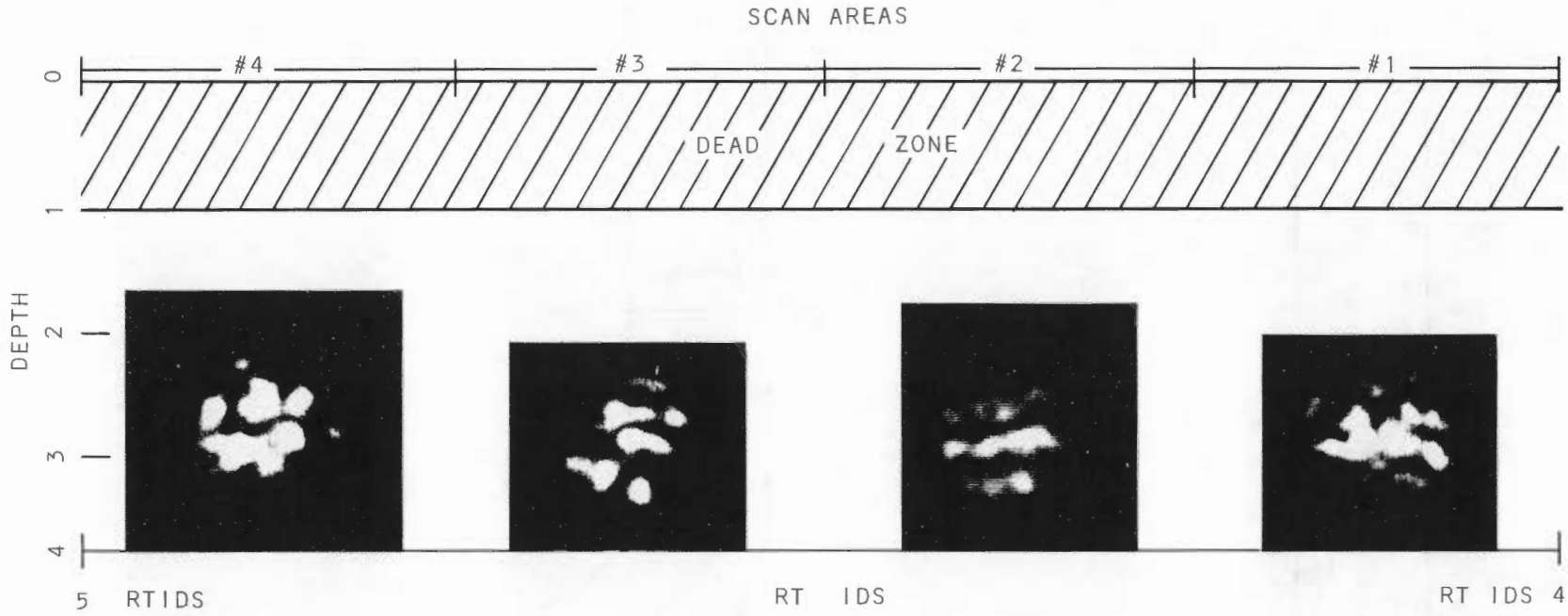

Figure 4-14 AH Images of Defect #2, Prior to Hydrotest

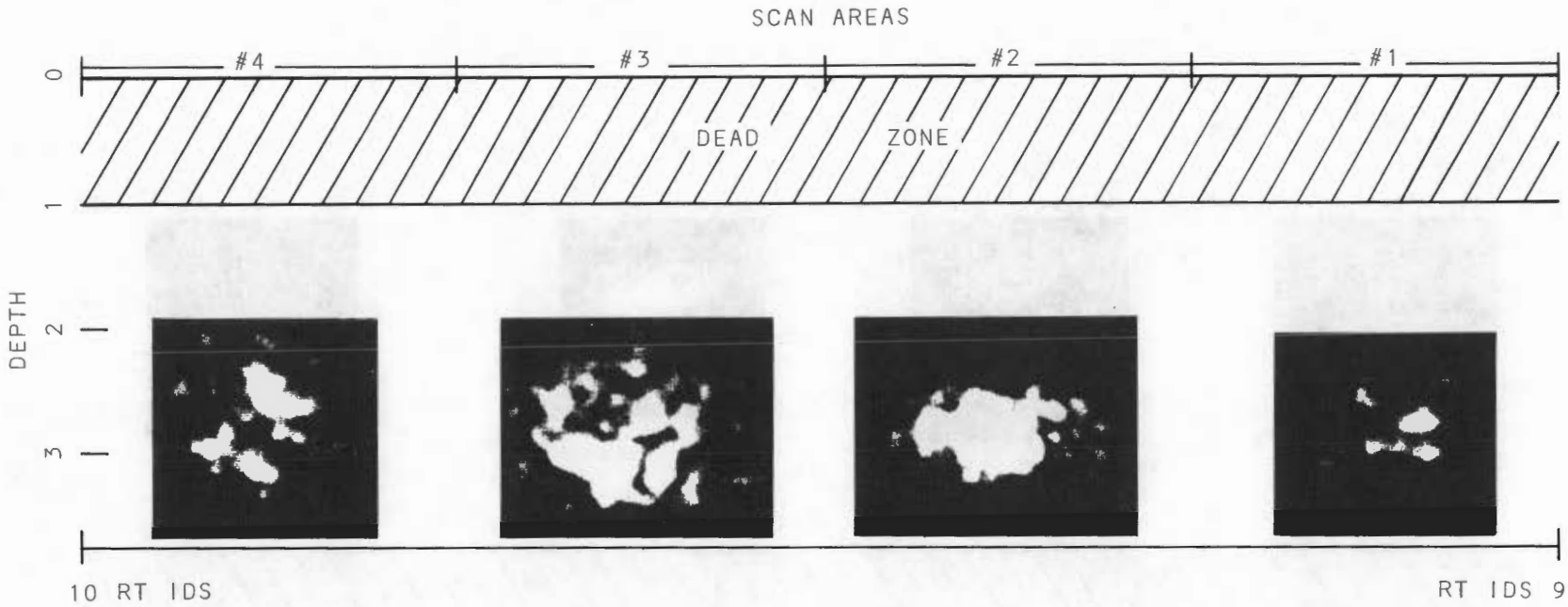

Figure 4-15 AH Images of Defect #4,Prior to Hydrotest

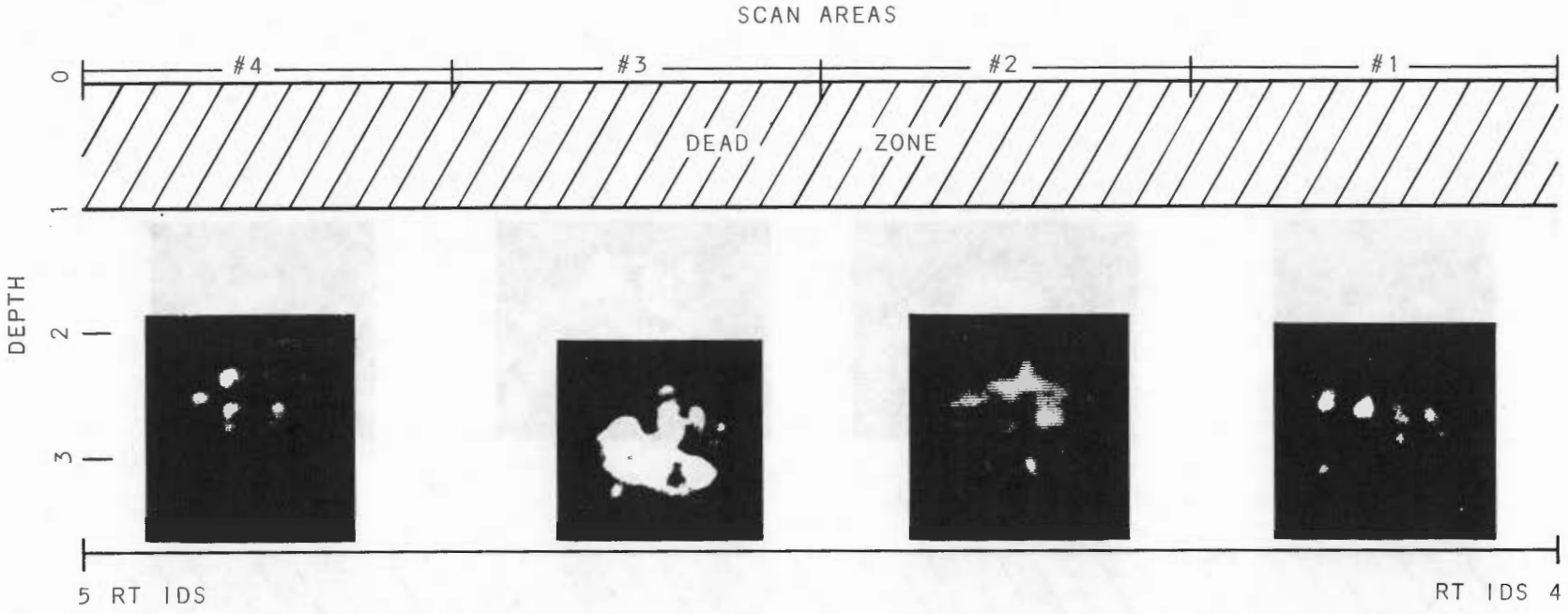

Figure 4-16 AH Images of Defect #2,Post-hydrotest

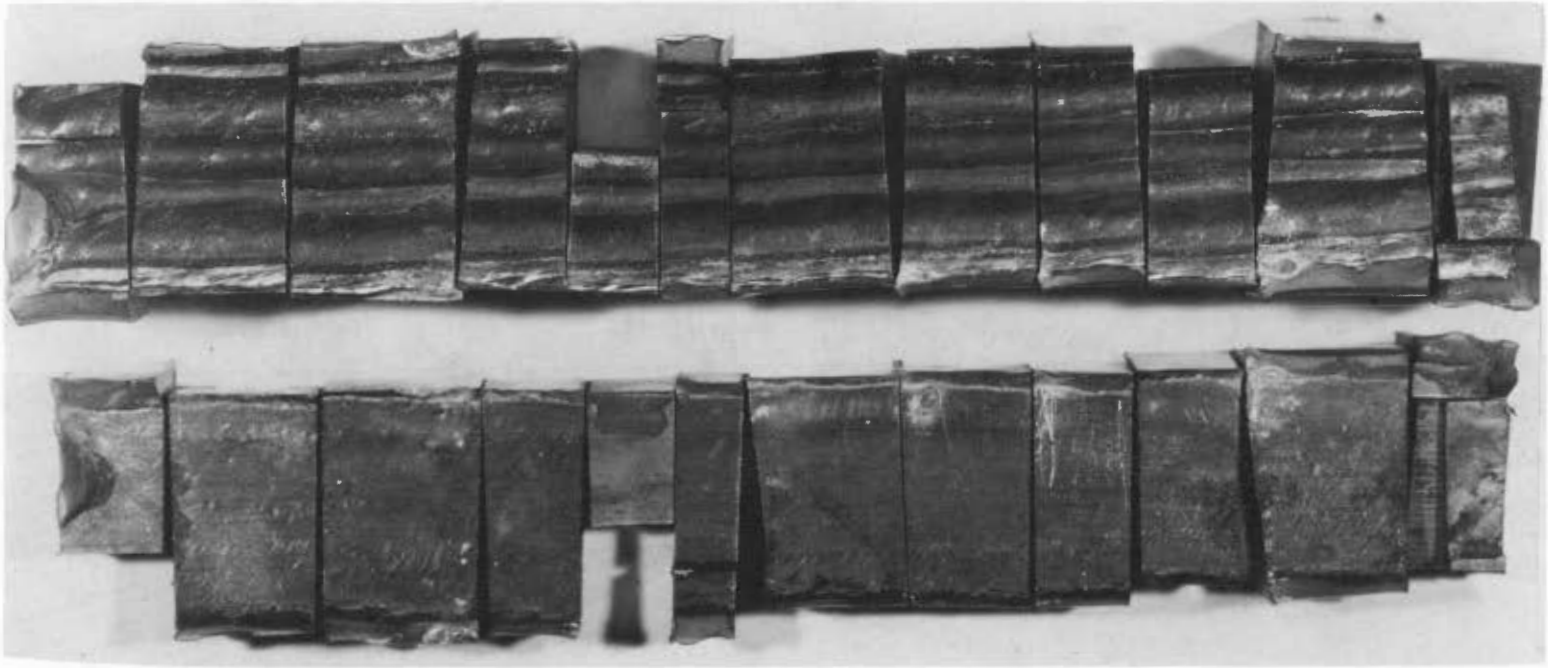

Figure 4-17 Full Length Fracture Surface of Defect #2

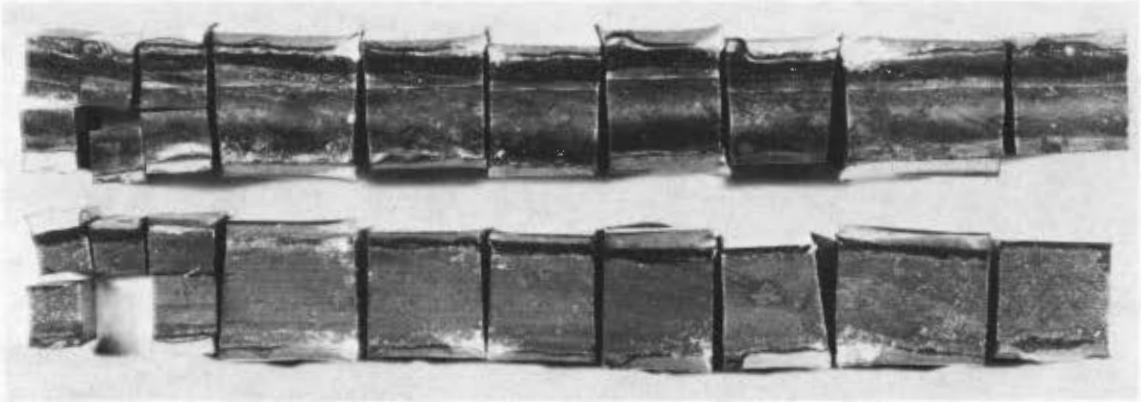

Figure 4-18 Full Length Fracture Surface of Defect #4

4.4 CLAD WELD TEST BLOCK INSPECTION

4.4.1 General

The inspections reported in this section were part of a cooperative exchange program. The test specimen was supplied by CEN, Saclay. The characteristics of the test block are shown in Figure 4-19 and 4-20, respectively. The tests were conducted in Saclay, France. The clad surface had ripples of up to 0.125 inches.

Two sets of AH equipment were used:

a. the Babcock and Wilcox equipment discussed in Section 5 of this report and

b. Babcock and Wilcox equipment with French supplied focused probes.

The focused probe differs from the B & W approach in that no image reconstruction is required because the image plane is the object plane. The B & W equipment focuses on the surface of the material to be examined, while the French probe focuses on the plane of interest. The results obtained with both types of equipment were in general agreement.

The test block had a double groove weld which contained both natural and artificial defects.

Three observation directions were used for each indication and holograms were made for both the clad and unclad surfaces of the block. Data were obtained for the unclad side with 3 MHz beams. 1 or 2 MHz beams were used for the clad surface inspections, and 4MHz beams for the focused probe tests. As shown in Figure 4-19, the test block was marked in each corner to aid orientation of the results. The side marked 7, 8 is denoted as plus, and the side marked 9, 10 is denoted as minus.

For a given discontinuity, i.e., the images obtained from each different viewing direction may be different (except for a symmetrically shaped flaw) due to the different reflecting elements of the defect. The information obtained from each viewing direction is a composite image of all reflecting areas of the defect, when viewed from that direction.

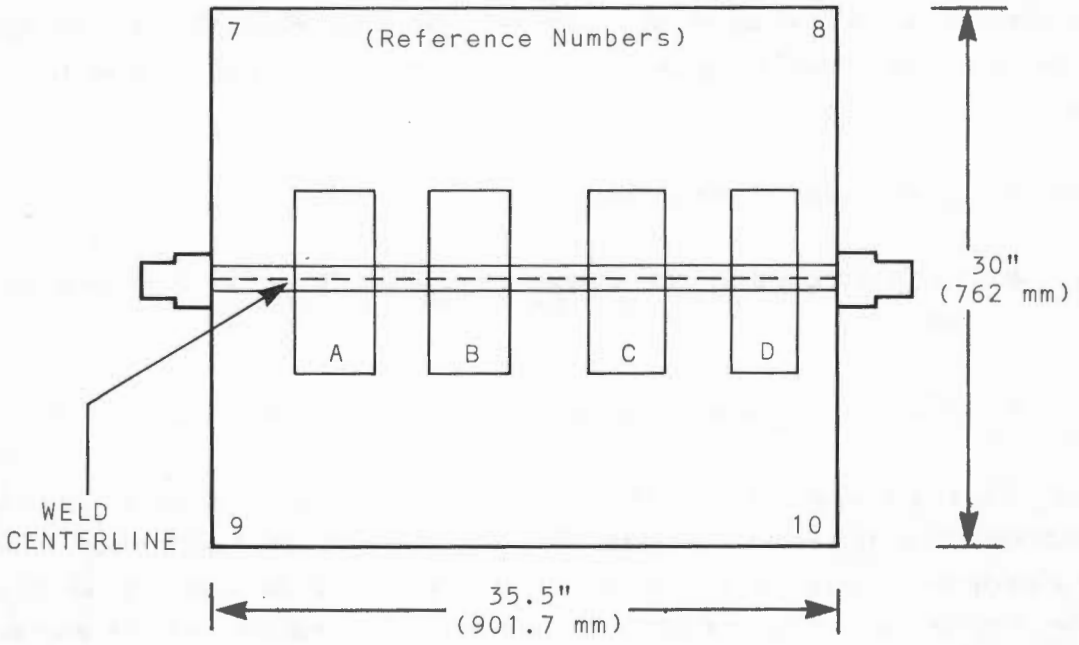

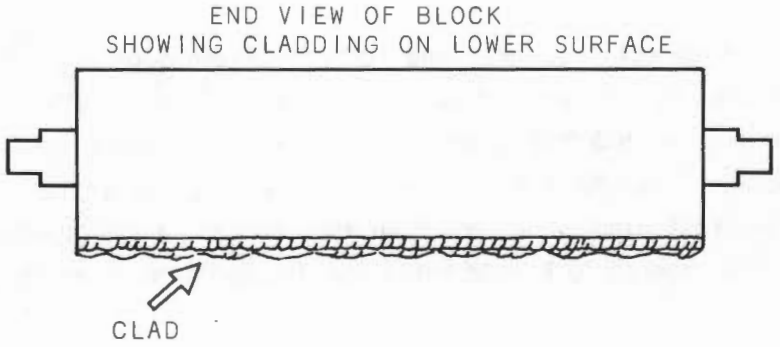

Figure 4-19 Sketch of French Test Block Showing the AH Scan Areas, Reference Numbers and Cladding

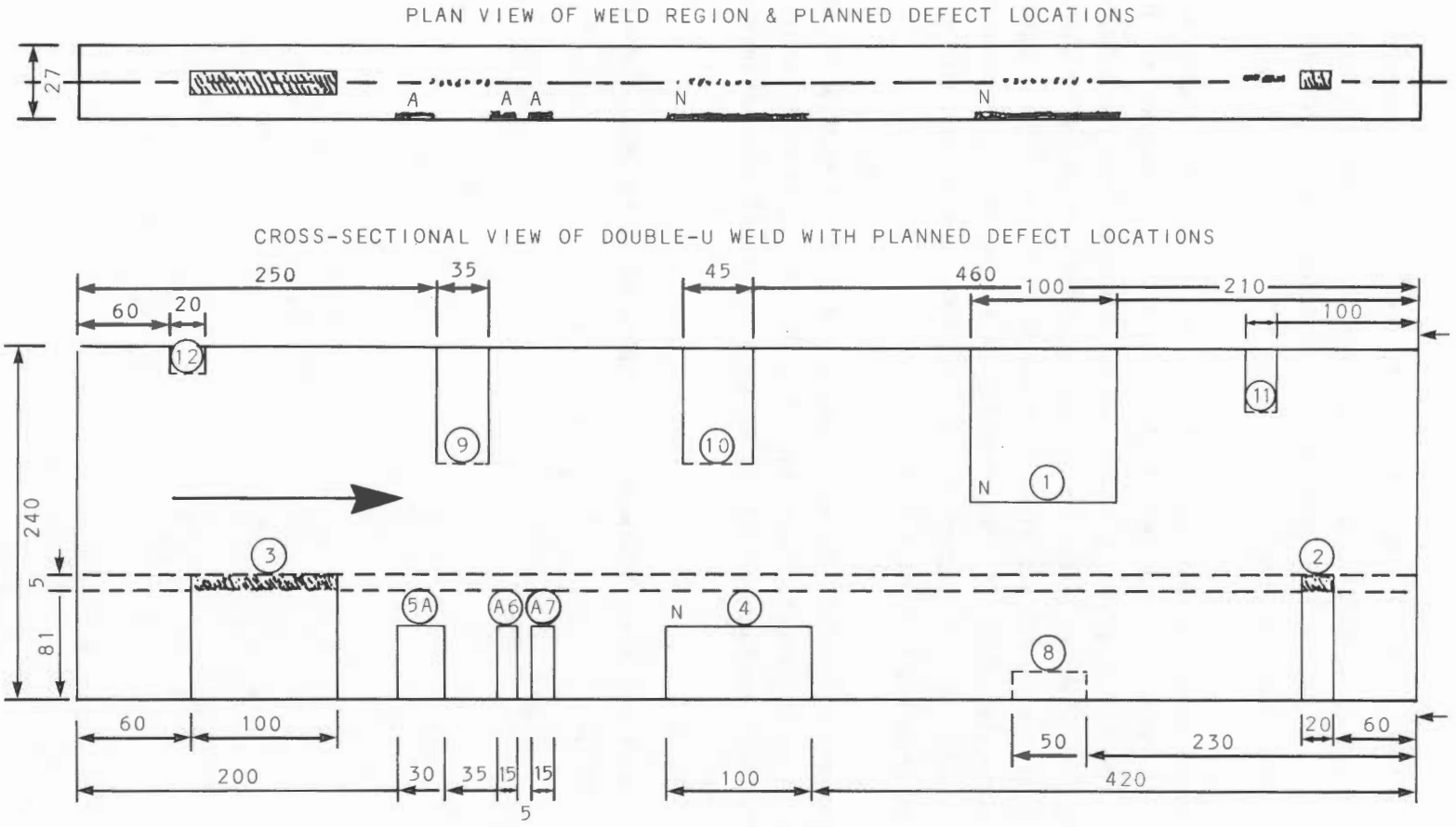

Figure 4-20 Reduced Sketch of the French Fabrication Drawing Used to Weld the Test Block

4.4.2 Test Results

All the discontinuities identified in Figure 4-20 were imaged except for defects Nos. 2, 11 and 12. Defects 2, 11 and 12 were located near the ends of the block and the rough ends of the test block introduced signals that masked the returns from these three defects.

Data obtained from AH images of the subject defects are presented in Table 4-3. The length (L) is the length of the defect along the length of the weld. The width (W) is the dimension transverse to (L) and was measured from the 0 degree beam images. The dimension (s) is the separation of images as viewed by the 45 degree beam. All of the dimensions given in Table 4-3 are the maximum values measured. The composite data, obtained from all AH images of each indication are presented in Table 4-4. One defect (No. 8) must have been planar, since it could only be seen from one view direction.

Cladding decreases the quality of the AH image. (Additional information on the effect of cladding on AH imagery is presented in Volume II of this series.) The focused probe test equipment configuration was not optimum because of physical constraints.

Destructive tests were not available when this report was compiled. They will be reported separately.

Table 4-3

SUMMARY OF RESULTS, CLAD TEST BLOCK

Identity of Defect Investigated	Surface From Which Defect Viewed	Orthogonal 45° Shear Angle		Longitudinal 0° Shear Angle		Orthogonal 45° Shear Angle		Depth Below Unclad Surface (mm)
		Lgth. (mm)	Sepr. (mm)	Lgth. (mm)	Width (mm)	Lgth. (mm)	Sepr. (mm)	
B&W Equipment								
1	Unclad	61.72	10.92	85.09	10.16	78	20.32	127
1	Clad	76	20.3	78	12.7	69	20.3	125
3	Unclad	85	17	56.4	9	90	15.2	157.5
3	Clad	58	20.3	-----	-----	44.7	13.5	155.5
4	Unclad	109	16.3	46.5	10	63	17.8	195.6
4	Clad	58.6	12.7	55.1	6	59.6	14	191
5	Unclad	30	13.7	24	15.2	30.2	12.7	183
5	Clad	13.2	8.1	18.8	7.6	----	-----	201.2
6/7	Unclad	21.3	13.7	11.5	15	18	12.7	183
6/7	Clad	24.8	11.2	14.7	3.8	----	-----	201.2
8	Unclad	----	----	-----	-----	35.2	12.7	223.5
8	Clad	----	----	-----	-----	----	----	-----
9	Unclad	55.4	15.2	35	8.4	43.7	20.3	89
9	Clad	68.8	15.2	32.3	14.5	76.5	20.3	87
10	Unclad	50.8	15.2	55.5	6.6	36.3	12.7	81.3
10*	Clad	64.8	35.6	----	-----	----	----	94.5
Focused-Probe								
9	Unclad	51.8	15.2	44.3	12.2	50.8	23.9	-----
10	Unclad	70.1	12.7	71.1	17.3	57.9	24.9	-----

NOTE: B&W Equipment - Unclad Surface AH Images - 3MH, Clad Surface AH Images- MHz (MHz for #9, #10 @ 45° Shear Angle).
Focused Probe AH Images - 4MHz.

* Questionable numeric values due to surface ripple.

Table 4-4
COMPOSITE DATA FROM ALL AH IMAGES
OF EACH INDICATION

Indication No.	Length (in)	Depth Variation (Through Wall Dimension) (in)	Depth (From Unclad Surface) (in)	Comments
1	4.25 (108 mm)	0.5 (12.7 mm)	5.0 (127 mm)	
3	4.1 (104 mm)	0.45 (11.4 mm)	6.2 (157.5 mm)	
4	4.29 (109 mm)	0.6 (15.2 mm)	7.6 (193 mm)	
5	0.84 (21.3 mm)	0.34 (8.6 mm)	7.2 (183 mm)	
6,7	1.2 (30.5 mm)	0.34 (8.6 mm)	7.2 (183 mm)	6 & 7 are connecting
8	1.4 (36 mm)	0.4 (10 mm)	8.8 (223.5 mm)	Discontinuity seen from only one direction; all others were three-dimensional.
9	2.3 (58.4 mm)	0.46 (11.7 mm)	3.5 (89 mm)	It appears as if there is an additional discontinuity at slightly lower position.
10	2.2 (55.8 mm)	0.5 (12.7 mm)	3.2 (81.3 mm)	

NOTE: There appeared to be more indications in the block than those reported. All holographic data was taken from the location specified and assumed the number of the indications specified was correct.

Section 5.0
AH EQUIPMENT AND TEST CONFIGURATIONS

5.1 GENERAL FINDINGS

RP 605 demonstrated that acoustic holography is practical in a field environment. The AH techniques and equipment modifications developed by Babcock and Wilcox in the four years preceding RP 605 (1972-1976) were appropriate for field use even though AH was an "Art" rather than a science up to 1978. Some practical operating procedures were developed during the program that facilitate AH in the field. In addition, areas where future improvements would help were also identified.

Field environments, as opposed to laboratory environments, contain a number of elements that could inhibit, or possibly preclude, the use of AH equipment for routine production operations. The major concerns were:

a. Would the time required to set up equipment, implement the test, reduce the data of the test, and remove the equipment be compatible with production operations?

b. Would the diversity of physical geometries allow AH to be used in field situations?

c. Would the results obtained be accurate enough to yield a pay-off for the effort?

5.1.1 Field Problems

A number of practical problems were encountered during the AH examinations reported in this study despite the fact that the investigators were familiar with the behavior of the equipment and the field environment. The problems were:

a. The commercially available laboratory equipment was not designed for field use. In particular, the equipment was not rugged enough for frequent transport by commercial carriers. Modifications were required to assure that transport vibration and shock did not dislodge screws and components. In some cases, additional fasteners had to be added to the equipment packages.

b. The quality of the prime power available at the site was a problem. In many cases, line transients and voltage levels variations required substantial prime power conditioning .

c. The production shops used welders and other equipment that drew large current pulses. Electromagnetic interference with the operation of the AH equipment was encountered.

d. Communication was needed between members of the field crew during setup and test. The Scanner was separated from the other equipment and required adjustment to obtain results. The B&W team anticipated this problem and used sound powered headsets to solve this problem.

e. The physical geometry of the test specimens was quite diverse. Each AH examination required some compensation or adjustment to deal with the physics of that particular examination. This involved consideration of end effects, beam angles, Scanner orientation, and masking effects.

5.1.2 Future Improvements

In the development of commercial equipment for use in the field, the designers should consider the following features:

a. Incorporation of power supplies that can accomodate a wide range of voltage swings, line transients, and frequency shifts.

b. Protection against high level electromagnetic interference would include the cabling to the Scanner as well as the individual equipment items.

c. Ruggedized packaging designed to withstand both transport and field handling.

d. Scanner mounting capability that allows the unit to be attached to a variety of surfaces and orientations from horizontal to vertical. In addition, the Scanner assembly must be able to operate on surfaces with substantial amounts of ripple and still maintain the integrity of the transducer/couplant system.

e. Incorporate an inter-team communication system for use in high noise environments.

f. Use computer reconstruction techniques rather than optical technique to improve the quality of the AH images. This requires substantial memory and data processing capability.

5.2 FUNCTIONAL DESCRIPTION OF AH EQUIPMENT

A functional block diagram of the overall system is shown in Figure 5-1. This system encompasses the test specimen, the test specimen scanner, electronics to generate acoustic pulses with megahertz repetition rates, electronics to detect the returned acoustic pulse, and optics equipment (or the digital equivalent) to reconstruct images from holographic data.

As discussed in Section 2.2, Acoustic Holography uses an acoustic transducer to propagate acoustic energy in a test specimen. This energy propagates throughout the test specimen and is reflected from discontinuities within and at the surfaces of the test specimen. A portion of the reflected energy is directed back to the transducer that initiated the acoustic wave and detected by the transducer (Backward Wave Propagation). Acoustic Holography looks at the distribution of the family of reflected signals that result when the transducer is moved in a prescribed way with respect to the test specimen. This pattern is known as the scan pattern. The function of the Scanner shown in Figure 5-1 is to position and move the acoustic transducer with respect to the test specimen.

The function of the Transceiver electronics is to generate a series of electronic pulses that are applied to the acoustic transducer which converts

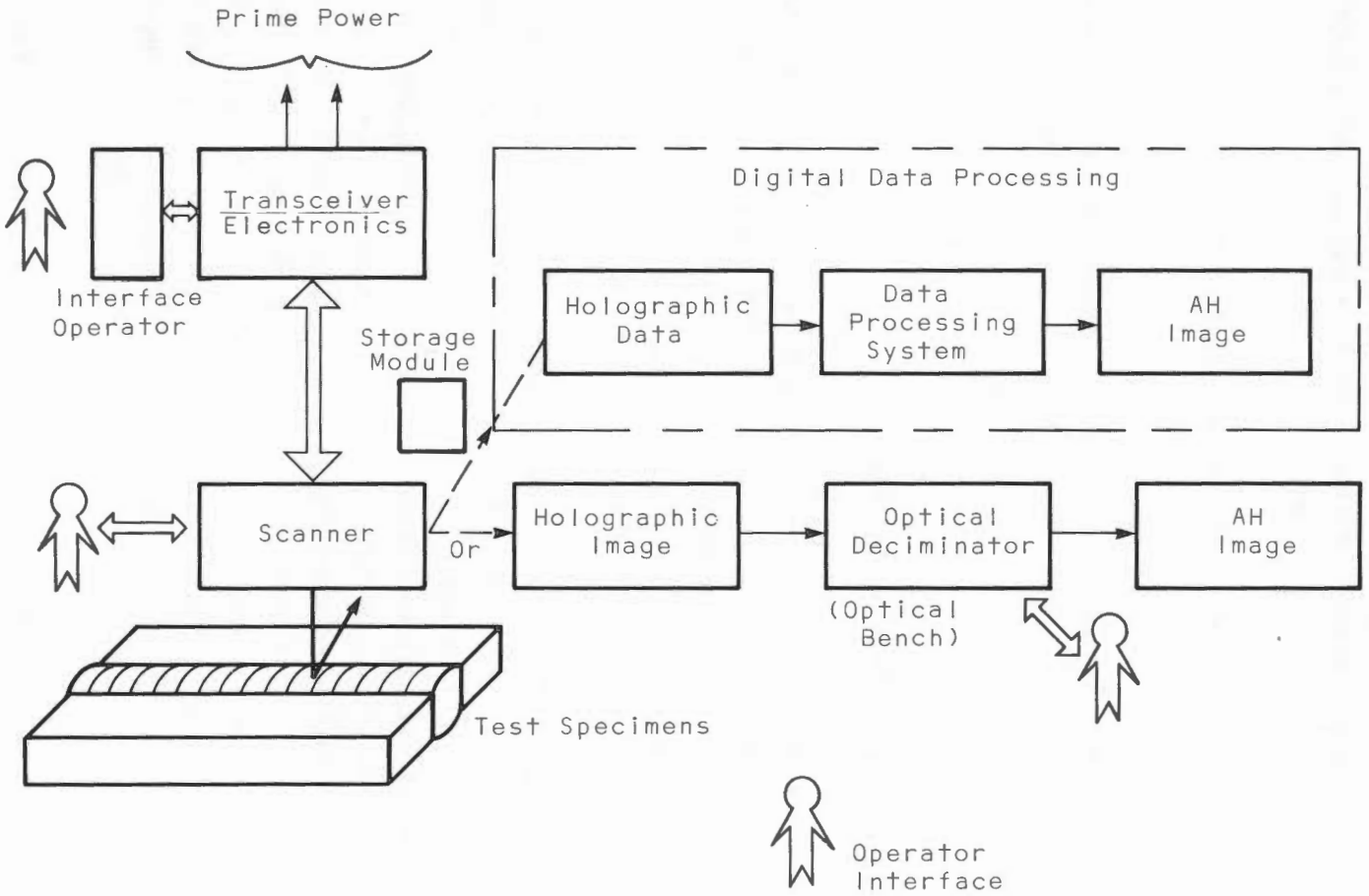

Figure 5-1 Simplified Block Diagram AH System

these pulses to acoustic energy. Typically, the acoustic transducers operate in a frequency range of 1 to 5 megahertz (MHz). The transducer also detects acoustic energy reflected back from the test specimen and converts the reflected acoustic energy back to electrical signals. The detected signals are used to drive a light source that exposes a film. During an acoustic holographic scan, the phase relationships of the reflected energy are recorded on the film as a set of patterns. In the tests reported in this volume, the Scanner included the transducer, scanning mechanism, and the photographic recording equipment.

The output of the photographic equipment on the Scanner is a transparency that contains a holographic image. This image is not a "picture" of the area of interest rather, the holographic data is a series of light and dark rings (fringe patterns) that have to be processed to produce a reconstructed picture of the defect of interest. Optical reconstruction techniques were used in the tests reported in this volume. Volume 2 of this series reports on the results obtained with computer-derived reconstruction techniques.

In optical reconstruction, the holographic image is placed in the optical path of an optical bench and a screen is placed in the focal plane of the optical bench. The operator then adjusts the optical equipment to produce an image on the screen. A laser is used to produce a phase coherent light source that interacts with the holographic image to produce the final "picture". The intensity of the image on the final "picture" is not important. The final image is interpreted in terms of the absence or presence of an image rather than the strength (intensity) of the image in the final "picture".

As shown in Figure 5-1, an operator interface exists at three points in the block diagram. In the tests reported in this volume, the experience and ability of the operator was an important determinant of the quality of the final result. In particular, "Art" was involved in:

a. Defining the physics of the test in configuration and adjustment of the equipment to operate in that situation.

b. Location and adjustment of the Scanner to achieve the desired results.

c. Operation of the Optical Bench to successfully reconstruct the acoustic holographic images.

5.3 EQUIPMENT DESCRIPTION

The equipment used for the AH examinations was a modified Holosonic 200 system with an optical reconstruction unit (Figure 5-2). The images were obtained using longitudinal wave transducers in water focused to a point source on the surface of the test specimen. Recirculated water was used as the couplant for ultrasonic energy transfer. The operator could choose a 0, 45 or 60 degree shear angle by changing the incident angle on the surface and an operating frequency of 0.5 to 5 megahertz (MHz). Physically, the AH system used for the field evaluations consisted of the Electronics, the Scanner and the Reconstruction Unit.

5.3.1 Electronics

A block diagram of the Electronics is presented in Figure 5-3. Detailed discussions of the Holosonics electronics are readily available in the open literature. (The Holosonic unit is no longer commercially available.) The operator uses the oscilli scope display to adjust the gate generator and other parameters to image the desired plane of the test specimen. The electronic circuits work exactly the same for both optical and computational reconstruction. The difference is that the electrical signals that drive the glow modulator are picked off and recorded when computational reconstruction is to be used, as opposed to optical reconstruction, in which the glow modulator exposes a poloroid film to generate the hologram.

The field environment required that the standard electronics package be made rugged enough for transport and field use. Effort was also required to make the electronics perform in accordance with the advertised specifications for that unit.

5.3.2 Scanner

The Scanner assembly is shown in relationship to the test specimen in Figure 5-4. The circled letters refer to the circled letters on the Electronics block diagram that was presented in Figure 5-3. Figure 5-5 indicates the coupler used in the AH examinations. This configuration allowed the transducer to be

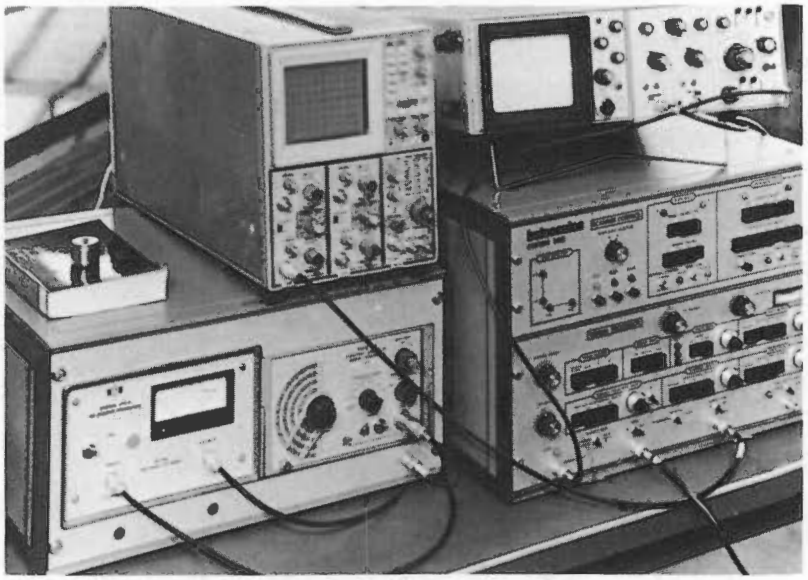

Electronics

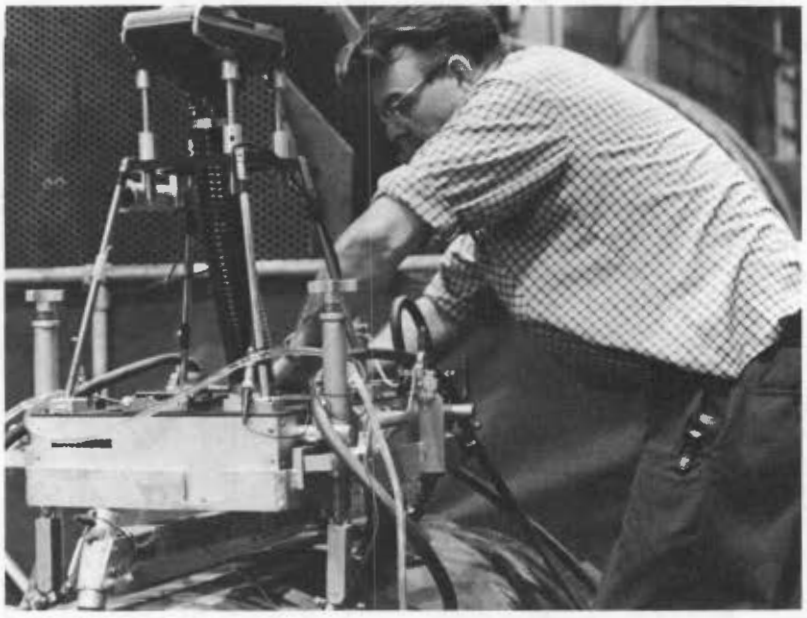

Scanner

Figure 5-2 AH Equipment

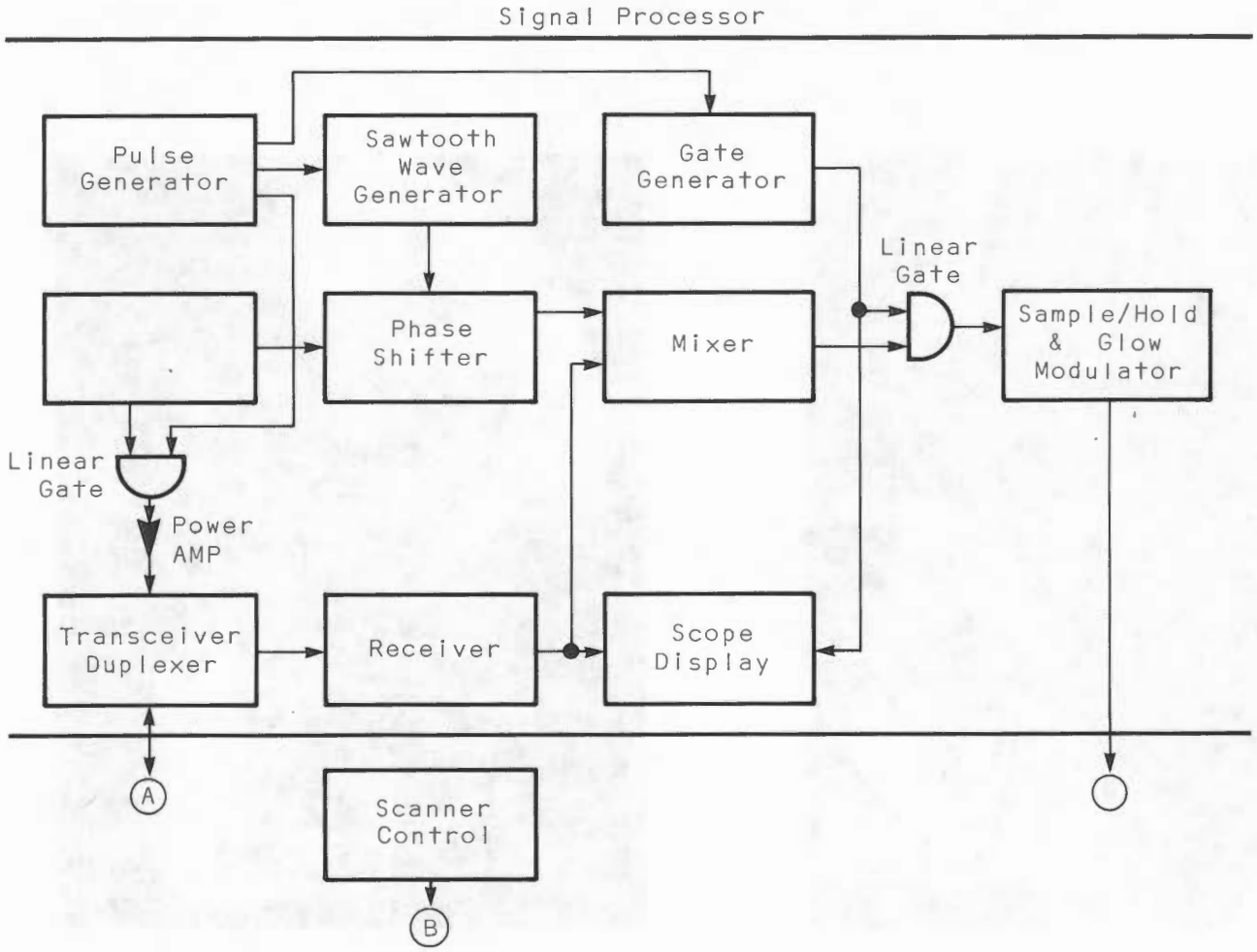

Figure 5-3 Electronics

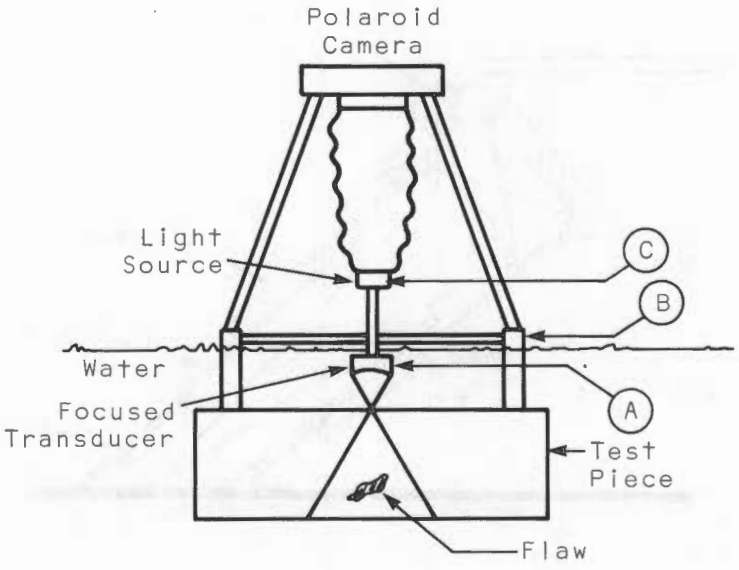

Figure 5-4 Scanner Assembly

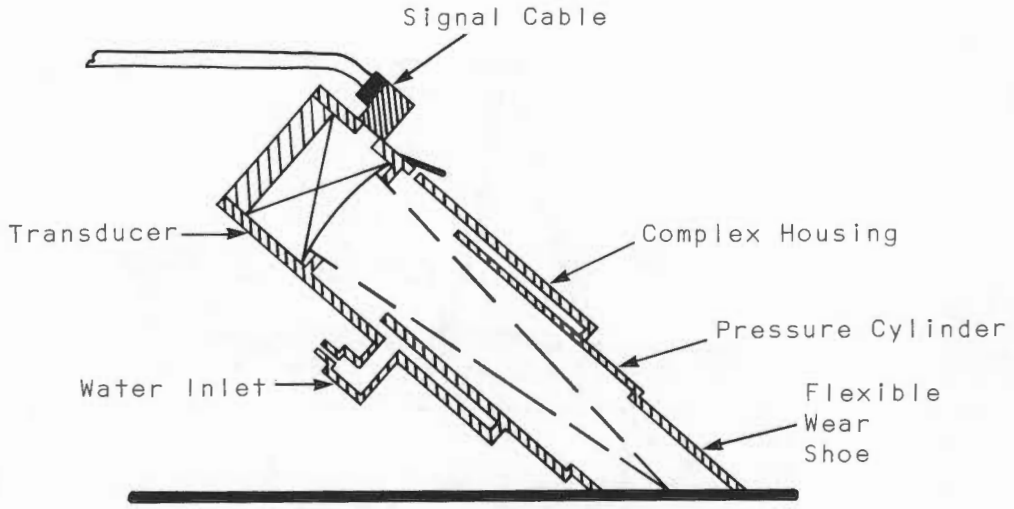

Figure 5-5 Transducer/Couplant Mechanism

to the surface during the arm movement. A cutaway view of the Scanner is presented in Figure 5-6. The Scanner contains a precision mechanism that moves the extension arm in a repeatable prescribed scan pattern. The physical construction of the scanning mechanism limits the travel of the arm, which means that for relatively long specimens, overlapping scan patterns had to be used. Figure 5-7 illustrates this point and shows the overlap areas for one of the HSST scans. The Holosonic Scanner was modified to facilitate field use and installation. The modifications included the extender arm and the addition of a mounting system that provided considerable flexibility in the field. In some instances, the Scanner had to be mounted to a vertical surface as shown in Figure 5-8. A vacuum system was used to mount the Scanner to the test specimens.

5.3.3 Optical Reconstruction

An optical bench was used to reconstruct the AH images. The primary elements of the optical bench are shown in Figure 5-9. The combination of the Helium-Neon Laser and the optics provides a coherent collimated light source that illuminates the hologram (which was made on the Scanner). The balance of the optics is used to focus the image on an Image Screen that is viewed by a TV camera and presented on a TV Monitor Screen. A camera is used to record the image presented on the TV monitor and some of these images are presented in the body of this report. There are a number of considerations that have to do with correction for surface curvature and correlation of the AH image to the actual size of the flaw. Surface curvature is readily analyzed on the basis of the physical relationship of the scanner and the test specimen.

The basic utility of the AH technique is true flaw size determination based on simple measurements of the reconstructed image of the flaw. The basic geometry used in deriving the flaw depth versus optical bench path length is shown in Figure 5-10. Refer to Figure 5-11 for a definition of the optical path parameters. The relation between the object to hologram distance (S to H) and the hologram to image distance (H to G) for a scanning pulse-echo system has been developed by Hildebrand and Brenden. (3). Based on the sign conventions used for distance measurements in this study the relationship can be expressed as:

$$1/R_a = 1/R_b \pm(\mu/m^2)\ (2/R_1)$$

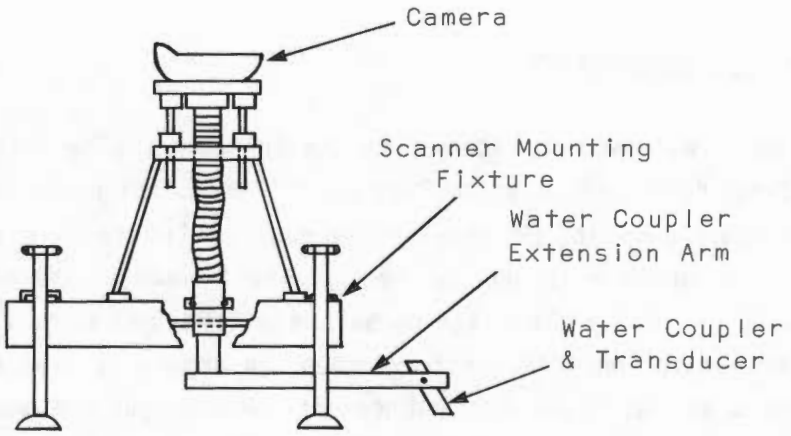

Figure 5-6 Cut Away View - Scanner

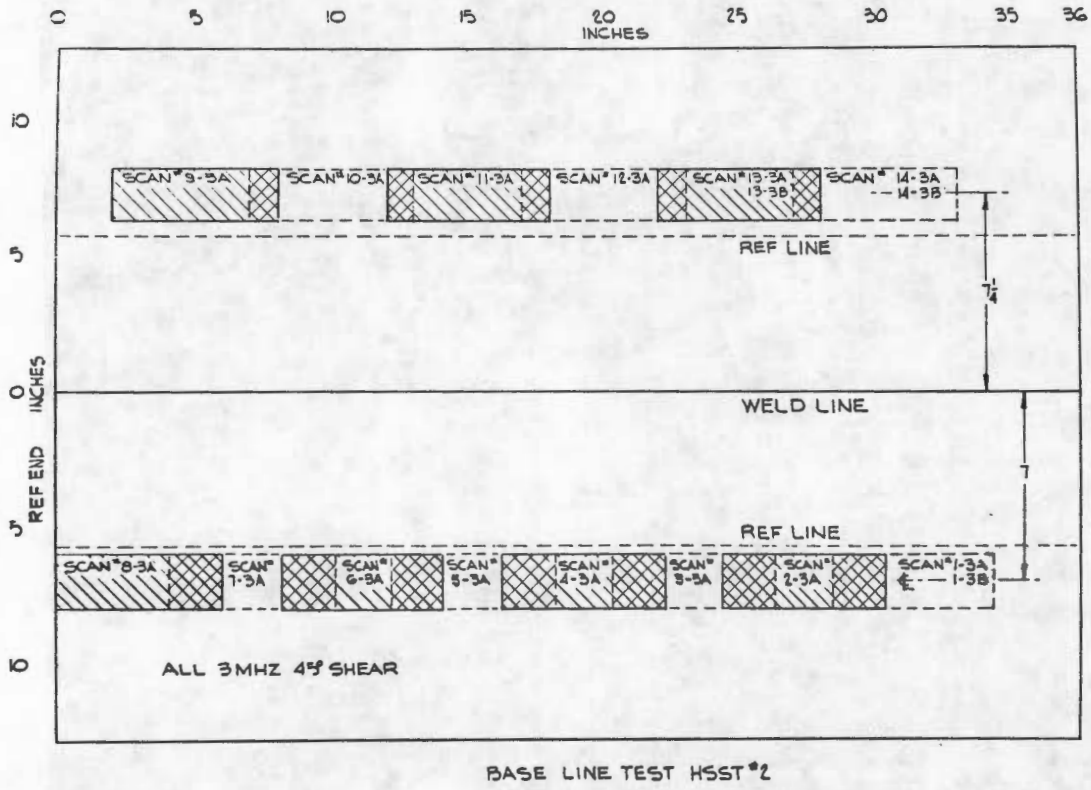

BASE LINE TEST HSST #2

Figure 5-7 Scan Areas for HSST #2

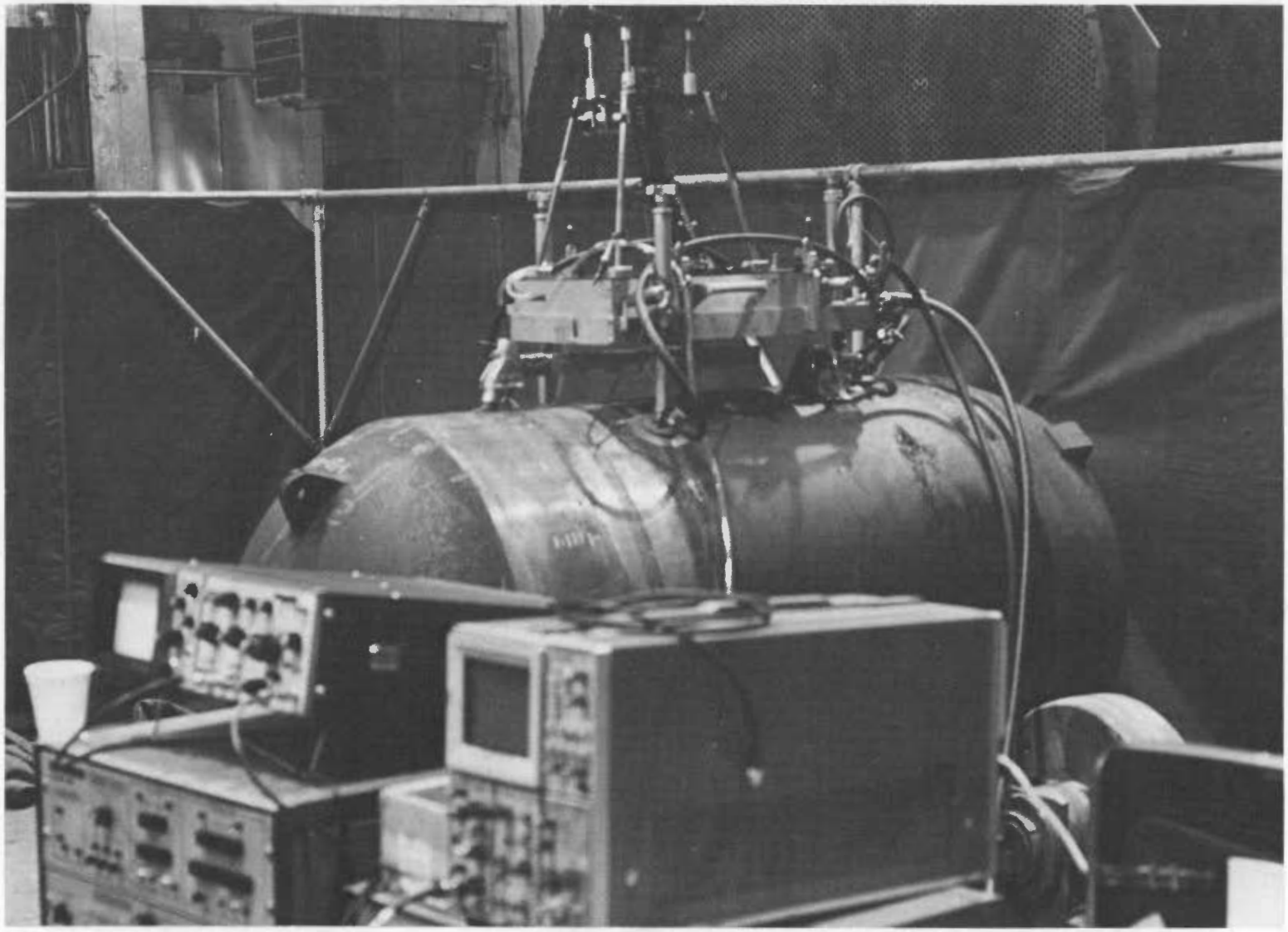

Figure 5-8 Scanner Mounted in Vertical Position

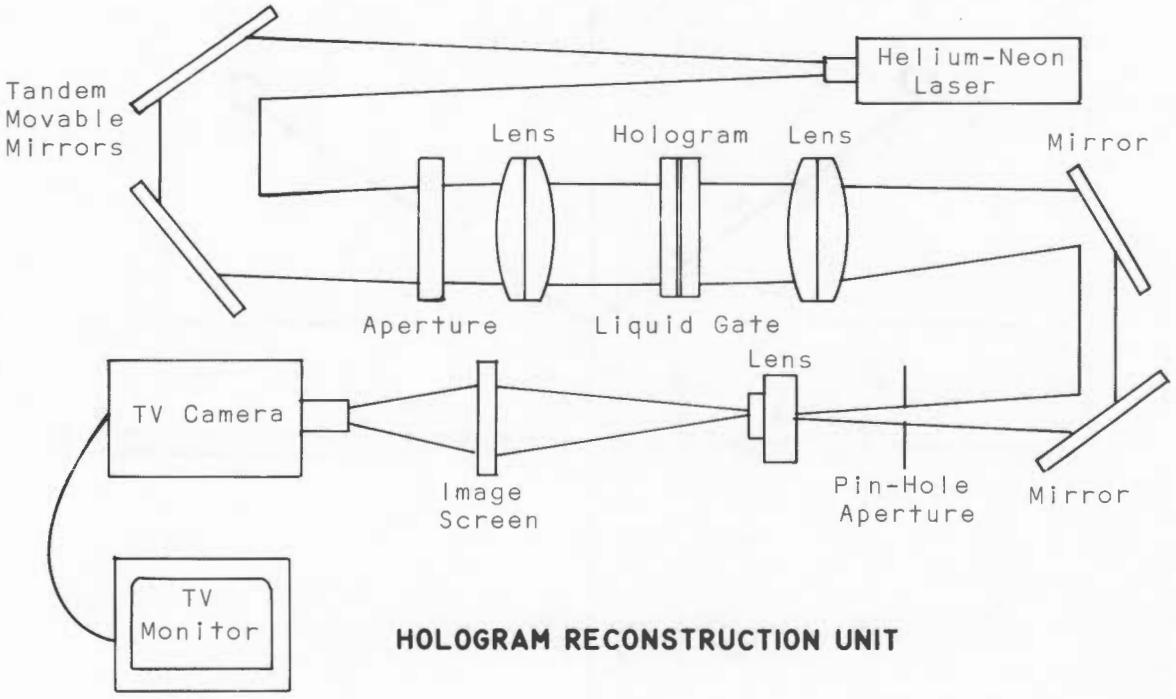

Figure 5-9 Optical Unit Schematic

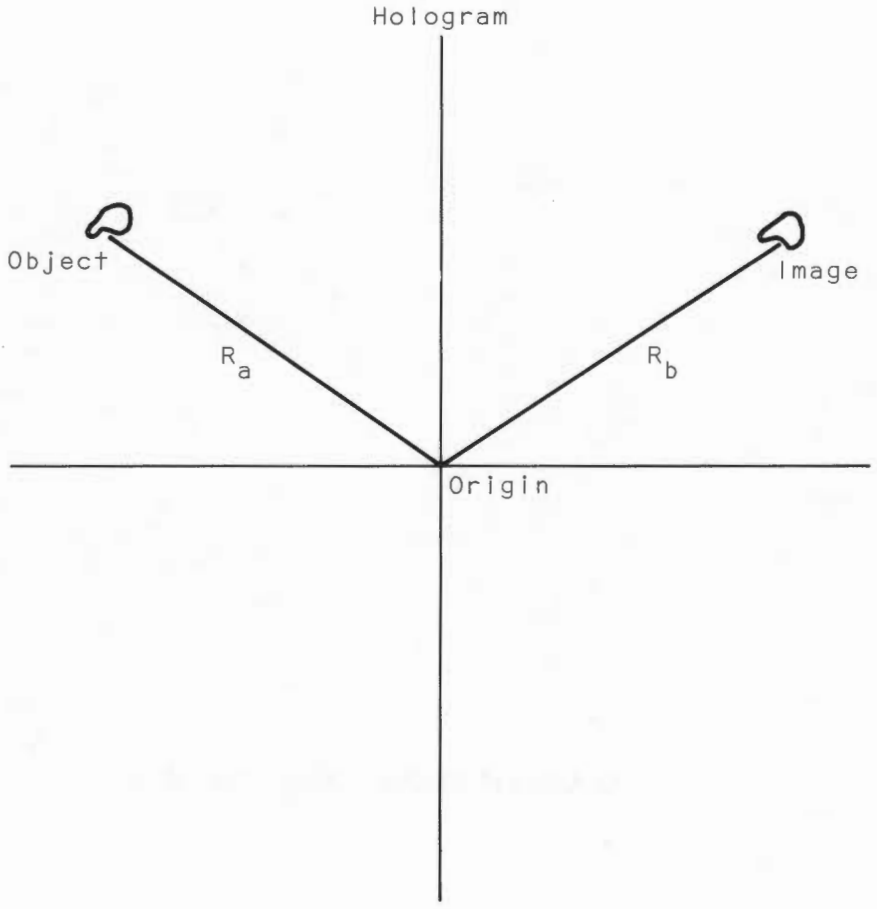

Base Geometry and Sign Conventions For Acoustic Holography Imaging.

Figure 5-10 AH Sign Conventions

Field Unit Optical Reconstruction System

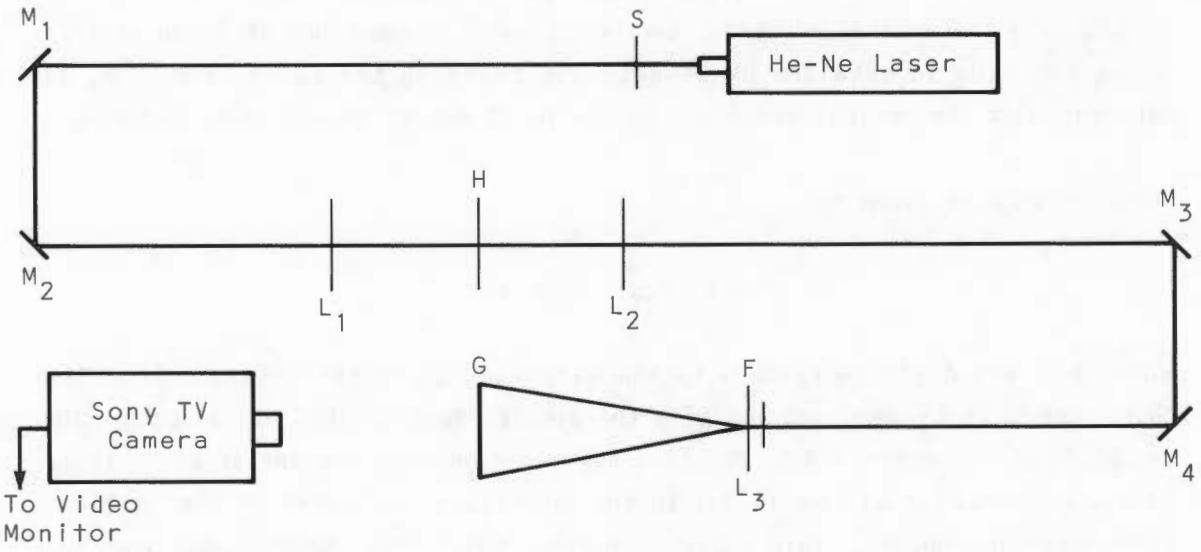

G= Ground Glass Screen For TV Imaging.
S= Point at Which Laser Becomes a Point Source.
H= Position of the Hologram.
F= Focal Plane of the Image.
H-F= Distance is Fixed.
S-H= Distance is Variable.
L_1&L_2=Collimating Lenses with Equal Focal Lengths.

L_3= 16X Enlarging Lenses.

Figure 5-11 Optical Path Parameter Definitions

where the $\pm$ sign refers to the true and conjugate image locations respectively. R_1 is the object distance in the material. R_1 and R_a are not equivalent because the ultrasonic path also encompasses a water path. $\mu = \lambda_R/\lambda_a$ where λ_R is the wavelength of the reconstructing laser and λ_A is the wavelength of the acoustic beam. m is the reduction factor of the hologram itself and is fixed at 0.25. In the optical processor the hologram to image plane is fixed so that image focusing is obtained by effectively changing the value of R_a. R_a is determined in the optical processor by the point source to hologram distance.

This distance is given by:

$$R_a = 2s + U_o + d$$

where d is the distance from L_1 to the hologram, U_o is the distance from the point source to L_1 when s=0 and s is the displacement of the optical path. The s=0 position is determined by focusing the laser beam to a point at the image plane. The factor of two is due to the mechanical behavior of the optical path change mechanism. This analysis implies that only precise measurements of the optical bench physical parameters and the wavelength ratio are necessary to relate s and R_1.

The ability to accurately determine R_1 from the optical bench setting is important because of the nature of the lateral magnification factor, which is given by: (1)

$$M = (\mu/M)(R_b/R_1)$$

Translating this equation into a form appropriate to the reconstruction unit we have:

$$M = 2(\mu/m)(f/R_1) \quad \sum_{i=1}^{N} M_i$$

where f is the total focal length of the lens system and ΣM_i accounts for the magnification due to lens L_3 and the cumulative effect of the TV camera, monitor and photographic procedure. A simple measurement of the physical parameters of the system is not sufficient for the magnificaiton factor computation due to the lack of a theoretical relation between the variables R_1

and ΣM_i. To account for this, a relative standardization of ΣM_i with respect to R_1 was performed using test blocks with known reflector sizes at different depths. Many were obtained from the test blocks at different frequencies. An effective magnification constant was calculated from the average value used to determine the actual reflector size from the reconstructed photographic images. The magnification factor then reduces to the equation:

$$M = 6.4009(N/R_1)$$

where $N = 1000\mu$ and the constant 6.4009 contains all the measurable and fixed values as well as the relation between ΣM_i and R_1. The standard deviation of the magification equation constant is $\pm$ 0.1373.

The Optical Bench was modified by B&W to meet performance criteria established by B&W.

5.4 TEST CONFIGURATIONS

5.4.1 Production Component Tests

As noted earlier, production and/or field environments frequently contain elements that are unfavorable for the use of sophisticated electronic equipment. As shown in figure 5-12 this can include problems with cleanliness and access as well as the points discussed earlier. Figure 5-13 and 5-14 are two views of the test configuration used for the Base Metal inspections. In the case of the Base Metal inspections the specimen surface was horizontal and access to the area requiring inspection was fairly easy.

The test configuration required for the Nozzle inspections was considerably more difficult than that for the Base Metal inspections. Figure 5-15 illustrates this difference. The Nozzle tests involved a curved vertical surface that was fairly rough as compared to the Base Metal surface. Figure 5-16 presents two more views of the Nozzle test configuration. As shown in Figure 5-16a the surface available for mounting the scanner was limited which increased the difficulties in mounting the scanner to the surface. Figure 5-16b illustrates the need for flexibility in locating the scanner electronics. In the case of the Nozzle tests the electronics had to be located inside the vessel and power had to be brought to the electronics.

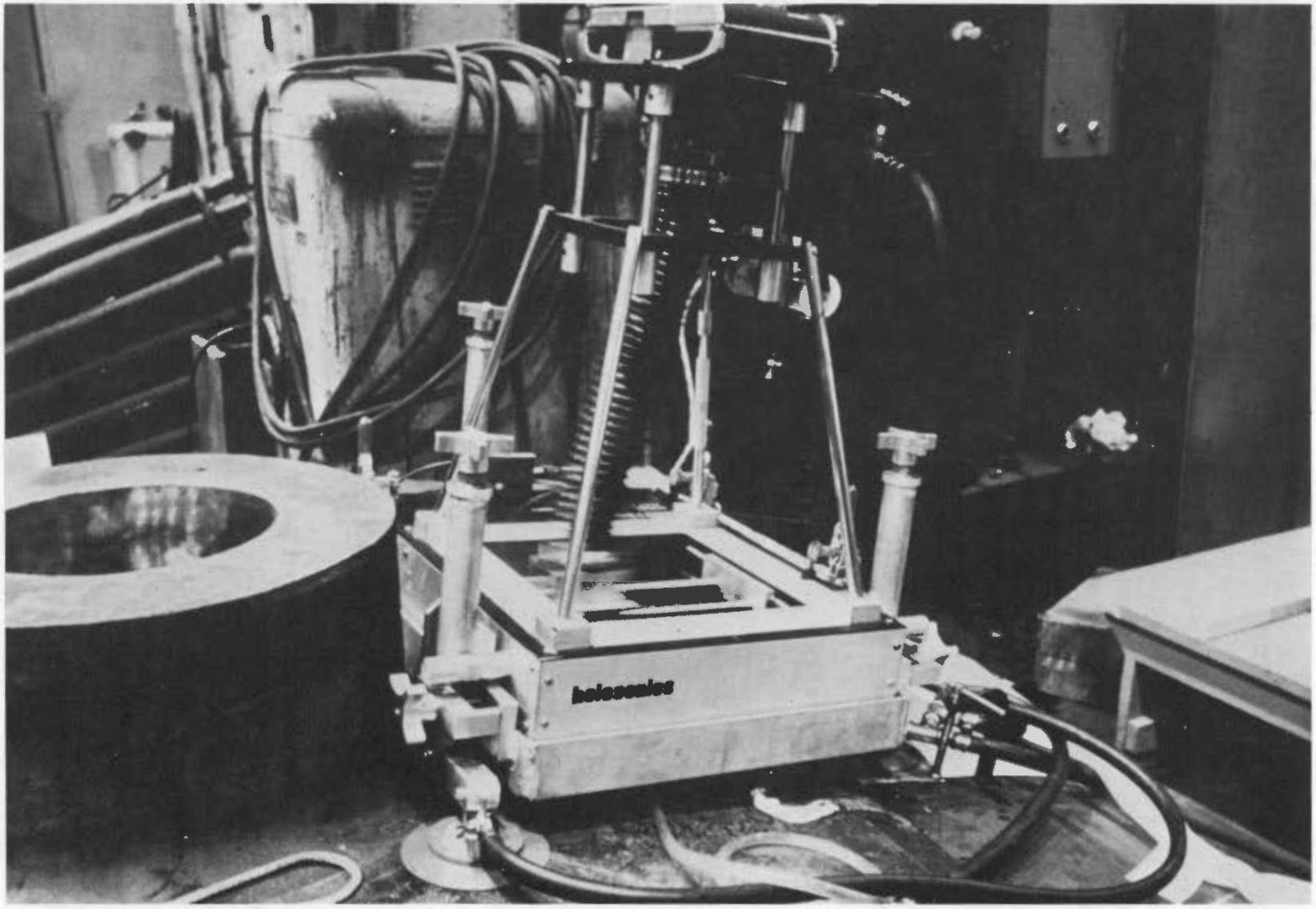

Figure 5-12 Production Environment

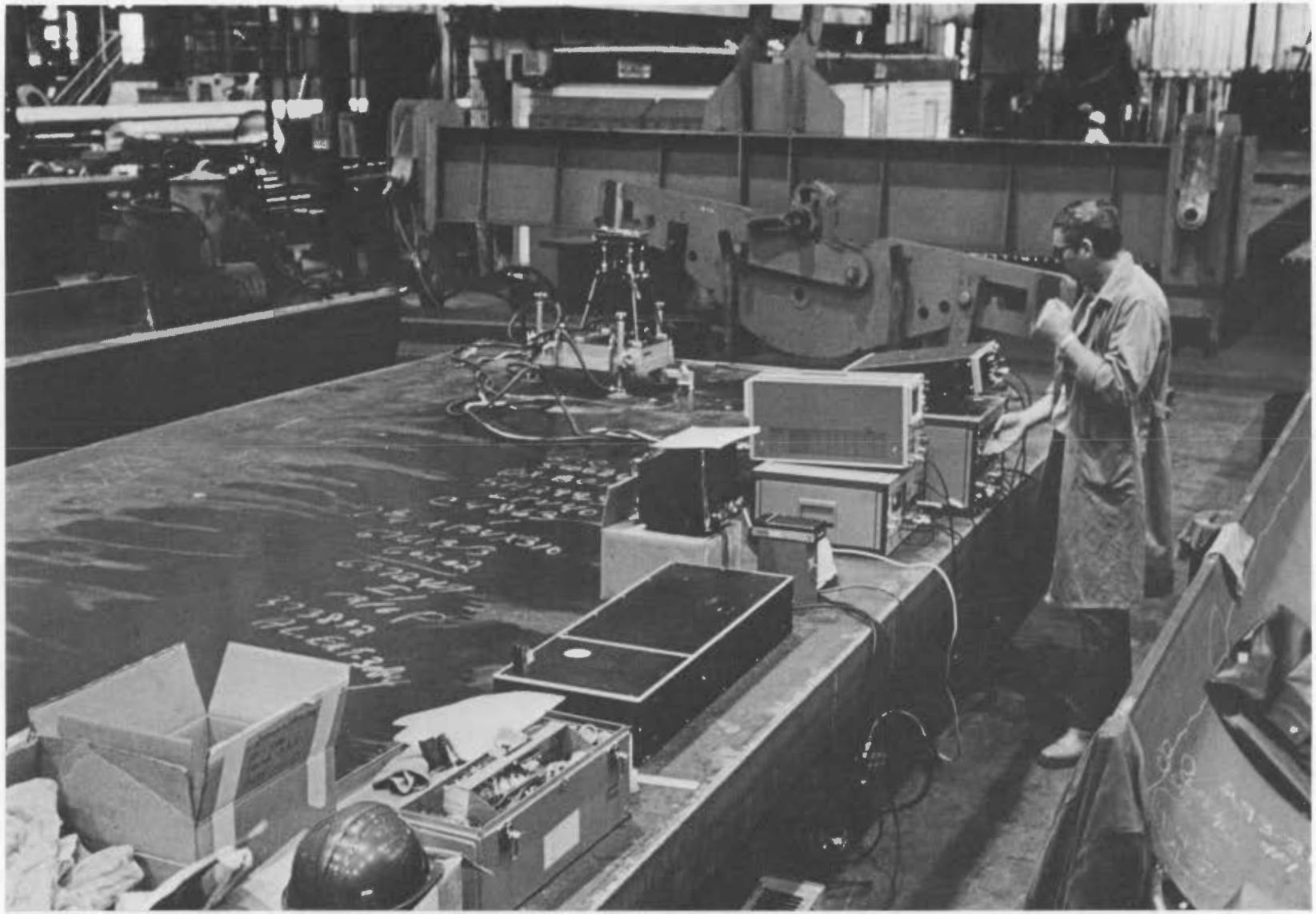

Figure 5-13 Base Metal Test Configuration

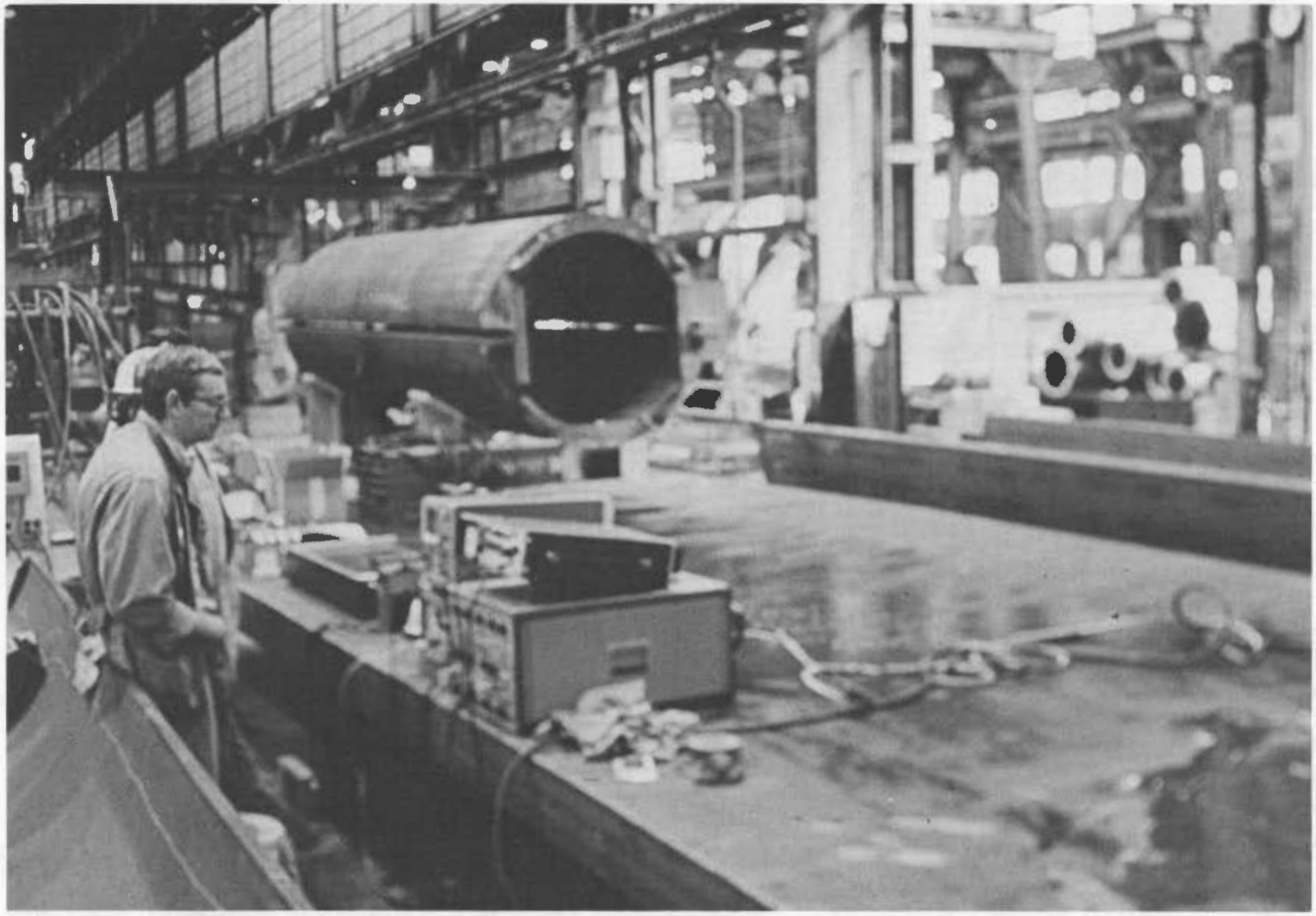

Figure 5-14 Additional View & Base Metal Test Configuration

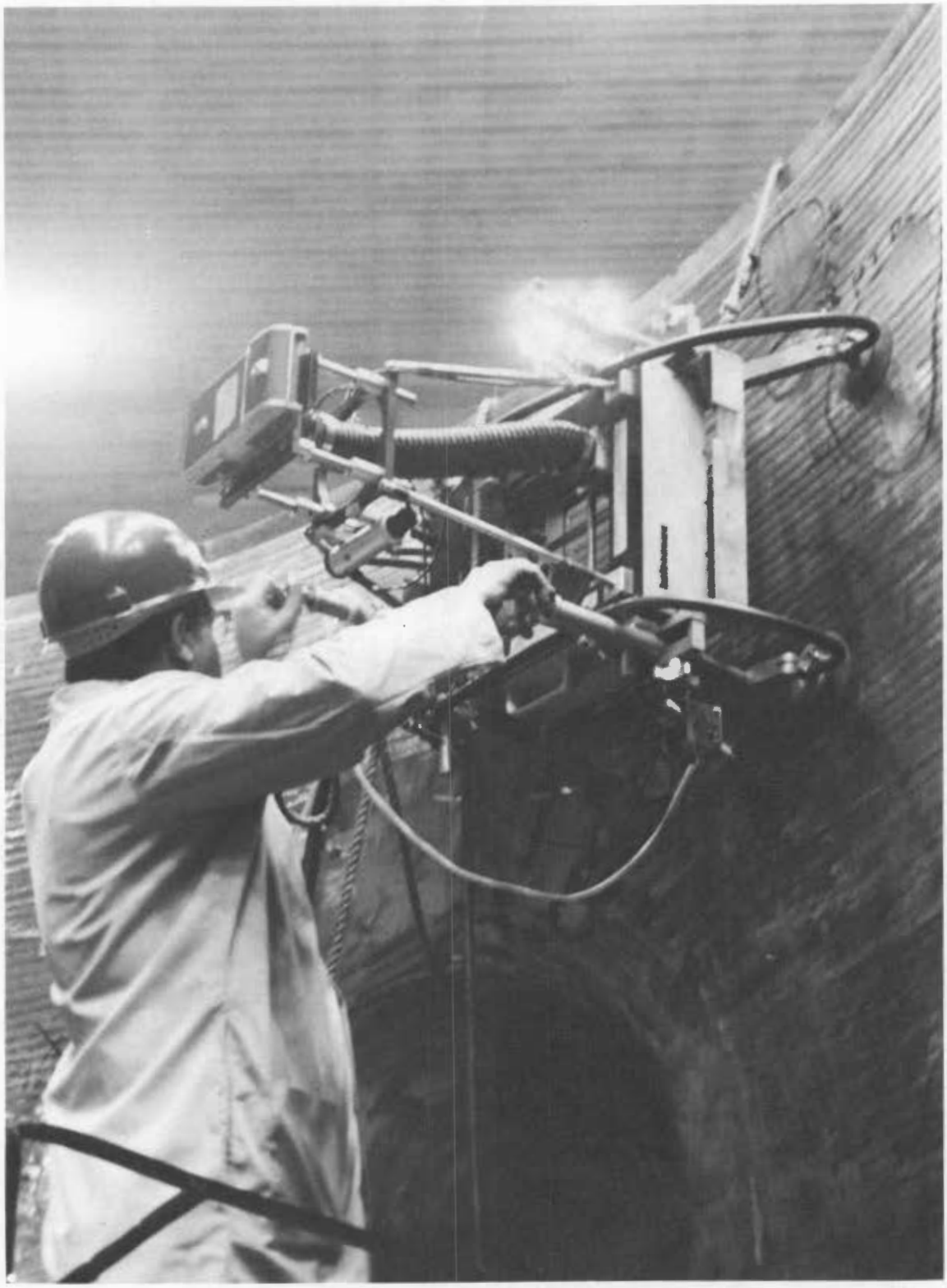

Figure 5-15 Operator Adjusting Scanner System During A Nozzle Weld Inspection (Mt. Vernon, Indiana)

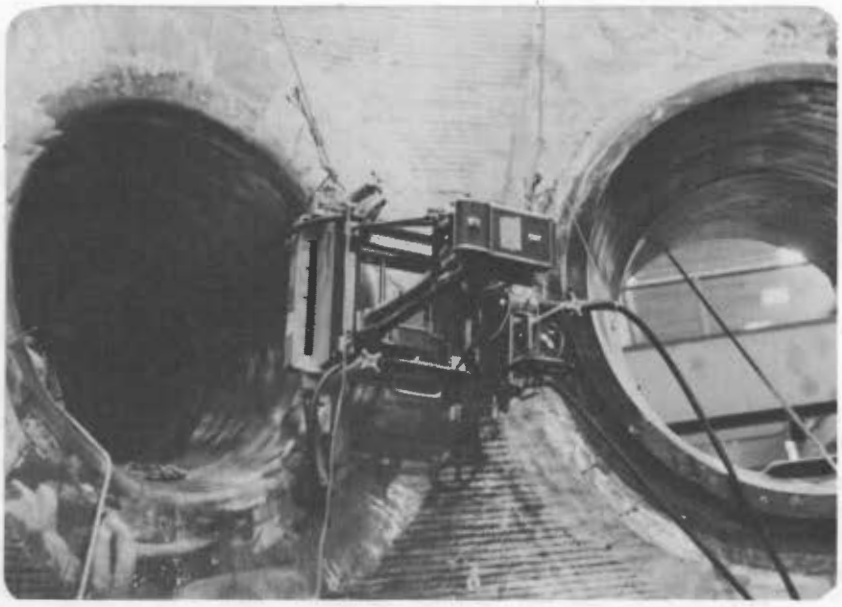

(a)

(b)

Figure 5-16 Additional Views of Nozzle Test Configuration

5.4.2 Non-production Component Tests

The inspections of the non-production components were generally made in a more hospitable physical environment. The set-up problems tended to relate more to the geometry of the test specimen. Figure 5-8 shows the test configuration for the AEPV inspections. The curvature of the test surface was a consideration in these tests. Figure 5-17 shows the test configuration used for the HSST inspections. The relationship of the scanner to the HSST surface is shown in Figure 5-18.

5.4.3 Summary Comments on Test Configurations

The size of the specimens and the diversity of surface shapes and conditions can require an extremely flexible arrangement for scanner mounting. While the inspections reported in this report did not involve suspension from an overhead curved surface it is conceivable that such a shape factor might be involved in a field inspection. Access to the surface to be inspected may be limited and the supporting electronics/reconstruction equipment has to be suitable for location inside as well as outside the vessel that is being inspected. Even with relatively crude equipment, it is feasible to successfully adapt available AH equipment to a variety of production environments and test specimens.

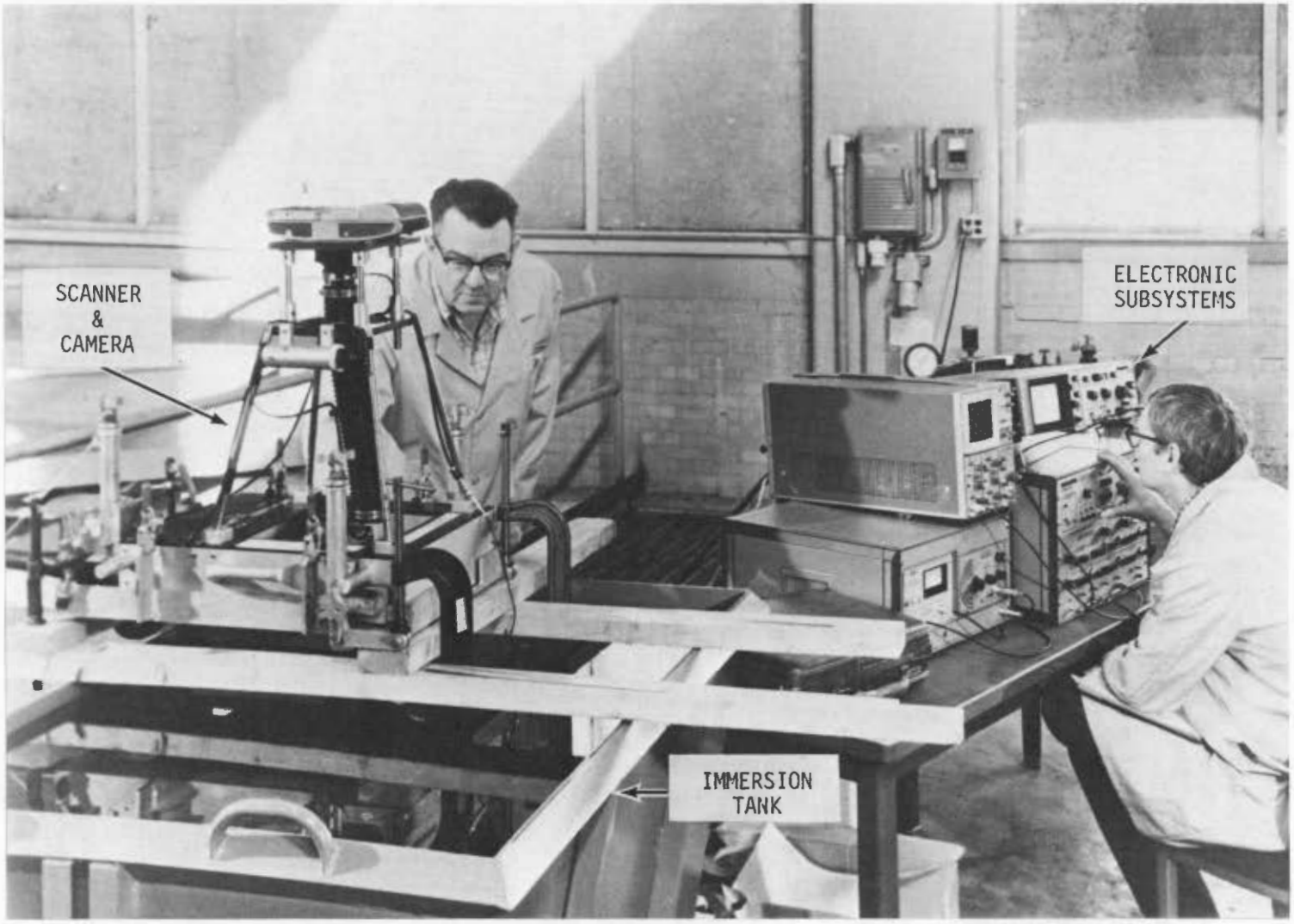

Figure 5-17 HSST Test Configuration

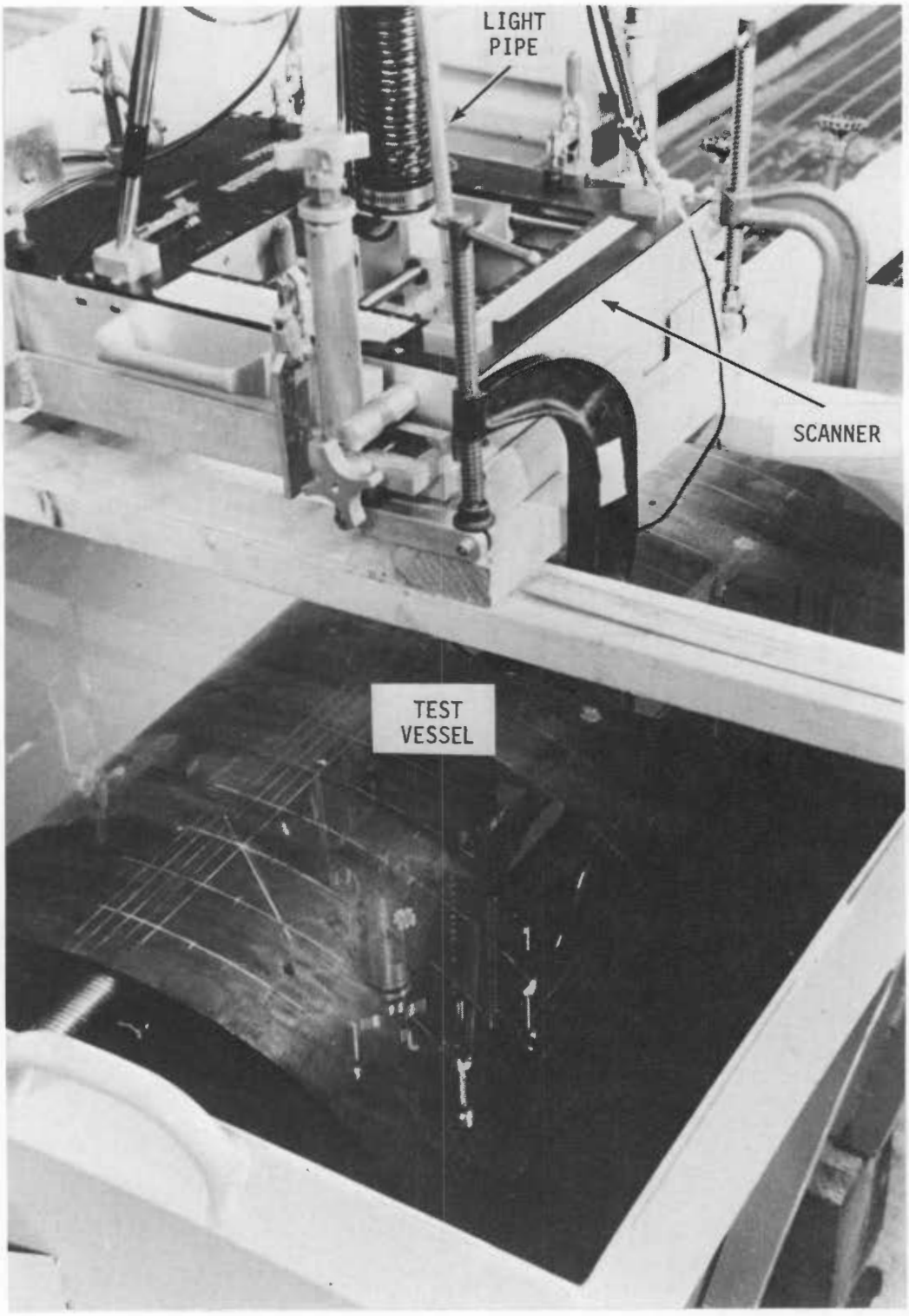

Figure 5-18 Relationship of Scanner and HSST Surface

Section 6.0
CONCLUSIONS

6.1 ACCURACY CONSIDERATIONS

The results obtained were generally encouraging. These results suggest that it is feasible and practical to characterize defects in production components with reasonable accuracy and in a timely manner. In many cases, the destructive tests used during RP-605 were relatively crude. As a result it is difficult to define the expected accuracy of the characterization by AH imagery in quantitative terms. Situations where satisfactory destructive test (DT) techniques were used suggested reasonably good agreement between the AH and DT results. As an example, Table 4-1 summarized the characterization results obtained with AH and DT on HSST #1 and HSST #2. In terms of AH results vs. the DT results the following ratios were obtained.

Item	AH/DT Result
HSST #1 - EB Weld Zone	1.0
HSST #1 - Trepan Diameter	0.95
HSST #1 - Max Crack Extent	0.91
HSST #2 - EB Weld Zone	1.0
HSST #2 - Avg. Crack Extent	1.0

Similarly for the Circle Seam Examination (Table 3-2) the following results were obtained.

Item	AH/DT Results
Defect No. 1 Length	0.9
Defect No. 1 Thru Wall Extent	1.07
Defect No. 1 Depth Below Surface	1.0
Defect No. 2 Length	1.0
Defect No. 2 Thru Wall Extent	1.0
Defect No. 2 Depth Below Surface	1.0

These above comparisons suggest that accuracies of 10% or better might be expected when optical reconstruction techniques are used by a skilled operator. The data base available in this report is quite small and it would be prudent to defer quantitative statements on specific AH characterization accuracies until a larger valid data base is available and more current versions of AH equipment are developed and used in the field. The results do suggest that design goals of accuracies of 10% or better for new equipment are feasible and practical.

6.2 OPERATOR SKILL CONSIDERATION

The RP 605 results were highly dependent upon operator skill in two ways:

a. Operation of the Holosonic equipment and interpretation of the AH images.

b. Dealing with the physics of the particular test specimen and the test configuration required to adapt the equipment to the test specimens.

One can anticipate that improved equipment designs and reconstruction techniques will reduce the operator skill required. It appears that for the next generation of equipment the operator (or test set up technician) will still have to be proficient in dealing with the physics/geometry of the particular test set up.

6.3 EQUIPMENT DESIGN

Significant improvements in AH equipment for field use are needed and are feasible. These needed improvements can be grouped into two areas:

a. Improvement focused on suitability of the equipment for operation in a field environment. Such improvements would include ruggedness, reduced susceptability to electromagnetic interference, internal power condition for a variety of prime power levels (and quality); scanner coverage; better mounting of the scanner to the surface of test specimen, general ease of operation; and reduced requirements for operator proficiency.

b. Improvements focused on AH image interpretation such as image enhancement, computer reconstruction or alternative presentation techniques that incorporate internal dimension measurement capability (e.g. Landsat Data Processing Techniques).

6.4 SUITABILITY FOR GENERAL FIELD USE

Acoustic Holography appears to be practical for use in field environments in terms of the results obtained and the set up of test equipment. Acoustic Holography supplements the existing NDE inspection techniques and offers an opportunity to improve on the current capability for defect characterization. While Acoustic Holography is not a panacea for the faults of the current NDE capability, it does complement current NDE in an important area, characterization of defects. A combination of NDE techniques is required to support field questions.

APPENDIX A

ADDITIONAL PHOTOGRAPHS-PRODUCTION COMPONENT TESTS

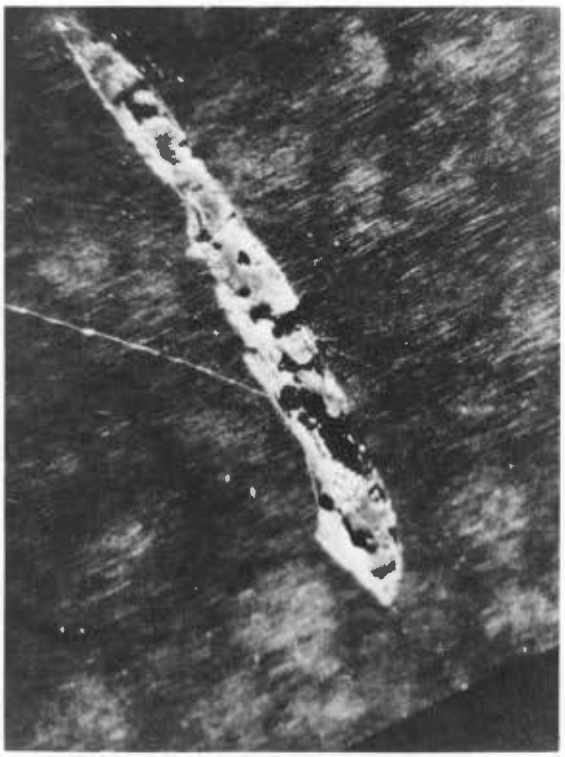

Figure A-1 Destructive Test Photo - Indication 21 (27th Slice)

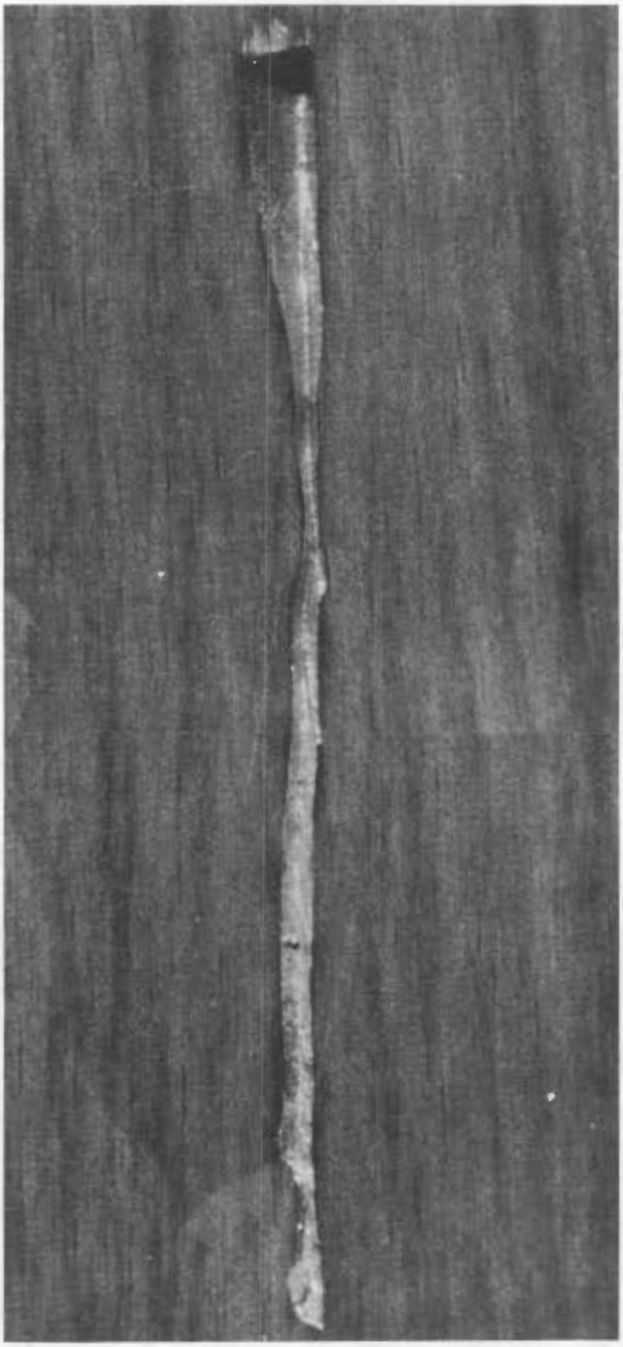

Magnified Montage Photo

Figure A-2 Destructive Test Photo - Indication 22

(a) BOTH DEFECTS

(b) A-3rd Slice

(c) A-5th Slice

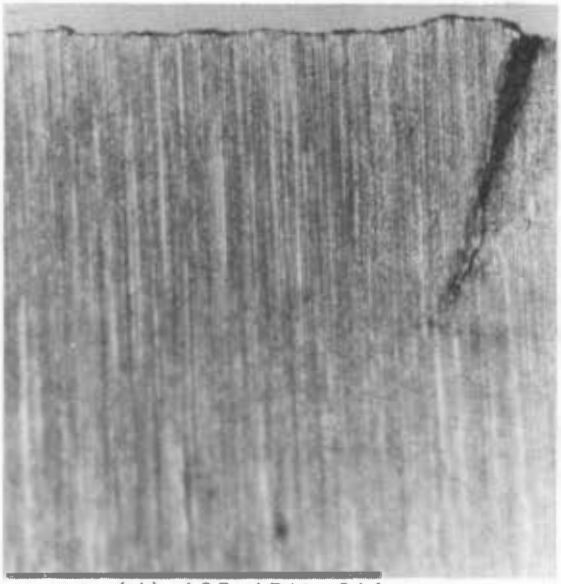

(d) A25-15th Slice

(e) A25-20th Slice

Figure A-3 Destructive Test Photos - Indications 25 and A

(a) 23rd Slice

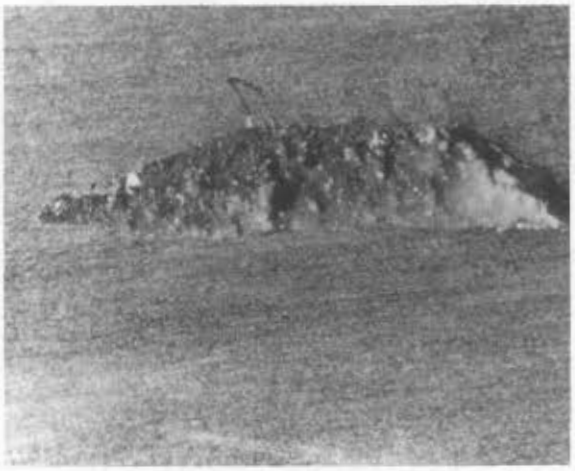

(b) 28th Slice

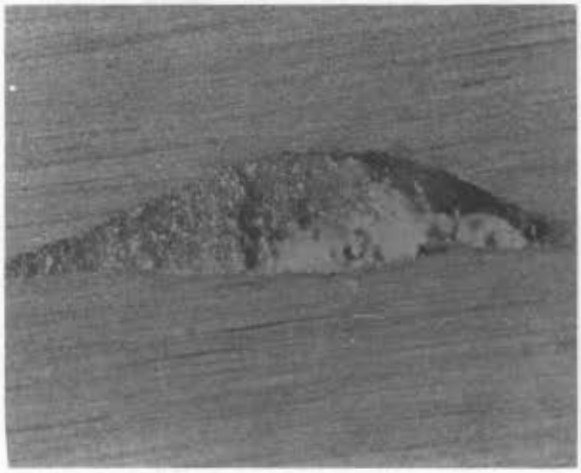

(c) 33rd Slice

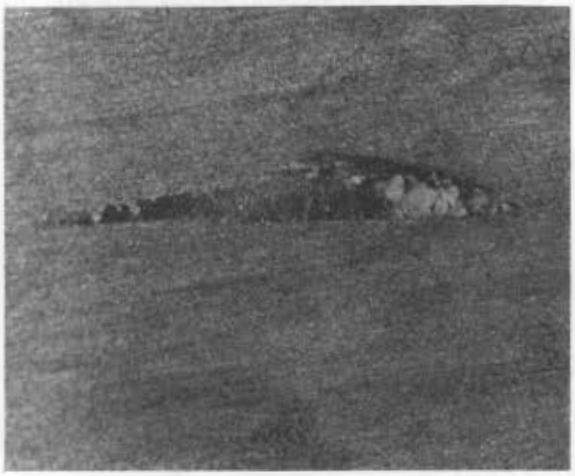

(d) 43rd Slice

Figure A-4 Destructive Test Photos - Indication 26

(a) 10th Slice

(b) 11th Slice

(c) 15th Slice

(d) 16th Slice

Figure A-5 Destructive Test Photos - Indication 27

APPENDIX B

ADDITIONAL PHOTOGRAPHS-NON PRODUCTION COMPONENT TESTS

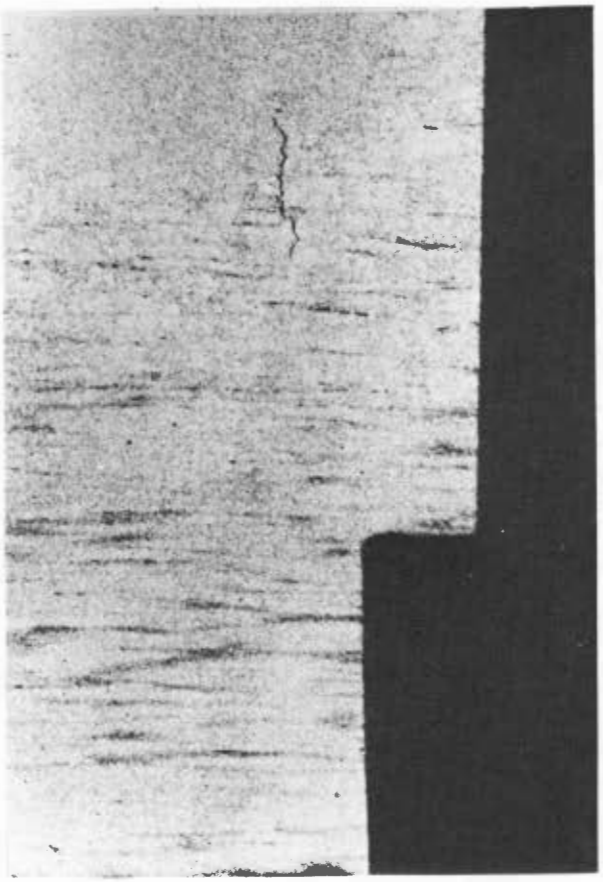

Figure B-1 Crack in Sample D X10 Ref: 140/10/76

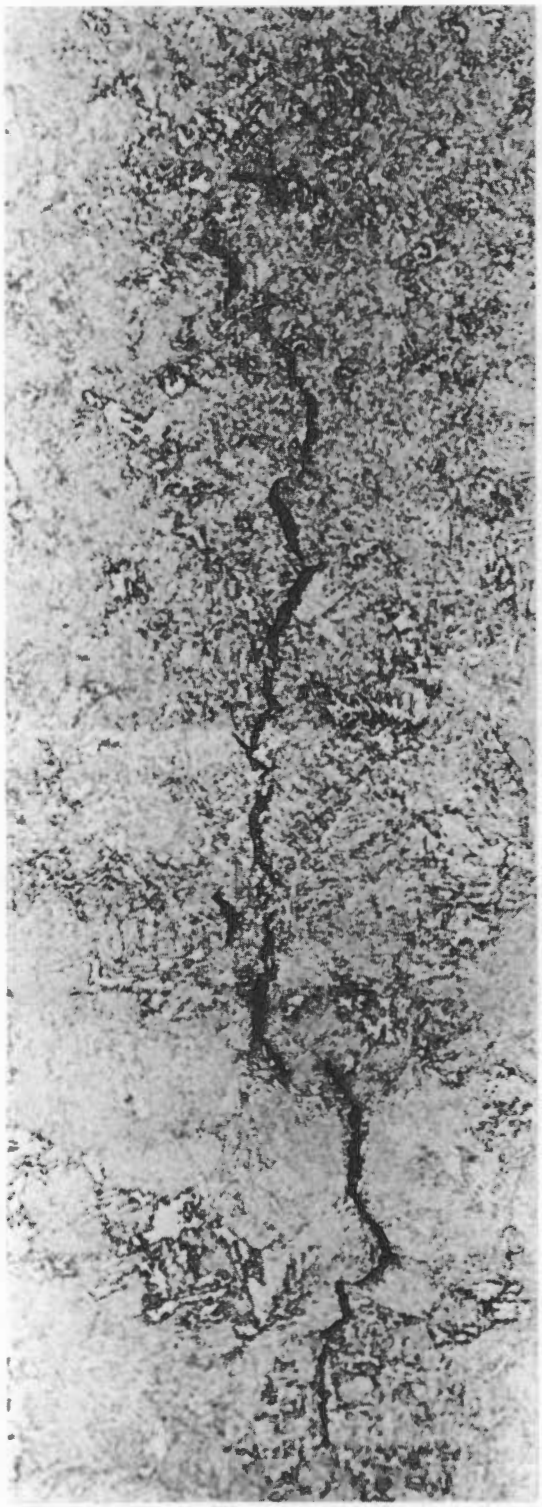

Figure B-2 Montage of Crack in Sample D X100
Refs: 111/10/76 & 112/10/76

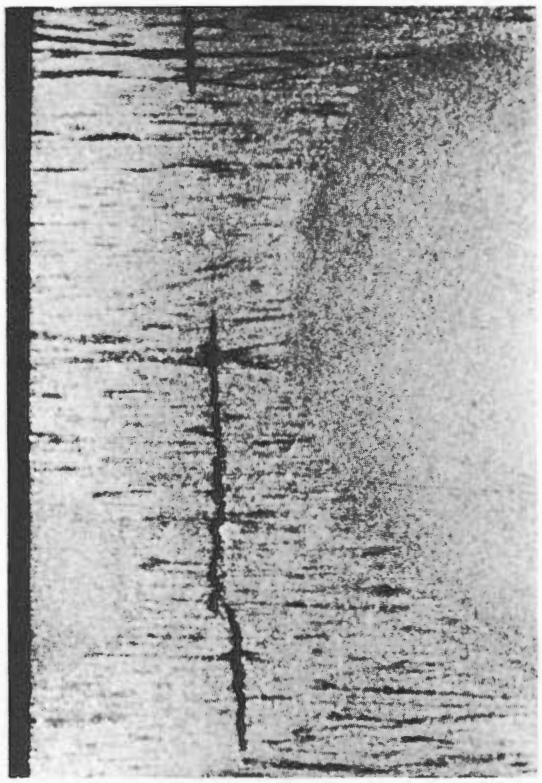

Figure B-3 Cracking in Sample E X6 Ref: 141/10/76

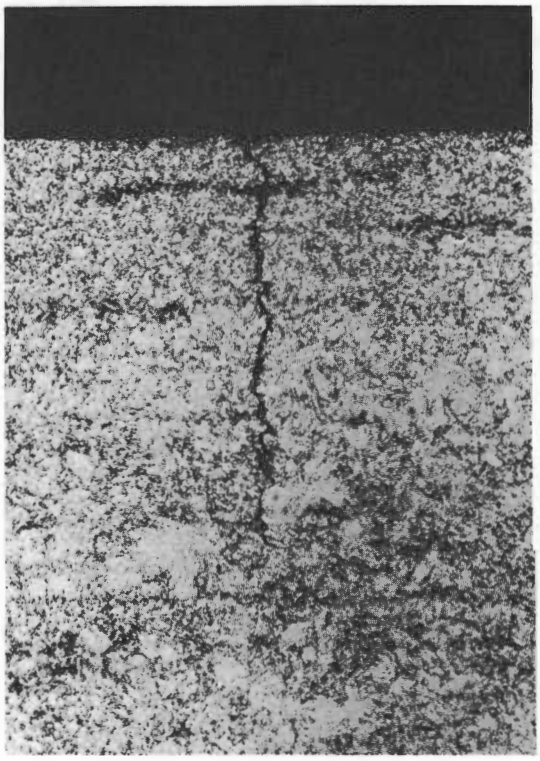

Figure B-4 Smaller Crack in Sample E X25 Ref: 92/10/76

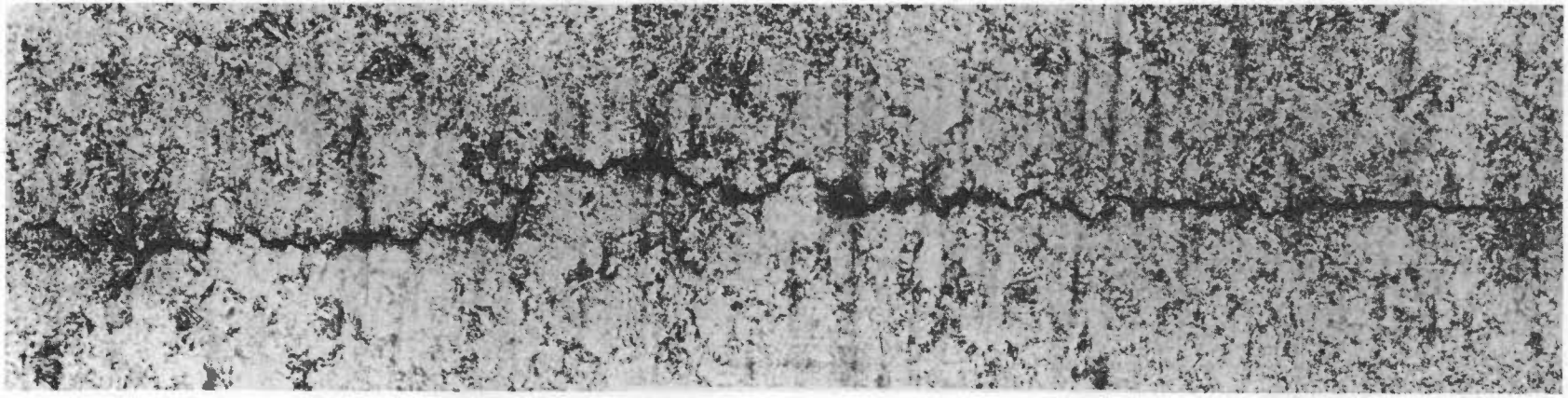

Ref: 104/10/76 Ref: 102/10/76 Ref: 103/10/76

Figure B-5 Montage of Largest Crack in Sample E X25

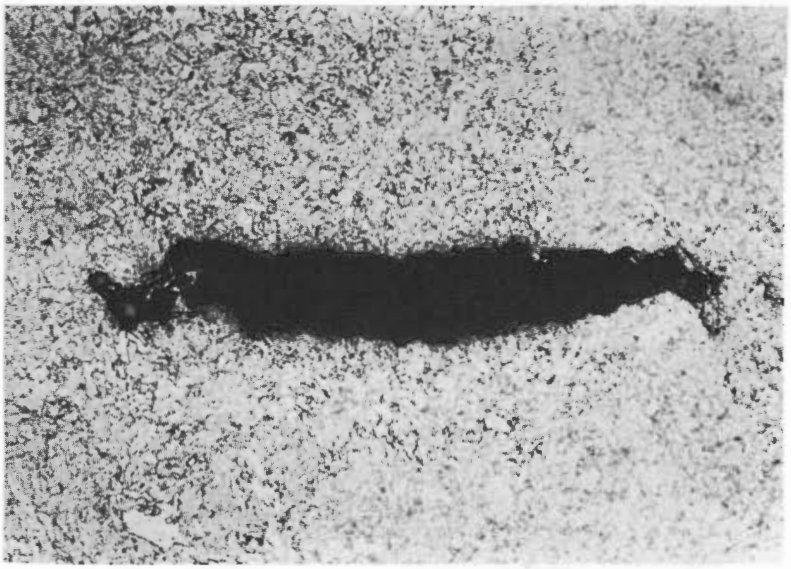

Figure B-6 Third Crack Found in Sample E X100 Ref: 84/10/76

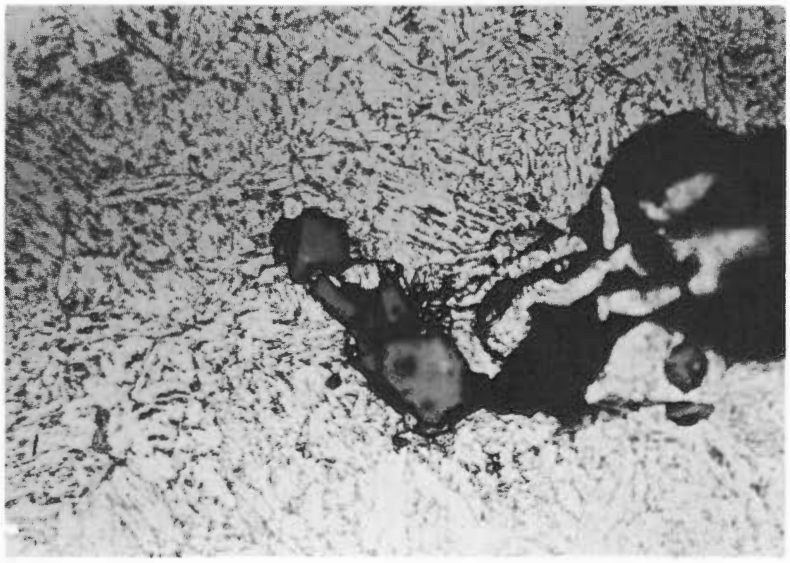

Figure B-7 Alumina Inclusion Associated with Crack X1000
Ref: 88/10/76

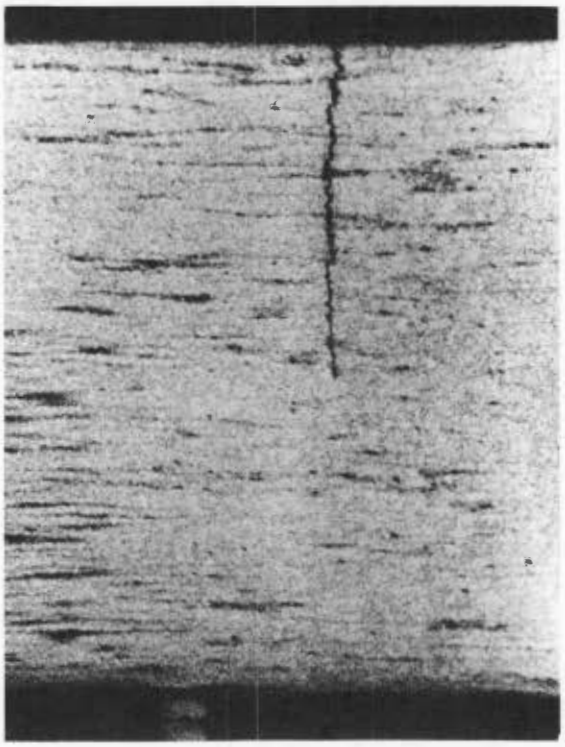

Figure B-8 Crack in Sample F X10 Ref: 142/10/76

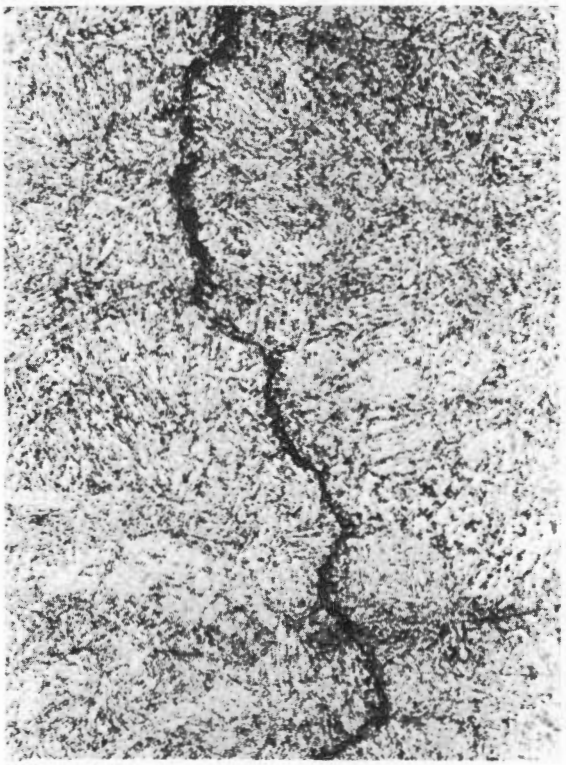

Figure B-9 Intergranular Nature of Crack in Sample F X1000
Ref: 73/10/76